The role of compartmentalised cyclic nucleotides in pulmonary endothelial barrier function

---

A thesis submitted for the degree of *Master of Science by Research*

University of Oxford

Prof. Dr. Manuela Zaccolo: Supervisor

Laura Schmidt

Keble College

Content

Acknowledgements

I would like to thank my supervisor Professor Manuela Zaccolo for giving me the opportunity to undertake this project at the University of Oxford. I really appreciate the contribution you have made to my career.

I would like to thank the members of the laboratory who have helped me over the past year: Konstantinos Lefkimmiatis for sharing his scientific knowledge and passion for science, Andreas Koschinski for all the work he put into developing the FRET-TER measurement chamber, Alex Burdyga for helping me with all kinds of practical FRET-microscopy challenges, Marcella Brescia, Oliver Lomas, Duangnapa Kovanich, Stefania Monterisi and Nicoletta Surdo.

Abstract

The barrier function of the endothelium has been found to decrease in response to cyclic adenosine monophosphate (cAMP) elevations in the cellular cytosol, while it seems to be rescued by increasing cAMP concentrations at the membrane. This suggests that cAMP compartmentalisation may be a regulatory mechanism of barrier function.

Barrier dysfunction has been implicated in disease, including chronic obstructive pulmonary disease and oedema. It remains unknown whether cAMP compartmentalisation plays a role in barrier dysfunction. Therefore, it is of interest to investigate whether cAMP is compartmentalised in human pulmonary microvascular endothelial cells (hPMEC) and how this affects barrier maintenance.

Here we describe the optimisation of methods to investigate the potential cAMP compartmentalisation in hPMEC. Fluorescence Resonance Energy Transfer (FRET) microscopy allows for high resolution live monitoring of spatiotemporal changes of cyclic nucleotides. FRET membrane targeted and cytosolic sensors, respectively, were developed to compare cAMP regulation in different subcellular locations in space and time. FRET imaging studies in hPMEC have not been undertaken before, therefore cell culture conditions were optimized for this specific purpose. In addition, a chamber that combines FRET imaging with transendothelial resistance (TER) measurements was designed and constructed to determine cAMP compartmentalisation in hPMEC and its contribution to cellular barrier function.

Fluorescence imaging confirmed localization of FRET reporters at the membrane and in the cytosol, respectively. Addition of 28 mM HEPES and omission of serum were judged to be appropriate in conducting future FRET experiments in hPMEC. Initial FRET-TER chamber experiments were conducted, confirming that both FRET and TER could be measured with this approach. Preliminary data, employing different stimuli and FRET reporters, are in line with the notion of cAMP is compartmentalised in hPMEC.

By further optimisation and development of the methods described here, insight will be gained into the localisation and regulation of cAMP at the subcellular level and its effect on endothelial barrier function. This will help clarify whether local manipulation of cAMP signals may offer alternative approaches to the treatment of barrier function-related pathologies.

1.Introduction

1.1 Endothelial barrier function and disease

Endothelial cells are at the interface of blood and tissue. They form a semipermeable cellular monolayer between the lumen and blood- and lymph vessel walls. Endothelial cells line the whole cardiovascular system. Therefore, they are in an optimal position to sense and relay physical and chemical cues to regulate processes including vascular tone and blood pressure, angiogenesis, inflammation and substance and gas exchange[1]. Involvement of endothelial cells in this plethora of functions explains why endothelial dysfunction can have significant physiological effects.

Endothelial barrier dysfunction (EBDF) is marked by inability of the endothelium to form a protective yet selectively permeable monolayer. The site of EBDF is a crucial determinant of disease phenotype. For example, when EBDF manifests in arteries it can be a significant contributor to inflammation and cardiovascular disease. Increased endothelial permeability enables easier passage and adherence of inflammatory cells to the endothelium. This process can increase plaque formation through oxidation of low density lipoproteins by macrophages[2–4]. Plaques increase the risk of blood flow obstruction and ultimately ischemia and tissue infarct.

Another site where adequate function of endothelium is crucial, is the' blood-brain barrier' (BBB). The main functions of this barrier include regulation of in- and efflux of ions and molecules, protection, and maintenance of brain

homeostasis. BBB dysfunction is characterised by junction disruption or impairment of transport processes and can lead to increased extravasation of immune cells and poorly regulated flux of molecules and ions across the BBB[5]. Dysfunction can occur through several processes, including inflammation and is associated with diseases including Alzheimer's disease, Parkinson's disease and stroke[6].

Endothelial barrier dysfunction as observed in sepsis and acute lung injury carries high morbidity and mortality. The most severe form of acute lung injury is acute respiratory distress syndrome, which develops if the lungs become severely inflamed as a result of an infection or injury. The inflammation causes barrier dysfunction, which leads to fluid extravasation into the alveoli; if untreated this can result in suffocation. Currently, therapies to counter this outcome are lacking.

Endothelial barrier dysfunction and the ensuing increase in endothelial permeability are significant contributors to many diseases and generally occur in conjunction with inflammation. The environment of endothelial cells can vary significantly between tissue types, making therapy development challenging. A better understanding of mechanisms underlying endothelial barrier function is crucial for future therapeutic developments in numerous pathologies, including cardiovascular, neurological and pulmonary disease.

1.2 Endothelial barrier

Endothelial cells are able to form structural barriers in support of vital homeostatic and protective tissue functions. Endothelial and epithelial cells are the most prominent example of cell types known to form barriers. Epithelium forms protective layers lining hollow organs including the lungs and digestive tract but also skin. Although endothelium has an epithelial origin, unlike epithelium it forms a semipermeable monolayer between the lumen and wall of blood- and lymph vessels. Under physiological conditions the different contributory components of endothelial barrier function remain in a dynamic balance. The components include the glycocalyx, cytoskeleton, cell–cell junction complexes, and cell attachments to extracellular matrix and basement membrane of endothelial cells. Under homeostatic conditions, the endothelial barrier maintains a low and selective permeability to fluid and solutes. When the balance between the different contributors to barrier function is perturbed endothelial dysfunction ensues and permeability increases. This is characterised by increased extravasation and fluid accumulation in tissue (oedema).

1.2.1 Glycocalyx

The glycocalyx is a negatively charged coating that lines the luminal surface of the endothelium. This meshlike structure consists of proteoglycans, glycosaminoglycans, and adsorbed plasma proteins.

The glycocalyx has been implicated in regulating endothelial barrier function in three non-mutually exclusive ways: it may act as a physical fiber matrix barrier[7–10], its negative charge may form a selective barrier for differentially charged macromolecules, or components of the glycocalyx may acts as receptors and regulate signalling in endothelial permeability[11]. Disruption of the glycocalyx has been shown to increase endothelial permeability to macromolecules in venules, capillaries and coronary arterioles[12–14]. The same holds true for neutralizing the negative charge of the coating by application of cationic ferritin or protamine, which increased the endothelial permeability for radioactively labeled albumin[15–17]. Furthermore, endothelial permeability was induced by cationic arginine and lysine polymers, models for neutrophil cationic peptides. These cationic peptides are released under inflammatory conditions by activated neutrophils that interact with endothelial cells[11]. Barrier permeability and actin stress fibers induced by cationic arginine and lysine polymers decreased significantly when cells were pre-treated with heparinase III[11]. Heparinase III recognises heparan sulfate proteoglycan as its primary substrate, which is a component of the glycocalyx. Heparan sulfate proteoglycans can act as receptors or co-receptors in cellular signal transduction[18,19]. These findings suggest that the glycocalyx may affect barrier function through signalling events.

Evidence for the importance of the glycocalyx in endothelial barrier function is increasing. Unfortunately, the glycocalyx is difficult to maintain and establish under *in vitro* cell culture conditions. Therefore, the glycocalyx is one of the most difficult variables to study in relation to endothelial barrier function[20].

1.2.2 Cytoskeleton

The cytoskeleton consists of all molecular components that provide cells with support, mobility and dynamic shape and structure. The molecular components can roughly be divided into microfilaments, intermediate filaments and microtubules.

1.2.2.1 Microfilaments

Microfilaments or actin filaments are the smallest of the cytoskeletal components. In vertebrates, three isoforms, α, β and γ, are differentially expressed in various tissue types[21]. Microfilaments consist of two-stranded helical actin polymers. These actin filaments are found throughout the cell and are present at increased density beneath the cellular membrane. This dense mesh of actin filaments, known as the cortical actin ring, is thought to be crucial for cell motility and shape dynamics through interaction with myosin.

Upon addition of barrier disrupting stimuli such as thrombin, endothelial cells present with actin stress fiber formation and actomyosin contraction[22–24]. In contrast, barrier enhancing stimuli, such as sphingosine-1-phosphate (S1P), reverse stress fiber formation by re-localisation of actin filaments to the cellular periphery and subsequent strengthening of the endothelial barrier[25].

1.2.2.2 Intermediate filaments

Intermediate filaments are constructed of a heterogeneous group of proteins that can be specific to a certain cell type. For example, keratins are found specifically in epithelial cells, whereas lamins are found in all cell types, where they form a meshwork that reinforces the inside of the nuclear membrane. Intermediate filaments are thought to be less dynamic than microfilaments or tubules and to support cellular stability mainly by reinforcing tubulin structures. The cellular function of intermediate filament proteins may be cell type dependent. For example, knock-out mice for glial fibrillary acidic protein, the main component of the intermediate filaments in cells of astroglial lineage, do not show any cellular or physiological abnormalities[26]. The same is true for mice deficient for vimentin, an intermediate filament expressed in mesenchymal cells. However, these animals showed delayed wound healing compared to wildtype mice as indicated by scanning electron microscopy. Another example is given by keratin filaments, which protect skin epithelial cells from mechanical and non-mechanical stresses[27]. Mutations in the keratin gene are known to cause several diseases that correlate with skin abnormalities, including blistering or cyst formation.

These examples indicate that intermediate filaments may fulfill various roles related to cellular function. The role of intermediate filaments in endothelial barrier function remains to be characterised.

1.2.2.3 Microtubules

The highly dynamic α and β tubulin polymer tubes known as microtubules, are found in the cytoplasm of eukaryotic cells. They lend structure and stability to organelles and the cell as a whole, in addition to directing intracellular transport. Microtubules are rigid straight hollow tubes that protrude from the centrosome outward to the plasma membrane.

The role of microtubule dynamics in barrier function is not well understood. However, recently there has been increasing evidence that microtubules may play a crucial role in maintaining the endothelial barrier. Birukova et al. found that thrombin decreased endothelial barrier function by stimulating peripheral microtubule disassembly in human pulmonary arterial endothelial cells[28]. These effects were attenuated upon pretreatment with taxol, a tubulin polymerization and stabilisation agent, indicating that microtubules are critical in thrombin-induced barrier failure. Interestingly, Birukova et al. also found that stimulation of lung endothelial cells with hepatocyte growth factor led to barrier function enhancement, as measured by an increase in transendothelial resistance. This was associated with increased peripheral microtubule growth[29]. Overall, these findings indicate that microtubules may play a role in endothelial barrier regulation.

1.2.3 Extracellular matrix interactions

Tissues consist of cells and interstitial space. This space is filled by an intricate network of macromolecules, which vary for each type of tissue, constituting the extracellular matrix (ECM). Through adhesive interactions with the endothelial cell surface, the ECM is able to provide an essential scaffold for maintaining the organization of endothelial cells in the vasculature.

The cell-ECM interactions, so called focal adhesions, are mainly established by transmembrane receptors called integrins. The intracellular domain of these heterodimers interacts either directly or indirectly with the cytoskeleton through linker proteins paxillin, talin, vinculin, or α-actinin. The large extracellular domains of integrins bind to matrix proteins, including fibronectin, vitronectin, collagen, fibrinogen, and laminin[30,31].

Moy et al. used an anti-vascular endothelial (VE)-cadherin blocking antibody to interfere with cell-cell adhesions of confluent endothelial monolayers grown on ECM[32]. In doing so, they were able to assess the contribution of ECM to the overall TER, a measure for endothelial barrier function. Indeed, the extracellular matrix accounted for 50% of the total measured resistance, a finding similar to earlier results with fibroblast monolayers[33].

In addition, several lines of evidence show that degradation of the ECM correlates with increased endothelial permeability[34–36].

Although integrin–matrix binding is essential to the establishment and stabilisation of endothelial barriers, the precise mechanisms by which focal adhesions contribute to the maintenance and regulation of endothelial barrier function are not completely understood[37,38].

On this note, it should be mentioned that certain integrins have also been shown to locate at cell-cell borders, implying that integrins may play a role in regulating endothelial barrier in both a lateral and basolateral fashion[39]. This is supported by *in vivo* research, which demonstrated that plasma leakage across microvessels caused by fibrinogen degradation products was significantly attenuated in integrin-β1-knockout mice[40].

Overall, the ECM and its interactions with the endothelium should be considered an essential component of endothelial barrier function and its regulation.

1.2.4 Permeability

Cellular permeability can be divided into paracellular and transcellular permeability. Under physiological conditions, transcellular permeability of vascular endothelium to albumin is crucial to maintain the oncotic pressure gradient. In addition, transcellular permeability allows for albumin cotransport of several hydrophobic molecules, hormones and enzymes across the endothelial membrane.

The paracellular route consists of interendothelial junctions and cell-matrix interactions. This route is the main regulator of endothelial hyperpermeability or barrier dysfunction under pathophysiological conditions.

1.2.4.1 Paracellular permeability: cell-cell junctions

Paracellular permeability refers to the interstitial space between adjacent cells, which is thought to be responsible for the majority of extravascular fluid leakage due to endothelial barrier dysfunction. Paracellular permeability is regulated by a complex interplay of centripetal forces generated by the cellular cytoskeleton and centrifugal counterforces of the proteins that establish cell-cell and cell-matrix interactions. The cell-matrix interactions are mainly established by integrins, whereas the overall cell-cell adhesive forces are formed by adherens, tight and gap junctions.

1.2.4.1.1 Adherens junctions

In all endothelial beds adherens junctions are established by proteins called VE-cadherins. It is thought to be crucial for cell-cell interactions and the forming of the endothelial barrier. This is compatible with the finding that the VE-cadherin knock-out mouse model is lethal due to immature vasculature[41,42]. Inter-endothelial barriers are established through formation of homotypic bonds between the extracellular domains of two VE–cadherin transmembrane receptors expressed on neighboring cells[16].

The intracellular domain of VE–cadherin is thought to be connected to the actin cytoskeleton via a family of catenins (α-, β-, γ-, and p120-catenins). The α-, β-, γ-catenins form a protein complex around the tail of VE-cadherin, which anchors it to actin microfilaments[43]. Notably, truncation of the cytosolic binding

domain of VE-cadherin for β-catenin proved to be lethal in mice, emphasizing the importance of this protein for functional cytoskeletal establishment[42].

γ-Catenins, or plakoglobins, and β-catenins have been shown to bind to the intracellular domain of VE-cadherin via association with α-catenin, thereby linking the cadherin complex to the actin cytoskeleton[44]. The VE-cadherin-actin cytoskeleton connection is further stabilized by α-catenin binding to other proteins, including α-actinin, vinculin, vasodilator-stimulated phosphoprotein and formin[45–49]. Keratinocytes lacking α-catenin were found to have leaky junctions, due to failure of polymerizing actin[48]. This suggests an important role for α-catenin in barrier function. In addition, α-catenin is able to bind to the protein Zona Occludens-1 (ZO-1), which is one of the main intercellular proteins involved in tight junction formation[50]. Interestingly, this implies regulatory communication between the different types of junctions in establishing a functional barrier.

P120-catenins bind to VE-cadherin, but do not directly interact with actin. Instead these catenins form a scaffold for proteins including kinases and phosphatases. These scaffolds enable further molecular interactions that regulate the dynamics of adherens junctions and ultimately of endothelial barrier function[51–55].

1.2.4.1.2 Tight Junctions

Tight junctions (TJ) differ from adherens junctions in their protein composition. TJs only represent ~20% of junctional complexes on endothelial cells[56]. Due to

lack of evidence the overall understanding of how TJs regulate endothelial permeability remains poor. Whereas adherens junctions are mainly made up of cadherin, tight junctions incorporate transmembrane proteins including occludin, claudins, and junctional adhesion molecules (JAMs)[16,57,58]. These associate with different intracellular peripheral membrane proteins, including the scaffolding proteins ZO-1, -2, and -3, which anchor the protein complex to actin microfilaments[59].

Occludin and claudin are membrane-spanning proteins. Each protein has four transmembrane domains and two extracellular loop domains, which enable homotypic binding with the extracellular domains of occludin or claudin, respectively, on the neighboring endothelial cells.

The expression level of occludin has been found to positively correlate with increased endothelial barrier function in various vascular cell types[60,61]. Interference with occludin expression by small interference RNA, or introduction of mutations into the amino terminal of the protein sequence was associated with leaky tight junctions[62,63]. Expression of occludin was found to be highest in the endothelial cells of the nervous system, which may relate to the superior resistance of the endothelial blood brain barrier compared to other vascular tissue[16,64]. Interestingly, occludin knock-out mice did not show any abnormalities in tight junction function, indicating that there may be other proteins compensating for the functional absence of occludin[65].

Of the claudin family, which consists of 24 proteins, only claudin-5 is expressed in endothelial cells[66,67]. In mice, deletion of claudin-5 resulted in death approximately 10 days after birth, which may suggests that claudins have a more crucial function than occludins[67]. This study suggested that the blood

brain barrier had become more permeable to small solutes, implicating claudin-5 to be a crucial regulator of blood brain barrier function[67].

JAMs, members of the immunoglobin superfamily of proteins, are single-pass transmembrane proteins that form homotypic binding with JAMs on opposite cells[68–70]. To date, the types JAM-1, -2, and -3 have been described, which show 30-40% homology and varying cellular expression patterns. All types are found in endothelial cells, but only JAM-3 is exclusively present in endothelium[69,70]. The overall role in barrier function of JAMs remains to be elucidated.

Very little is known about the overall contribution to barrier function of the ZO protein family. Of these proteins, ZO-1 is thought to play a prominent role in cellular permeability. This perspective is supported by evidence that ZO-1 interacts directly or indirectly with transmembrane proteins occludins, claudins and JAMs via bridging proteins[59]. Furthermore, the expression of ZO-1 has been found to be an important factor in tight junction physiology. Cellular treatment with different pharmacological agents, including glucocorticoids or interferon-γ, have been shown to increase or decrease ZO-1 expression[71,72]. This finding was negatively correlated with the respective endothelial or epithelial resistance, indicating a facilitatory role of ZO-1 in barrier function. Although specifically enriched at tight junctions, ZO-1 has also been found in fibroblasts, Schwann cells, astrocytes and various types of cancer[73,74].

ZO-2 has been shown to have a nuclear export and sorting domain. This fact, in conjunction with increased accumulation of ZO-2 at nuclei of non-confluent cellular layers, suggests a shuttling function for this protein[59,75]. The function of

ZO-3 remains to be elucidated.

1.2.4.1.3 Gap junctions

Gap junctions can form pores between neighbouring endothelial cells, and other surrounding types of cells, and allow for current flow and exchange of second messengers[16]. The channels are formed by two hydrophilic connexons, one contributed by each neighbouring cell. In turn, each connexon consist of six connexin subunits, which each have four transmembrane domains[76]. Endothelial cells have been shown to express connexins 37, 40 and 43, which are present in varying ratios within endothelial connexons[77,78].

Although gap junctions are generally thought to play a less prominent role in endothelial permeability, there is evidence supportive of their role in barrier function. Simon and McWhorter[79] found that deletion of connexin 37 or 40 showed no detrimental effect to the vasculature or viability of mice. However, double knock-out mice for both connexins died before or shortly after birth, due to vascular abnormalities that resulted in hemorrhaging in several tissues. This is compatible with a role for connexin 37 and 40 in barrier function.

Other connexins may be implicated in barrier function as well. For example, connexin 43 has been shown to associated with the tight junction scaffolding protein ZO-1, as well as spectrin[16]. This suggests integration gap and tight junctions, and the actin cytoskeleton.

In summary, there is evidence supporting a role of gap junctions in endothelial barrier function; however, the overall contribution and underlying mechanisms need further elucidation.

1.2.4.2 Transcellular permeability: vesicular transcytosis

The transcellular pathway has been defined as the receptor-regulated transport of albumin from vessel lumen to interstitial space, although other solutes and fluids are transported through this pathway as well[80].

Transcellular transport can occur through endocytosis of extracellular molecules by different types of vesicles into the cell. These vesicles are part of different endocytic pathways: phagocytosis, macropinocytosis and micropinocytosis. Phagocytosis is a highly regulated, particle specific process that occurs in cells such as macrophages, which are able to engulf and internalize cell debris and microorganisms.

Macropinocytosis is a process common to most cells, which occurs at membrane regions that are highly ruffled, enabling large vesicle formation. Because macropinosomes are quite large, they provide an efficient route for non-selective endocytosis of macromolecules. This type of endocytosis has been described to aid antigen uptake in immune cells, but also to aid virus uptake into cells[81,82].

Interestingly, Bruewer et al. have found evidence supportive of a role for macropinocytosis in TJ regulation[83]. They found that interferon-γ induced internalization of tight junction proteins occludin, JAM-A and claudin-I was unaffected by inhibition of clathrin- and caveolae-mediated transport. Treatment with pharmacological inhibitors of macropinocytosis abolished this internalization of tight junction proteins in epithelial cells. This study did not establish a direct relation between TJ protein internalization and a decrease in barrier function. However, the data is compatible with a regulatory function of

macropinocytosis in paracellular permeability through TJ protein internalization. Under homeostatic conditions, micropinocytosis and vesiculo-vacuolar organelles (VVOs) seem to contribute to transcellular permeability of endothelial cells by trafficking macromolecules, including albumin, to maintain cellular homeostasis and oncotic pressure within the vasculature[16].

Endocytosis by clathrin-coated vesicles and caveolae is also known as micropinocytosis as the vesicles are much smaller compared to macropinocytic vesicles. Clathrin-coated vesicle and caveolae-mediated transport is highly regulated through receptor binding by molecules which are to be internalized. Clathrin-coated vesicles obtained their name through the characteristic presence of the cytosolic protein clathrin, which forms a coating around endocytosed vesicles[84]. Clathrin-mediated endocytosis is found in virtually all cells and is fundamental to physiological processes including neurotransmission, signal transduction and the regulation of many plasma membrane activities[85].

Another equally important transcellular transport route is thought to be mediated by caveolae, which are small non-clathrin-coated plasma membrane buds[86,87]. They consist of the cholesterol-binding protein caveolin with a bilayer enriched in cholesterol and glycolipids. Caveolae can constitute up to a third of the plasma membrane surface area of the cells of some tissues, being especially abundant in smooth muscle, fibroblasts, adipocytes, and endothelial cells[86].

In 2001, Dvorak et al. reported a new endothelial cell permeability organelle in microvascular endothelial cells[88]. These organelles were termed VVOs, because they consist of an agglomeration of several interconnected vesicles, of

which the components remain to be elucidated, that form sessile channel-like structures spanning the cell interior[88]. Interestingly, the VVO density in capillary endothelium is generally significantly higher than in arteries, veins, arterioles and venules, with the exception of the blood-brain barrier where the amount of caveolae is decreased compared to the other types of endothelium[89,90].

It should be noted that the contribution of endothelial transcytosis to overall barrier function and pathophysiological permeability is not well understood. This is illustrated by studies using knockout animals of caveolin-1[91–93]. Endothelial cells of caveolin-1 deficient mice did not show any caveolae-mediated transcytosis. In addition, this deficiency caused endothelial nitric oxide synthase upregulation and increased levels of the vasodilator nitric oxide (NO), which led to increased paracellular permeability[94]. The exact molecular mechanisms behind this observation remain to be elucidated; however, this suggests that there may be cross-communication between paracellular permeability and transcellular permeability pathways[94]. Thus, caveolae do not only transport molecules in a transcellular fashion, they may also regulate paracellular permeability indirectly.

Another example illustrating the relation between endocytosis and paracellular permeability stems from research undertaken by Zhang et al[95]. They found that 1 hour after vascular endothelial cell stimulation with lipopolysaccharide, permeability increased in conjunction with a cytosolic co-localisation of VE-cadherin and clathrin as shown by immunofluorescence and immunoprecipitation[95]. Furthermore, several hours after stimulation, they found an increased cytosolic co-localisation of VE-cadherin with caveolin-1 and an increase in cellular permeability[95]. This confirms that lipopolysaccharide

induced hyperpermeability in vascular endothelial cells is mediated by caveolae and clathrin-coated vesicle internalization of the AJ protein VE-cadherin, thus illustrating the importance of crosstalk between trans- and paracellular pathways in homeostatic and pathophysiological endothelial permeability.

1.2.4.3 Modulation of endothelial permeability

The endothelial barrier is in a continuous state of dynamic homeostasis. It is at the interface of different environments, including blood or lymph and the respective tissue type through which the vessels travel. This complex environment necessitates endothelial cells to adapt barrier function and permeability to the needs of specific situations. For example, during inflammation due to a bacterial infection it may be beneficial for the endothelium to become more permeable. This allows leukocytes and other anti-inflammatory cells to enter into the tissue and obliterate bacteria and infected cells. In contrast, barrier function stabilisation would be beneficial during angiogenesis and development. The maturation process of new vasculature can be aided by increased barrier function, which strengthens the interendothelial junctions, thus stabilizing vessels.

On a molecular level, incorporation of extracellular cues into intracellular signals is crucial to the modulation of endothelial barrier function. Endothelial permeability is regulated by myosin light chain phosphorylation and reorganization of the actin cytoskeleton, which is tethered to intercellular junctions of cells (discussed in more detail in section 1.5 and Figure 3). Various

endogenous molecules are known to modulate barrier function by regulating the actin cytoskeleton. Examples include the G protein coupled receptor (GPCR) ligands adenosine, histamine, thrombin and S1P.

Adenosine is a widely distributed endogenous signalling molecule. Extracellular adenosine levels are quite variable, depending on tissue type and the degree of stress experienced by the tissue. Extracellular adenosine concentrations increase due to release by so-called equilibrative nucleoside transporters or as a result of cell damage[96–98]. Adenosine has been shown to have cellular protective effects, not limited to, but crucial in acute lung injury and sepsis[99–101]. It binds to four GPCRs designated A_1, A_{2A}, A_{2B}, and A_3[102]. A_{2A} and A_{2B} are expressed in several endothelial cell types, in which they can increase cellular cAMP levels and ultimately barrier function.

In contrast, histamine transiently increases microvascular permeability *in vivo*[103,104]. These transient changes are associated with a decrease followed by a restoration of cell adhesion in endothelial cells[105–108]. Although these rapidly resolving changes in cell adhesion are clearly described, the underlying mechanisms remain uncertain.

Thrombin is predominantly known for its role in blood coagulation and tissue damage. Next to a plethora of effects in the vasculature, thrombin induces increased permeability and cell shape changes in cultured endothelial cells, which are ultimately thought to aid oedema formation and extravasation[22,109]. The underlying barrier-disruptive signalling mechanisms remain to be elucidated.

Comparable to adenosine, endogenous S1P induces barrier protective signalling. Both *in vitro* and *in vivo* models of acute lung injury determined a

vascular endothelial barrier enhancing role for S1P[110–112]. This is further supported by a murine knock-out model of sphingosine kinase 1. Sphingosine kinases catalyse the formation of S1P from sphingosine to maintain intracellular and circulating levels of the short-lived S1P[113,114]. The sphingosine kinase 1 knock-out animals showed significantly increased oedema formation when challenged with lipopolysaccharides, compared with wild type animals[115]. Comparable to histamine, thrombin and adenosine, S1P is thought regulate barrier function through signalling that involves myosin light chain phosphorylation and reorganization of the actin cytoskeleton[25,111,116].

1. 3 Cyclic nucleotide signalling cascade

Cyclic adenosine monophosphate (cAMP) has been widely recognised to enhance barrier function. Raising intracellular cAMP has been shown to decrease endothelial permeability both *in vitro* and *in vivo* in different endothelial cell types in canine limb, hamster cheeks and bovine lung[22,117]. However, a more recent study showed that increasing cAMP concentrations in the cytosol of rat human pulmonary microvascular endothelial cells actually led to intercellular gap formation[118].

These findings were confirmed in a later study by Sayner et al.[119] in which permeability of rat human pulmonary microvascular endothelial cells increased upon high levels of cytosolic cAMP[119]. Cytosolic cAMP was increased by a genetically engineered soluble adenylyl cyclase (sAC), which upon activation synthesizes cAMP from ATP. It localises in the cytosol, rather than at the

plasma membrane as most endogenous adenylyl cyclases (ACs) do. When the genetically engineered sAC was targeted to the membrane and activated, the barrier dysfunction was abrogated. These findings suggested that increases of membranous cAMP were responsible for the barrier protective effect, whereas stimulation cytosolic cAMP pools induced endothelial permeability[119].

To understand the mechanism by which cAMP may modulate barrier function, thorough understanding of both the cAMP and cyclic guanosine monophosphate (cGMP) signalling cascade is necessary.

The second messengers cAMP and cGMP are known to mediate a myriad of hormone-induced cell responses. cAMP signal transduction regulates cardiovascular processes, gene transcription, cell metabolism, proliferation and development[120,121]. The main known role of cGMP is to regulate cardiovascular processes, including the regulation of vascular tone, cardiac contractility and cardioprotective responses to ischemia[122–124].

The cyclic nucleotide (CN) signalling machinery is a complex network of independently regulated proteins. A simplified schematic of the CN signalling cascade is shown in Figure 1. Activated GPCRs can couple to stimulatory G proteins (G_s). The $G_s\alpha$ subunit relocates and binds to membrane-bound ACs.

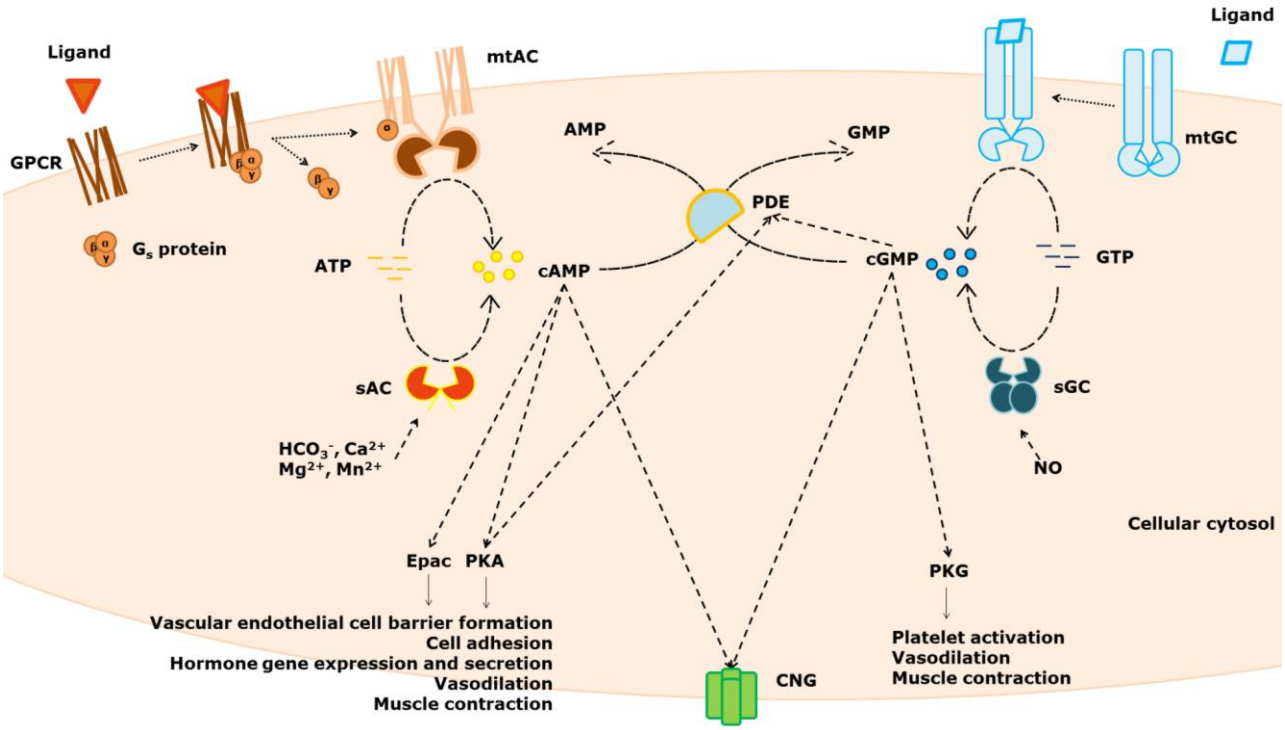

Figure 1: Schematic representation of intracellular cyclic nucleotide signalling pathways. GPCR, G-protein coupled receptor; mtAC, membrane-targeted adenylyl cyclase; sAC, soluble adenylyl cyclase; ATP, adenosine triphosphate; cAMP, cyclic adenosine monophosphate; AMP, adenosine monophosphate; PDE, phosphodiesterase; cGMP, cyclic guanosine monophosphate; GMP, guanosine monophosphate; mtGC, membrane-targeted guanylyl cyclase; NO, nitric oxide; sGC, soluble guanylyl cyclase; GTP, guanosine triphosphate; Epac, Exchange protein directly activated by cyclic AMP; PKA, protein kinase A; PKG, protein kinase G; CNG, cyclic nucleotide gated channel.

The bound α subunit induces the AC to produce cAMP. Cellular GPCR ligand stimulation can significantly increase the cytosolic cAMP concentration via ACs. An endogenous sAC is also expressed in endothelial cells. The sAC, however, is not activated by G-proteins, but by ions including Ca^{2+}, Mg^{2+}, Mn^{2+}, and HCO_3^-[125,126].

cGMP is produced by ligand activated membrane bound guanylyl cyclases (mtGCs) or through direct activation of soluble GCs by nitric oxide (NO). To balance the intracellular CN increases, CN breakdown is mediated by phosphodiesterases (PDEs).

The main effectors of cAMP are protein kinase A (PKA), exchange protein directly activated by cAMP (Epac), and cyclic nucleotide gated (CNG) ion channels. CNGs change their conformation upon binding of cAMP or cGMP from a closed to an open state. Activated CNGs allow Na^+, K^+, Ca^{2+} and Mg^{2+} to pass through. Physiological functions of CNGs include signal transduction in vision and smell[127]. An in depth discussion of CNG function is beyond the scope of this thesis. Known effectors of cGMP are protein kinase G (PKG) and CNG ion channels.

PKA and cGMP have been reported to mediate cAMP-cGMP crosstalk by activating PDE isoforms specific to either cyclic nucleotide, which subsequently hydrolyse the targeted cyclic nucleotide (refer to Figure 2)[128–130].

1.3.1 G protein-coupled receptors

The first of a chain of endogenous proteins involved in cAMP synthesis are GPCRs. Their major role in physiological function and ubiquitous expression throughout the body, make this superfamily of proteins a major target for therapeutic intervention and explains why they cover an estimated 30–40% of all drugs currently on the market[131–133]. Additionally, approximately 50% of all newly introduced drugs target GPCRs[134].

An analysis of GPCRs in the human genome identified more than 800 receptors, making GPCRs one of the largest and most diverse protein families known[135,136]. On the basis of their amino acid sequence and structural differences, GPCRs can be grouped into five major families and various subfamilies[136–138]. The five major families according to the GRAFS system are: Rhodopsin, Secretin, Adhesion, Glutamate and Frizzled/taste receptor 2[139]. All families contain receptors that are implicated in diabetes, neurodegenerative disease, cardiovascular disease, taste and smell, development and immunological responses[140–144].

The rhodopsin family, or class A, is by far the biggest group of GPCRs, counting more than 700 of the more than 800 total receptors within its ranks. Examples include the β-adrenergic receptors, the muscarinic acetylcholine receptors, the histamine receptors (H1R-H4R), adenosine (A_1, A_{2A}, A_{2B}, and A_3), thrombin (PAR1-4) receptors, and S1P (S1PR1-5) receptors[102,145–150]. The adenosine, thrombin, histamine and S1P receptors have in common that they play a role in endothelial barrier function. For example, the thrombin receptor PAR1 is a drug target of major interest in thrombosis[151]. Ideally, PAR1 antagonists would obstruct the thrombotic process to prevent detrimental events including vascular occlusion and embolus formation[151]. The therapeutic challenge would be to target PAR1 signaling in order to inhibit platelet aggregation and endothelial barrier disruption, while maintaining or activating barrier protective signals. Currently, several antagonists have been proven effective in preventing thrombosis in clinical trials[151]. The most advanced PAR1 antagonist, Vorapaxar, has shown to reduce the risk of cardiovascular death or ischemic events in patients with stable atherosclerosis[152,153]. However, the risk

of moderate to severe bleeding, including intracranial hemorrhage, was increased[153,154].

This example illustrates the need for combinatorial treatments that decrease side effects and improve barrier function as well as a better understanding of GPCR signalling in vascular endothelial barrier function. Within this context, so-called orphan GPCRs are interesting drug targets. More than 140 orphan GPCRs are known, which are poorly characterized and have not been linked to endogenous ligands[155]. Orphan GPCRs offer tremendous promise as they may provide novel and more selective therapeutic targets, with diminished side effects, compared to the ones known.

1.3.1.1 Structure and function

The GPCR family is as diverse in relation to its physiological relevance, structure and ligands as it is big. Regardless, all GPCRs share a common mechanism to relay intracellular signals their intracellular domains interact with heterotrimeric G proteins.

Generally, for proteins to be classed as GPCRs they must fulfill two requirements: they contain seven membrane-spanning helices and interact with a G-protein. In addition to the transmembrane domain, GPCRs contain N-terminal extracellular loops, which play a role in ligand binding. At their intracellular C-terminus, GPCRs have domains that can couple to various G-proteins, depending on their specific structure. G-proteins are responsible for propagation of the signal. GPCR ligand binding induces intra-molecular conformational changes that enable G-protein coupling and intracellular signal

propagation.

The extracellular domains of GPCRs that consists of the upper parts of the transmembrane helices and the N-terminal loop are generally thought to be the main orthosteric binding sites specific for a plethora of endogenous ligands. Interestingly, despite the differences in the identity of receptors, comparisons of inactive and active ligand-bound receptor structures have shown common intracellular conformational changes of GPCRs. Reports indicate that the conformational change of transmembrane helices four to six are pertinent in signal transduction[156–159]. Conformational changes in the extracellular and transmembrane domain initiate the intracellular structural shift necessary for G-protein coupling and intracellular signal transduction.

1.3.1.2 Regulatory and modulatory mechanisms of GPCR signalling

GPCR signalling can be modulated by GPCR kinases (GRKs), arrestins, allosteric binding ligands, and receptor dimerization. These modulatory processes diversify and fine-tune the signalling mechanisms, adding additional specificity and complexity to GPCR signalling.

GRKs and arrestins function in concert to desensitize receptors to prolonged or repeated exposure to high agonist concentration[160]. GRKs are able to identify activated GPCRs and phosphorylate various sites on the intracellular tail of the receptor. These phosphorylated sites are recognized by arrestins. The arrestin binds to the GPCR and in doing so blocks the binding sites for G-protein, leading to cessation of G-protein signalling and the initiation of the arrestin signalling cascade. Arrestin signalling can lead to internalization of GPCRs via

clathrin coated pits and consequently to desensitization[161].

In parallel to orthogonal ligand binding, GPCR signalling can be modulated by allosteric binding molecules. These molecules are thought to sensitize or desensitize the receptor rather than triggering actual GPCR signalling, which makes them interesting drug targets[162–165].

Complexity of the GPCR signalling is increased by the homo- and heterodimerization of these receptors[166]. Dimerization may affect signalling properties of receptors, ligand binding, agonist mediated endocytosis and crosstalk between GPCR pathways[167–170].

1.3.2 G proteins

Activated GPCRs relay signals through the trimeric G-protein complex, made up of α, β, and γ subunits. In fact, activated GPCRs act as Guanine nucleotide exchange factors (GEF) for Gα subunits by catalysing the release of GDP and binding of GTP to activate G proteins. Several GPCRs can couple to the same type of trimeric G protein, which consequently dissociates into an α subunit and βγ heterodimer; these two activated units are then able to activate independent signalling pathways and various downstream effectors[171,172]. The βγ heterodimer has been implicated in GRK recruitment, activation of potassium and calcium channels and activation of phosphatidylinositol 3-kinase, to name a few[172].

To date, twenty-one different human Gα proteins have been discovered that can form heterotrimers with five different types of Gβ subunits and twelve types

of Gγ subunits[135,173–175].

The widely distributed G-protein heterotrimers are generally divided into four classes based on their primary sequence similarity of the Gα subunit: $G\alpha_{12/13}$, $G\alpha_q$, $G\alpha_s$, and $G\alpha_i$[172,176].

$G\alpha_{12}$ has been reported to interact with a variety of proteins, including protein kinase C, proto-oncogene tyrosine protein kinase Src, and RasGAP. RasGAP deactivates Ras, the rat sarcoma protein, which has been associated with cytoskeletal integrity, cell adhesion and migration[177,178]. $G\alpha_{12/13}$ is thought to activate the protein RhoA through stimulating p115RhoGEF. Interestingly, RhoA has been implicated in endothelial barrier function regulation (Figure 3). Suppression of p115RhoGEF, and thus possibly RhoA, has been shown to diminish the permeability inducing effect of thrombin in human umbilical vein endothelial cells[179].

The G_q pathway has been mainly implicated in calcium signalling. G_q is thought to stimulate phospholipase-β to produce intracellular messengers inositol trisphosphate and diacylglycerol. Inositol triphosphate consequently triggers the release of calcium from intracellular stores, while diacylglycerol activates and recruits protein kinase C (PKC) to the membrane[180]. Interestingly, PKC has been suggested to activate nitric oxide synthase in endothelial cells treated with vascular endothelial growth factor (VEGF). This suggests a role for PKC and NO in VEGF induced permeability in endothelial cells[181]. Although calcium was not found necessary for VEGF mediated permeability induction, presence of calcium is required for the maintenance of basal barrier function and NOS activity[182,183].

The $G\alpha_s$ and $G\alpha_i$ classes have been shown to couple to the protein family of

ACs. $G\alpha_{s,i}$ modulate synthesis of the second messenger cAMP. The $G\alpha_s$ subunits stimulate all transmembrane ACs to synthesise cAMP from ATP, whereas $G\alpha_i$ units inhibit specific ACs. The ACs are responsible for signal transduction of GPCR ligands through production or inhibition of the intracellular second messenger cAMP.

1.3.3 Adenylyl and guanylyl cyclases

1.3.3.1 Adenylyl cyclases

cAMP is generated in mammalian cells by nine membrane-bound ACs and one sAC. All cyclases have two hydrophobic domains, each consisting of six transmembrane helices. The catalytic site responsible for cAMP synthesis is made up of two cytoplasmic domains, C1a and C2a. Due to the high homology of the catalytic core, ACs share several characteristic regulatory mechanisms: activation by the α subunit of G_s proteins, G-protein independent activation by forskolin, and inhibition by P-site inhibitors. The Gα subunits of G_s proteins generally stimulate ACs, whereas the Gα subunits of $G_{i,z,o}$ proteins inhibit specific ACs[184]. $G_s\alpha$, $G_i\alpha$, P-site inhibitors and forskolin regulate AC activity by binding different sites on the AC catalytic domains. In addition ACs can be regulated by $G_{\beta\gamma}$ subunits, magnesium, calcium, calmodulin or phosphorylation in a isoform specific fashion[185–187]. The $G_{\beta\gamma}$ subunit can be either stimulatory or inhibitory depending on the coupled AC isoform[188]. The different regulatory mechanisms are determined by various isoform specific sites on the catalytic

C1a and C2a domains and possibly additional regulatory sites on the C1b and C2b domains. C1b and C2b link the catalytic core to AC transmembrane regions[184,189,190].

Further specificity and complexity of signalling is related to discrete expression patterns of AC subtypes. Expression of ACs in tissue types has been difficult to determine, due to low protein expression levels and the lack of high-affinity antibodies. Most ACs seem to be widely distributed throughout the body, although expression patterns can differ depending on tissue type. For example, AC3, 5 and 6 were found to be expressed in endothelial cells of the aorta, vena cava and lung[191,192]. Interestingly, AC3 expression was highest in lung endothelium, whereas AC5 and 6 were most highly expressed in the vena cava[193].

The sAC is activated by bicarbonate and has been shown to 'fertilise' sperm through hyperactive sperm motility induction in testis[194]. sAC is expressed in a variety of mammalian tissues, including testis, kidney and choroid plexus[126194]. As the name suggests, the sAC can be found in the cellular cytosol and lacks the mtAC specific transmembrane domains. sAC can also locate to other sub-cellular domains including nuclei, mitochondria and microtubules and possibly vacuoles[195,196].

The sAC is structurally and biochemically different from the transmembrane cyclases[190]. In contrast to transmembrane adenylyl cyclases, sAC is insensitive to heterotrimeric G protein regulation and forskolin stimulation. Instead, sAC activity is directly modulated by bicarbonate and divalent cations of magnesium, calcium and manganese[125,197]. The buffering ability of bicarbonate in combination with gaseous carbondioxide, would suggest a relation between

cAMP levels and pH. However, reports remain contradictory and thus far a sAC activity pH-dependency has not been shown[125,126,198].

1.3.3.2 Guanylyl cyclases

Guanylyl cyclases (GCs) convert GTP to cGMP. These proteins occur as differentially regulated cytosolic and transmembrane GCs. GCs share an overall similarity in structure. Unlike ACs they are not regulated by G protein coupling following GPCR activation. However, there have been reports of cGMP-cAMP crosstalk via PDEs, which suggest that cGMP indirectly regulates intracellular cAMP levels[129]. Therefore, cGMP may play a role in endothelial barrier function.

Seven transmembrane GC isoforms have been identified: GC-A to G. All transmembrane isoforms are highly conserved homodimers with an N-terminal extracellular single ligand-binding site, formed by two extracellular amino terminal domains. These GCs generate cGMP through their catalytic domain at the C-terminus[199].

The GC isoforms are activated by various ligands. GC-A and B bind natriuretic peptide A, B and C (A-, B- and CNP) and are called natriuretic peptide receptors. All natriuretic peptides are thought to play a role in vasodilation and blood pressure regulation[123]. The exact underlying mechanisms remain to be determined. GC-C is activated by guanylyl, uroguanyly and lymphoguanylyl and is thought to play a role in electrolyte homeostasis. Ligands for GC-D, -E, -F are as of yet unknown.

The receptors GC-A, -B and –G are broadly expressed in many tissues. GCs-C, -D, -E, and F are mainly expressed in sensory organs.

NO is the only known endogenous ligand of soluble GCs (sGC)[200]. By NO binding, sGC is activated and catalyses the conversion of guanosine triphosphate to cGMP in the cytosol. sGC has been implicated in a myriad of physiological functions, including inhibition of platelet aggregation, immunomodulation, neuronal signal transduction, relaxation of smooth muscle and vasodilatation[201,202]. sGCs are heterodimers, consisting of α- and β-subunits, with amino terminal regulatory domains. These domains contain a core that can bind NO. In addition, sGCs possess dimerization domains and C-terminal catalytic domains that are responsible for cGMP synthesis.

1.3.4 Cyclic nucleotide effector proteins

Cyclic nucleotides can bind various proteins. cAMP is known to bind protein kinase A (PKA) and exchange proteins directly activated by cyclic AMP (Epacs). cAMP and cGMP can activate PKA and G, respectively; specific PDEs and CNG ion channels through binding. A detailed discussion of cyclic nucleotide-gated channels is beyond the scope of this report.

1.3.4.1 PKA

Once ATP is converted into cAMP it activates its downstream effectors PKA and Epac. PKA has many physiological functions, which include lipid and glucose metabolism, cardiovascular and reproductive function, and hormone synthesis and secretion[203].

PKA is a heterodimer kinase made up of two catalytic subunits (C) and two regulatory units (R)[204]. Two types of PKA exist: PKA(I) and PKA(II). The type of R subunit determines which C subunits are bound based on their structure. Three C subunit genes, Cα, Cβ, and Cγ have been identified, as well as four different R subunit genes, RIα, RIβ, RIIα, and RIIβ[205–207]. The expression patterns and subcellular localisation between R isoforms differ, which suggests specificity in downstream PKA signalling[208,209]. PKA RI has been found to be more sensitive to cAMP and mainly located in the cytosol. PKA RII is mainly located at subcellular organelles. cAMP binds to two highly conserved cAMP binding domains on each regulatory PKA subunit[210]. cAMP binding initiates conformational changes that lead to dissociation of the regulatory dimer from the catalytic dimer[204]. Once free, the C subunits can exert their physiological function by phosphorylating an array of cytoplasmic and nuclear protein substrates, including enzymes and transcriptional factors[208].

cAMP has been suggested to exert its barrier protective function through both Epac and PKA. PKA strengthens cellular barriers by stimulating dephosphorylation of the myosin light chain (MLC). Previously published results suggest that PKA inhibits the small GTPase RhoA through phosphorylation, which then cannot activate Rho kinase (ROCK) to phosphorylate and inhibit

MLC phosphatase. Therefore, MLC phosphatase retains its active state, inhibits MLC through dephosphorylation and promotes actin cytoskeletal stabilisation. MLC in its active state interacts with actin to promote myosin cross-bridge cycling and tension development, inducing cellular barrier dysruption[23,108,211,212].

1.3.4.2 Epac

Epac1 and Epac2 were first identified in the late 1990s[213,214]. Previously, PKA had been thought to be the main effector of cAMP. Now Epac emerged as a regulator of several pivotal processes, including calcium handling, ion transport, vesicle trafficking and secretion, and barrier function[215–217].

Two widely distributed isoforms of Epac exist. Structurally they differ in that Epac2 contains a low affinity cAMP binding domain, which determines the intracellular localisation and biologic properties of Epac2[218,219]. Epac activity is determined by cAMP binding to the high affinity cAMP binding domain. Epac is then activated by relief of the auto-inhibitory function of one of the regulatory domains. Upon activation, Epac1 has been reported to translocate to the plasma membrane, a process dependent on its Dishevelled, Egl-10 and Pleckstrin domain (DEP) domain, which is responsible for membrane association[220]. Other domains may be involved in Epac localisation as it has been found in various subcellular regions including mitochondria, nuclear membrane and the actin cytoskeleton[219].

Epac has been shown to increase VE-cadherin mediated cellular barrier

through Rap1 activation and actin rearrangement, independent of PKA[221]. Several studies indicate that Epac, acting either alone and/or in concert with PKA, reduces barrier leakage through inhibition of RhoA by Epac-activated Rap.

Epacs are GEFs for Rap proteins[222]. Rap belongs to the Ras family of small G proteins, which cycle between an inactive guanosine diphosphate (GDP)-bound state and an active guanosine triphosphate (GTP)-bound state. Epac exchanges GDP for GTP and thereby activates Rap. Rap downstream effectors include adaptor proteins implicated in modulation of the actin cytoskeleton and regulators of G proteins of the Rho family[223].The Epac-Rap1 signalling pathway has been associated with increased cellular adhesive stability, accumulation of VE-cadherin at cell-cell borders, enrichment of cortical actin and a decrease in RhoA activation[221,224–230]. Without ROCK activation by RhoA, ROCK is not able to inhibit MLC phosphatase. Therefore, MLC phosphatase dephosphorylates and inhibits MLC re-arranging, thus stabilising the cytoskeleton and endothelial barrier function (refer to Figure 3). In addition, Epac's barrier enhancing effect is suggested to be mediated through Rac activation, by Rap1, and subsequent Rac association with activated Tiam and Vav2 proteins[29,231].

1.3.4.3 PKG

PKG is the principal intracellular effector of cGMP. Two types of PKG exist: cytosolic PKGI and membrane-bound PKGII. PKG is generally thought to be a regulator of blood pressure. PKG I acts as a modulator of intracellular calcium, regulating smooth muscle contraction and relaxation. PKG II is implicated in

fluid homeostasis at the cell membrane, by phosphorylating the cystic fibrosis transmembrane conductance regulator, which induces a chloride current across the membrane and subsequent water secretion in the intestine[199].

The PKG N-terminal domain contains several regulatory sites that allow for dimerization, autoinhibition of PKG in the absence of cGMP and specific intracellular localisation. The N-terminal domain that dictates PKG localisation differs between PKGI and II. The PKG regulatory domain contains two cyclic nucleotide binding domains (CNBD), A and B. The C-terminal catalytic domain contains the binding site for target proteins[232–234].

Cytosolic PKG I is widely expressed in mammalian tissue, whereas membrane-bound PKG II is excluded from the cardiovascular system[233,235,236].

PKG and PKA are homologous proteins that differ in their selectivity for cGMP and cAMP binding. Despite the 50- to 200-fold selectivity for cGMP and cAMP, respectively, PKG and PKA can be activated by either CN within physiological ranges of the respective nucleotide[237–241]. Indeed, studies have shown that introduction of several point mutations into the catalytic domain of PKA can significantly shift the selectivity from cAMP to cGMP[242].

1.3.5 Regulatory proteins: phosphodiesterases

PDEs are the main negative regulators of cyclic nucleotides, cAMP and cGMP. PDEs are a large superfamily of proteins of which some specifically target cAMP or cGMP and others degrade both[243,244]. Mammalian PDEs are subdivided into 11 different families, PDE1-PDE11, on the basis of their amino

acid sequences, substrate specificities, endogenous and exogenous regulators and pharmacological properties[245].

The mammalian PDEs share a common structural organization, with a conserved catalytic and regulatory domains located near the C-terminus and an additional regulatory domain at the N-terminus of the protein. The catalytic domain of PDEs is highly conserved between types and determines the ability of all PDEs to suppress cyclic nucleotide concentrations. The N-terminal domains are responsible for CN binding-mediated allosteric regulation and dimerization of GAF containing PDEs. PDE5 and 6 have been reported to prefer cGMP as a substrate. PDE1–3, 10 and 11 hydrolyse both cyclic nucleotides. Interestingly, isoenzymes within a dual-specificity family can differ significantly in preference for cAMP or cGMP as occurs among the PDE1 isoenzymes[246]. PDE1, PDE3, PDE4, and PDE7–9 have no GAF domain. PDE4, 7 and 8 hydrolyse cAMP specifically, PDE9 only targets cGMP and PDE1 and 3 can break down both. PDEs can be regulated by CN effector proteins, cyclic nucleotides but also other small molecules, including calcium. For example, PDE1 contains a Ca^{2+}/calmodulin (CaM)-binding site, allowing it to be activated by intracellular rises of cAMP. PDE3 has a transmembrane domain, thus localising it uniquely to the membrane. PDE8 contains a response regulator receiver domain, which implicates it in expression regulation. In addition PDE8 has a per–arnt–sim domain. These domains are found in various regulatory proteins and detect a wide variety of physical and chemical stimuli and in response, regulate the activity of effector domains[247]. The distribution and functional significance of PDE enzymes vary in different tissues. In most cells, PDE3 and PDE4 provide the major portion of cAMP-

hydrolyzing activity[245]. Pharmacological targeting of specific PDE isoenzymes should thus allow for tissue or even cell-type selectivity of drugs.

Presently, the main PDEs known to be expressed in endothelial cells are PDE2, 3, 4 and 5, but PDE1 and 7 have also been described[248] (for an overview refer to Figure 2). PDEs have been shown to mediate interplay between cAMP and cGMP signals. This is determined by the ability of cGMP to activate PDE2 and to inhibit isoform 3[249]. In addition, PKA is thought to activate PDE3 and the presence of crosstalk between cGMP and cAMP has been proposed as a contributive regulatory mechanism in cardiac cyclic nucleotide signalling[130]. One could therefore hypothesise that cGMP-cAMP crosstalk may be an important effector of cellular regulatory mechanisms, due to the expression of the relevant PDEs and the prominent role of NO in vascular cell signalling.

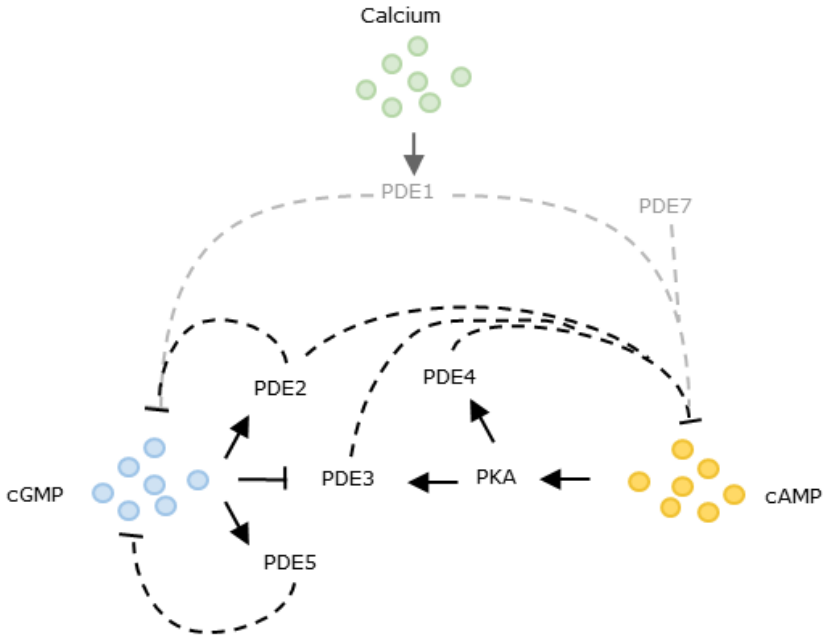

Figure 2: Potential cAMP-cGMP crosstalk mediated by PDEs in endothelial cells. cGMP activated PDE2 is thought to hydrolyse both cGMP and cAMP. In contrast, cGMP inhibits PDE3, which therefore cannot reduce cAMP and cGMP levels. The PKG activated PDE5 is implicated in a negative feedback loop and hydrolysis of cGMP. cAMP is known to regulate PDE activity indirectly through PKA binding and stimulation. PDE3 and 4 are activated by PKA and degrade cAMP. The Ca^{2+}/Calmodulin-regulated PDE1 hydrolyses both cGMP and cAMP. PDE7 is thought to degrade cAMP. Upstream PDE7 signalling remains to be elucidated.

1.4 The concept of compartmentalisation

Specificity in signalling is dependent on protein isoforms, specific tissue expression, allosteric modulation, crosstalk and interactions between proteins. In the introduction to cyclic nucleotide signalling, one factor of crucial importance to specificity of signalling has not been touched upon: subcellular localisation.

The subcellular localisation of proteins adds an additional layer of specificity to the CN signalling cascade. For example, depending on type, GPCRs have been found to localise differentially at the cellular membranes. Certain GPCRs have been found to locate to lipid rafts, whereas others are excluded from lipid rafts[250,251]. Cytosolic or membrane bound forms of adenylyl and guanylyl cyclases suggest specifically localised generation of cyclic nucleotides. The same holds true for PKA and PKG. PDE subcellular localisation has been shown to be type and isoform dependent, with for example PDE3 having a transmembrane domain that the other PDE family members lack[245,246].

However, PDE localisation is more complex than simply a matter of membrane-bound versus unbound. Indeed, PDE4B and D have been shown to be co-expressed in mouse embryonic fibroblasts[252]. However, PDE4B localises to the membrane, whereas PDE4D has an intracellular punctate pattern of localisation[252]. In contrast, PDE4D has been shown to localise to the plasma membrane, where it interacts with Epac and forms a barrier stabilizing microdomain by association with VE-cadherin in human arterial endothelial cells[253]. These findings suggest that the 'specialised' role of PDEs is highly complex and may be tightly regulated in specialized microdomains.

Visualization of microdomains by live-cell imaging and FRET has allowed for differentiation between low and high subcellular concentration cAMP sites. This indicates that cAMP accumulation is restricted to specific locations within the cell[254]. Compartmentalised pools of cAMP are controlled in space and time by endogenously expressed ACs and PDEs. Indeed, over the years the specific subcellular localisation of CNs and proteins involved in CN second messenger signalling have been established as crucial factors in signalling specificity[120,254].

The importance of this CN compartmentalisation is further underlined by the presence of A-kinase anchoring proteins (AKAPs), G-kinase anchoring proteins (GKAPs) and specifically localized signalosomes[255,256]. A- and GKAPs are a group of structurally diverse proteins, which have the common function of "anchoring" PKA or G, respectively, to discrete subcellular locations. They function as adaptor proteins for several proteins, including PDEs, to form signalling platforms where the signal is channelled toward a specific task. Recently, in human dermal microvascular cells, AKAP220 was found to contribute to barrier function via tethering PKA to the plasma membrane[257]. AKAP9, located near the Golgi apparatus and centrosome and Epac1 interact to enhance barrier properties through effects on microtubule growth in human umbilical vein endothelial cells[258]. GKAPs have thus far been found in mouse testis, rat brain, intestine and most interestingly, the aorta[256,259]. Their role in endothelial cellular signalling remains largely unknown.

Evidence indicates the presence of plasma membrane signalosomes in human arterial endothelial cells that consist of PDE4D, Epac and Rap1, which are suggested to play a role in regulating endothelial permeability (Refer to Figure 3)[253].

1.5 The relevance of cyclic nucleotide signalling and compartmentalisation in endothelial barrier function

Endothelial cells are connected through gap junctions, TJs and AJs. AJs are thought to be pivotal in barrier function maintenance and are comprised of VE-

cadherin complexes. These complexes are formed by α, β and γ catenins which tether the VE-cadherin complex to the actin cytoskeleton and therefore strengthen the AJs[260]. TJs are also known to play a crucial role in barrier function, possibly through crosstalk with AJs. AJ barrier function is maintained through its interaction with the cytoskeleton and most prominently with actin filaments. Barrier regulation occurs at the anchoring sites of AJs, actin cytoskeleton and microdomains that bring regulatory proteins to the anchoring site.

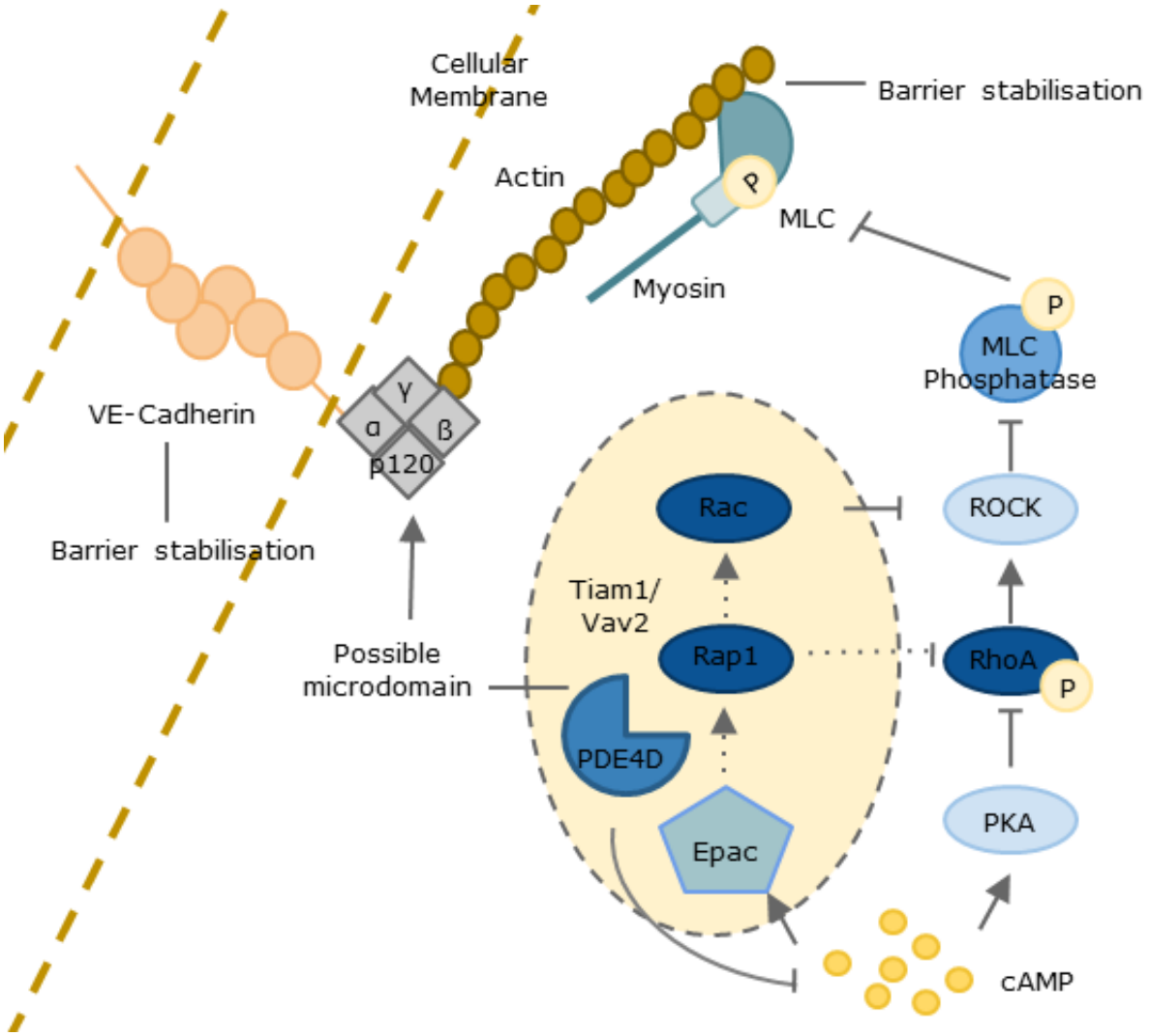

Figure 3: Simplified schematic of proposed cellular barrier regulation by cAMP. cAMP stabilises barrier function through PKA and Epac mediated dephosphorylation of MLC. PKA and Epac can function independently to affect the MLC phosphatase inhibitor ROCK. Epac may form a barrier function regulatory microdomain with Rap1, Rac, Tiam1, Vav2 and PDE4D. cAMP, Cyclic adenosine monophosphate; PKA, Protein Kinase A; Epac, Exchange protein activated directly by cAMP; RhoA, Ras homolog gene family, member A ; Rap1, Ras-related protein 1; Rac, Ras-related C3 botulinum toxin substrate; ROCK, RhoA activated kinase; VE-cadherin, Vascular Endothelial Cadherin; MLC, Myosin Light Chain; Vav2, Guanine Nucleotide Exchange Factor VAV2 ; Tiam1, T-cell lymphoma invasion and metastasis 1.

The general consensus over the last few decades has been that cellular increase of cAMP protects against endothelial barrier permeability. Through

stimulating downstream effectors, cAMP was thought to stabilise the actin cytoskeleton and AJ complexes (refer to Figure 3). Interplay of the cytoskeleton, cAMP and its downstream effectors seem to be crucial for endothelial barrier function. Both PKA and Epac have been implicated in barrier stabilisation. They are thought to mediate barrier function through different cAMP dependent signalling pathways, which ultimately converge in stabilising the VE-cadherin complex (for an overview, refer to Figure 3). PKA and Epac have both been implicated in endothelial barrier stabilisation, however, which of the two proteins may be the main regulator remains to be elucidated[208,253,257]. Together with the vast array of GPCRs that can modulate intracellular cAMP and the notion of protein compartmentalisation this illustrates the complexity of EC barrier signalling. Therefore, it seems unlikely that EC barrier regulation would simply depend on an increase or decrease of intracellular cAMP. Indeed, recent evidence suggests that the barrier protective signalling mechanisms underlying cellular cAMP are more complex than originally thought.

A study in rat human pulmonary microvascular endothelial cells showed that cAMP increases specific to the cytosol actually led to endothelial permeability[118]. Cells were inoculated with bacteria of the *Pseudomonas aeruginosa* strain, which expressed ExoY. ExoY is a soluble adenylyl cyclase that catalyzes high-level synthesis of cytosolic cAMP when transferred into target cells. Endothelial cells inoculated with ExoY showed an increase in whole cell cAMP and intercellular gap formation over the course of four hours[118].

The notion that cytosolic cAMP induces endothelial barrier permeability was

confirmed in a later study by Sayner et al. They treated rat human pulmonary microvascular endothelial cells that expressed an active mammalian sAC with forskolin, to increase cytosolic cAMP levels, and observed subsequent gap formation[119,261]. This sAC was a chimera of the catalytic loops of mammalian forskolin-sensitive AC 1 and 2 (sACI/II), from which the membrane targeted domains were deleted. When the soluble adenylyl cyclase was targeted to the membrane and stimulated to produce cAMP here, the barrier dysfunction was abrogated. These findings suggested that increases of membranous cAMP were responsible for the barrier protective effect, whereas stimulation cytosolic cAMP pools induced endothelial permeability[119].

This phenomenon of cAMP compartmentalisation is compatible with the notion of regulatory microdomains in endothelial barrier function. For example, Epac's barrier enhancing effect is suggested to be mediated by Rac upon association with Tiam and Vav2 proteins. This protein complex has been suggested to be part of a microdomain that regulates barrier function, possibly through AKAP220 anchoring to VE-cadherin by catenins (α, β, γ, and p120), actin and PDE4 at the plasma membrane[253].

Less is known about the role of cGMP in endothelial barrier function. Evidence regarding NO and PKG involvement in barrier permeability is contradictory[262–266]. For example, the natriuretic peptide A has been shown to both decrease and increase cellular permeability[231,267]. Furthermore, the involvement of PKG remains unclear. Interestingly, cAMP/cGMP crosstalk via PDE2 and 3 (refer to Figure 2) has been shown to differentially regulate endothelial cell permeability *in vitro*. PDE2 is GMP-activated, whereas PDE3 is cGMP-inhibited and both PDEs hydrolyse cAMP. Indeed, it was recently demonstrated that cGMP

elevating agents such as ANP and NO have biphasic effects on cAMP inhibition of thrombin-induced endothelial permeability[128]. This suggests a far more prominent role for cGMP in endothelial barrier function than was previously thought[128,268]. Regulators and effectors of cAMP and cGMP: PKA, Epac, PKG and PDEs, respectively, have been shown to locate to specific subcellular sites. In addition there is mounting evidence of the importance of cAMP compartmentalisation in barrier regulation. Therefore, the notion of specifically localised subcellular cGMP pools would be a possibility.

1.6 Methodologies to assess endothelial barrier function and intracellular cyclic nucleotide levels

When assessing endothelial barrier (dys) function/permeability, the method applied can vary substantially depending on the barrier model that is used. A distinction can be made between animal and *in vitro* studies.

1.6.1 *In situ* methods

Some of the earliest endothelial barrier function studies were conducted in vessels isolated from mammals. Several techniques have been developed, all of which were based on perfusing the isolated macro and micro vessels with different solutes. For example, isolated hind limbs of cats can be suspended from a balance to determine changes in tissue fluid content via perfusion at

constant pressure. Consecutively the amount of fluid leakage was recorded, giving an indication of the amount of filtration of fluid over a specific membrane area in time, known as the filtration coefficient[269,270].

These initial efforts were later refined and adapted into methods such as the perfused microvessel permeability assay developed by Yuan and Granger[271]. They canulated venules at each end of the vessel and submerged it in a physiological salt solution. The setup allowed for switching between perfusion solutions, including a fluorescent tracer (e.g., FITC-albumin) or a chemical treatment. Consequently the permeability of venules could be observed as recorded by fluorescence video microscopy.

Other approaches took advantage of tissue staining methods to assess the general status of plasma leakage *in vivo.* Coloured dyes were injected into the blood circulation. After the treatment of interest, the animal was sacrificed and dye accumulation was quantified in harvested organs[272]. More recently, intravital microscopy has been used to monitor microvascular leakage in intact tissues[273,274]*.* These experiments make use of macromolecules (albumin or dextran) conjugated to a fluorescent probe (e.g. FITC or TRITC). This method can be applied in semi-transparent tissues that allow imaging, including the cremaster muscle and hamster cheek pouch[275].

Although these approaches allow for a physiological perspective on vascular permeability, they are technically limited. Only vessels that can be canulated are compatible with perfusion studies. This excludes experiments in vascular beds and smaller vessels. Furthermore, the data of these studies is limited to assessment of permeability. The staining techniques do not allow for *in vivo* assessment. *In vivo* imaging on the other hand can only be used on surface

tissues that can be imaged with a microscope setup. All described approaches do not permit the study of molecular mechanisms that underlay endothelial barrier function.

1.6.2 *In vitro* methods

In vitro approaches allow for more controlled manipulation of molecular or pharmacological variables than isolated vasculature. However, i*n vitro* models show limited resemblance to real physiological structures and functions. This becomes clear through the lack of pressure and flow, luminal glycocalyx or the endothelial environment, which are complex *in vivo* and lacking in cell culture. Therefore it cannot be assumed that treatments affecting cultured monolayer permeability will have similar or comparable effects *in vivo*. Despite these limitations, *in vitro* assessments of endothelial barrier function are crucial to uncover underlying signalling pathways and molecular interactions. Well established *in vitro* methods include permeability assays, barrier resistance measurements and immunocytochemistry.

Endothelial permeability assays were first employed by Malik et al[276]. Briefly, cells are grown on a porous membrane, which is inserted into cell culture wells to divide the space into two compartments. A tracer molecule (e.g. FITC-dextran) is introduced to the upper or luminal compartment at a known concentration. The increase of tracer in the lower compartment is sampled at various time intervals. This type of assay enables investigators to determine solute permeability and size selectivity in cultured endothelial cell monolayers.

Note that these characteristics are specific to the cell line of choice and can vary depending on the porous membrane on which cells are grown as well as the tracer molecule employed.

More recently, approaches that measure the resistance of cellular monolayers have become available. TER measurements take advantage of the electrical insulating properties of cells. Endothelial membranes are composed of lipophilic molecules (predominantly phospholipids and cholesterol), which restrict the passage of aqueous solutions and function as electrical insulators. In contrast, open fluid filled pores of the membrane on which cells are grown do allow for free passage of aqueous solutions. Thus, a cellular monolayer has a high electrical resistance, whereas uncovered open pores allow electrical conductance that decreases measured resistance. TER has been measured in a variety of animal models[277]. Interestingly resistance of *in vivo* endothelial barriers has generally been observed to be significantly higher than in cell culture[278,279]. TER can easily be measured using the two-compartment transwell configuration of permeability assays. In this setup, electrical resistance is measured directly across the cell monolayer using probes positioned above and below the cellular monolayer. Measurements are performed by coupling the probes to an electrical resistance meter. The TER method is often used in conjunction with transwell solute flux assays, as an alternative approach to assess barrier function.

A more sophisticated method to determine endothelial monolayer resistance is with an electrical cell–substrate impedance sensor (ECIS)[275,280]. In this setup, cells are grown directly on two golden electrodes. After cell confluence is reached, an alternating current is sent across the monolayer and impedance in

voltage is measured. Impedance is analogous to resistance, but accounts for resistance measured in an alternating current system. Main advantages of the ECIS system are measurements of impedance in cells under cell culture conditions (e.g. growth medium, 5% CO_2 and 37 °C) over longer periods of time.

Finally, immunocytochemistry is a technique that visualizes the localisation of a protein in cells by use of a specific primary antibody that binds to it. When a secondary antibody, conjugated to a fluorophore, binds to the primary antibody, the targeted protein can be imaged under a fluorescence microscope. Immunocytochemistry can therefore be employed to assess the effect of endothelial barrier modulatory drugs on the cellular cytoskeleton or proteins that may re-localise or have altered expression patterns. This method is useful for localisation studies, but in contrast to endothelial permeability assays and TER or impedance measurements, it does not allow for a quantitative read-out of endothelial permeability.

The methods described here to assess endothelial barrier function, focus solely on endothelial monolayer resistance or permeability. With the exception of immunocytochemistry, these methods do not allow insight into the molecular mechanisms that explain changes in barrier function on a molecular level. However, immunocytochemistry cannot be performed in living cells. To investigate the role of specific molecules, such as cAMP in the context of barrier function, methods that allow measurement of the second messenger targets in parallel with endothelial permeability studies are crucial.

1.7 Methodologies to assess cellular cAMP concentrations

To date, a plethora of assays exist to measure changes in cAMP concentrations. Available assays can be divided into two categories: cAMP accumulation systems and reporter-gene methods.

1.7.1 cAMP accumulation assays

Examples of cAMP accumulation assays include enzyme-linked immunosorbent assays (ELISA) and I^{125} radioimmunoassays. Although there are many more comparable assays, they are all based on the same principle: changes in intracellular cAMP are detected by competitive binding of cellular cAMP and labelled cAMP to an anti-cAMP antibody. For cAMP ELISAs, wells are coated with an antibody for cAMP. Then cell lysate with endogenous unlabelled cAMP and a solution with for example fluorescently labelled cAMP are added. When labelled cAMP binds, the fluorescent signal is stabilised through the relative immobility of the flourophore. High levels of endogenous cAMP outcompete the labelled form, increasing the mobility of the fluorophore and decreasing the fluorescent signal.

This principle is the same for I^{125} radioimmunoassays, with the exception that reading of the signal does not require a fluorescence plate reader, but a scintillation counter.

1.7.2 Reporter gene assays

Luciferase and β-galactosidase assays are examples of well-known reporter-gene methods to detect cAMP. The principle behind all reporter-gene assays relies on detection of intracellular cAMP concentrations via changes in the expression level of a particular 'reporter' gene. The transcription of the reporter is regulated by the transcription factor cAMP response-element binding protein (CREB), which binds cAMP and then translocates to the nucleus. Here CREB binds to upstream cAMP response elements, which initiate downstream transcription of the reporter gene.

The classic bioluminescence based assays employ the luciferase gene from the firefly Photinus pyralis as reporter gene. Increases of intracellular cAMP increase expression of luciferase, which can catalyse the oxidation of its substrate luciferin to produce oxyluciferin and an increase in measurable light. Notably, cells need to be lysed to free the luciferase and allow it to react with luciferin. The light resulting from the catalysis of luciferin can be measured by bioluminescence plate readers as an indication of intracellular increase of cAMP.

The methods described above all have advantages and disadvantages. The reporter-gene methods may offer greater benefits when employed with weak GPCR agonists as they effectively amplify the signal. However, this means that the compound activity detected may not be physiologically relevant. cAMP accumulation assays on the other hand may give more physiologically relevant results, but are more expensive and less sensitive[281]. For a more exhaustive review of different cAMP measurement methods available please refer to the

paper by C. Williams[281].

1.7.3 Fluorescence Resonance Energy Transfer

Both cAMP accumulation and reporter gene assays have a crucial shortcoming that makes them unemployable to gain a better understanding of subcellular spatiotemporal cAMP regulatory events: only overall intracellular cAMP endpoint changes upon treatment can be monitored, usually after cells have been lysed. To understand the subcellular CN regulatory effects in space and time a method that allows for intracellular high resolution cAMP measurements in real time and in living cells is crucial.

The combination of fluorescent labelling of biological materials and modern high magnification microscopy provide tools with which to visualize the spatial distribution of cellular structures of interest. FRET combines spectrally different fluorescent proteins in one approach. This allows for monitoring subcellular distribution of molecules and real-time molecular interactions in living cells.

1.7.3.1 Principle of FRET

FRET is named after the German scientist Theodor Förster, who first described the transfer of energy between chromophores in close proximity. Energy transfer between donor and acceptor molecule can occur when the donor fluorophore is in an electronically excited state and transfers excitation energy

to a nearby acceptor chromophore. The Jablonski diagram in Figure 4A depicts the relevant energy transfers between donor and acceptor chromophore during FRET.

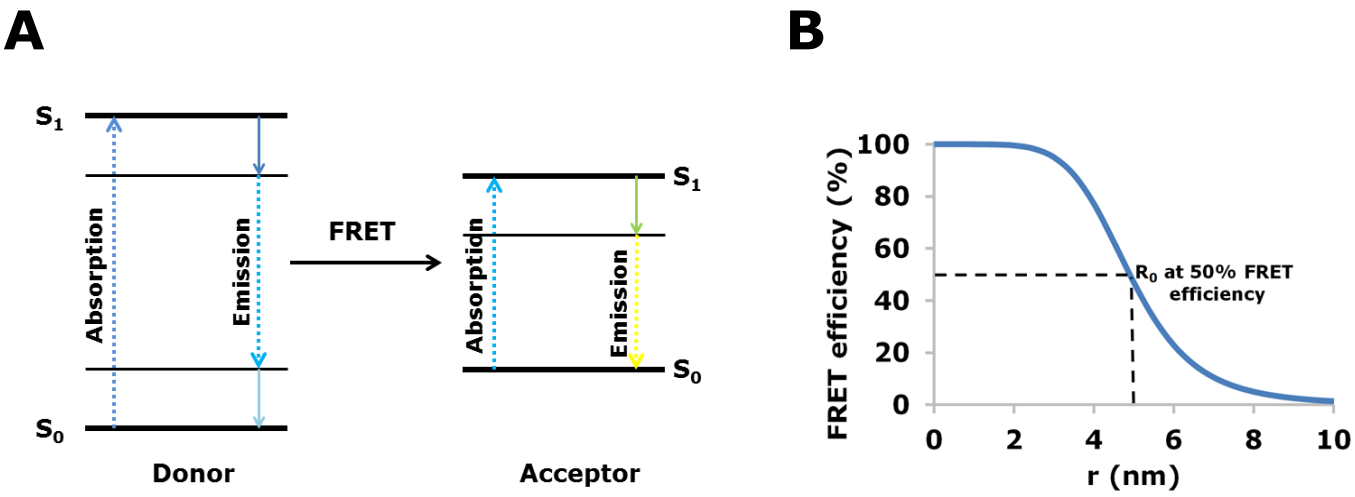

Figure 4: Theory of FRET transfer. A) The Jablonski energy diagram illustrates coupled excited state transitions between the donor emission and acceptor absorbance in FRET. FRET can occur when the donor molecule is excited by absorbing energy in the form of light. Then the donor transitions from the ground state (S_0) to the excited state (S_1). To return back to the ground state, the donor molecule releases the energy in form of emission (bright blue dotted arrow) or via vibrational relaxation (small solid lines). The donor emission energy can be absorbed by the acceptor (bright blue dotted arrow), allowing for transition of electrons from S_0 to S_1. The energy is emitted as fluorescence or sensitized emission by the acceptor molecule (yellow dotted arrow) allowing it to go back to the ground state. Absorption and emission transitions are represented by straight dotted arrows (blue and yellow). The smaller solid lines indicate vibrational relaxation of the donor and acceptor molecules. B) Depiction of the relation between r, the distance between dipoles of the acceptor and donor molecule and the FRET

efficiency of a theoretical donor-acceptor pair. R_0 for this fluorophore pair is 4.9 nm (r), which holds true for a molecular pair of enhanced yellow and cyan fluorescent proteins.

FRET can only take place when the donor and acceptor molecule are 'compatible'. Compatibility is determined by overlap of the donor molecule fluorescence emission spectrum with the absorption spectrum of the acceptor molecule. This means that the emitted light of the donor molecule needs to be of a certain energy, and thus wavelength, that allows for efficient uptake of said energy by the acceptor chromophore. Apart from compatible chromophores several criteria must be satisfied in order for resonance energy transfer to occur. Close proximity of donor and acceptor is necessary and their relation is depicted in the formula below (the accompanying graph is shown in Figure 4B):

$$\mathbf{E_{FRET} = 1/ (1 + (r/R_0)^6)}$$

R_0 denotes the characteristic distance between chromophores, where FRET efficiency is 50 percent, termed the Förster radius. R_0 is specific for any pair of fluorescent molecules. r Is the actual distance between dipoles of the acceptor and donor molecule. From this equation it becomes clear, that a smaller distance between donor acceptor dipoles will favour FRET efficiency. Figure 4B shows that the distance between donor and acceptor dipoles must be 1-10 nm.

The value of R_0 for fluorophore pairs in an aqueous or buffered solution may be calculated from the following expression:

$$\mathbf{R_0 = 2.8 \cdot 10^{17} \cdot K_2 \cdot Q_D \cdot E_A \cdot J(\lambda)^{1/6}}$$

K_2 represents the relative orientation in space between the transition dipoles of the donor and acceptor, thus determining the coupling efficiency. Q_D is the donor quantum yield, E_A denotes the maximal acceptor extinction coefficient and J(λ) is the overlap integral in the region of the donor emission and acceptor absorbance spectra. Q_D and E_A are characteristic for the donor and acceptor molecule, respectively. Q_D is a measure of how efficiently the donor can transfer its energy to an acceptor molecule. E_A indicates to what degree the acceptor fluorophore absorbs light at its characteristic excitation wavelength. Thus the Förster radius incorporates individual properties of the donor and acceptor molecules, Q_D and $E_{A,}$ as well as their relation to each other in terms of orientation, distance (r), and amount of energy transferred based on the overlap of their respective light spectra J(λ).

Fluorophore pairs with the most favourable characteristics are crucial for efficient FRET sensors. This implies choosing the highest quantum yield donor, the highest absorbing acceptor, and fluorophores that have a significant overlap in their emission and excitation spectra, respectively.

1.7.3.2 FRET microscopy

The combination of fluorescent labelling of biological materials and modern high magnification microscopy provide tools with which to visualize the spatial distribution of cellular structures of interest. FRET combines spectrally different fluorescent proteins in one approach. It does not only assess cellular distribution of molecules, but also real time subcellular molecular interactions in living cells. FRET has seen multiple applications over the last years and microscopic setups have been modified and improved for specific use with FRET reporters.

There are many types of methods that employ FRET; however, a discussion of these is beyond the scope of this report. Our laboratory studies subcellular cAMP distribution by means of several FRET reporters expressed by the cells of interest. With a fluorescent microscope setup specifically adapted for this purpose (a simplified schematic of our FRET setup is depicted in Figure 7 in the materials and methods section), we measure so-called acceptor sensitised emission. Briefly, the donor-acceptor pair is excited with light of the excitation wavelength specific for the donor molecule. When donor and acceptor are in close proximity, the donor transfers part of its energy to the acceptor molecule, as depicted in Figure 4A, at the expense of its own emission. The light emitted from both fluorophores is detected and measured. The distance between donor and acceptor can alter due to interference by the molecule of interest. This results in an altered amount of energy being transferred to the acceptor and, consequently, in the light emitted by both donor and acceptor. The ratio of donor to acceptor emission signals will reflect the change in concentration of

the molecule of interest. Ultimately, the ratio represents the final read out of sensitized emission.

1.7.3.3 FRET sensors

FRET reporters can be employed to assess intermolecular interactions. FRET sensors can be expressed in living cells, either by viral transduction or transfection. FRET reporters can be either uni- or bimolecular. Bimolecular FRET sensors are two independent 'sensor' molecules with a donor and acceptor fluorophore attached, respectively. They are co-expressed but not linked and float independently in the cytosol. Under favourable conditions, e.g. activation of one of the molecules, the two 'sensor' molecules will find each other and bring together the donor and acceptor fluorophore. Consequently, FRET will increase. In practice, measuring FRET ratio changes with this type of reporter is challenging as the expression of both acceptor and donor are not at a ratio 1:1, which can substantially affect the detected light emission. Other factors that may distort accurate representation of bimolecular FRET ratios, are donor emission signal bleedthrough and direct acceptor excitation[282,283]. Bleedthrough occurs because of overlap between the emission spectra of donor and acceptor chromophores. The signal detected for acceptor is actually a combination of both donor and acceptor emission. Direct acceptor excitation stems from overlapping excitation spectra of donor and acceptor molecules. In this case, exciting the donor with light of the appropriate wavelength also results in excitation of the acceptor and thus increased emission. This can be

detected as a false increase in FRET. Bleedthrough and direct acceptor excitation can be exacerbated by varying concentrations of donor and acceptor molecules, and thus varying fluorescence signals that distort the detected emission signals, of bimolecular FRET reporters.

These challenges can be diminished by employing unimolecular FRET sensors. Unimolecular FRET reporters have a linker and sensitivity domain in between the donor and acceptor molecule. This design increases the proportion of real FRET signals versus artifactual signals by decreasing background fluorescence of bleedthrough and direct acceptor activation[282,283]. In addition, unimolecular FRET sensors are less likely to perturb endogenous signalling through uncontrolled protein interactions of the reporter[284]. However, depending on the specific research question, it may be worthwhile choosing a bimolecular FRET reporter. In the case of monitoring an interaction between two proteins, it would be intuitive to choose a bimolecular sensor. The proteins of interest would each be tagged with a donor and acceptor chromophore, respectively, and upon protein-protein interaction FRET would occur. In contrast, unimolecular sensors are better suited for visualizing changes in single molecule concentration or activity. Examples include PKA activation, calcium concentration and changes in intracellular cyclic nucleotide concentration. As we focus on cyclic nucleotide and protein activity changes, we exclusively employ unimolecular reporters.

FRET sensors can be described as “loss of FRET” or “gain of FRET”. To assess changes in intracellular CN changes we work with cAMP and cGMP FRET reporters, H187 and Cygnet2.1, which are “loss of FRET”. AKAR4 is a “gain of FRET” sensor for PKA activity, the main downstream effector of cAMP.

Figure 5A and B illustrate the two types of sensors and their respective states of activation. In the absence of cyclic nucleotides (CN), the donor and acceptor fluorophores of “loss of FRET” reporters are in close proximity to each other. Upon excitation of the donor fluorophore with light of the appropriate wavelength, part of the excited state energy of the donor is transferred to the acceptor fluorophore at the expense of its own emission. The acceptor fluorophore will then emit light at its own emission wavelength (sensitized acceptor emission). Binding of cyclic nucleotides, cAMP or cGMP, to the Nucleotide Binding Domain (NBD) induces a conformational change in the NBD resulting in increased distance between donor and acceptor fluorophores. Therefore, the donor can no longer efficiently transfer energy and will emit a more intense signal at the emission wavelength of the donor itself; concomitantly there will be a decrease in emission coming from the acceptor. FRET changes are typically calculated as acceptor emission intensity divided by the donor emission signal. This mechanism applies to the reporters H187 (kindly provided by Dr Kees Jalink, The Netherlands Cancer Institute, Amsterdam) and Cygnet2.1 (kindly provided by Dr Wolfgang Dostmann, The University of Vermont, Burlington) employed in this study, which are sensitive to changes in cAMP and cGMP concentrations, respectively[285–288].

In “gain of FRET” reporters (Figure 5B), the fluorophores of the sensor are initially in a position that does not allow for efficient resonance energy transfer. However, when the Substrate Recognition Sequence (SRS) is phosphorylated by the kinase for which it is specific, the SRS is recognised by the Ligand Binding Domain (LBD). Upon binding of the LBD to the SRS, the conformation of the sensor changes in a way that the fluorophores come into close proximity

and energy can be transferred between donor and acceptor fluorophores upon excitation. This mechanism applies to the reporter AKAR4[289], which is employed in this study to assess intracellular PKA-mediated phosphorylation. The three cytosolic reporters were chosen based on their favourable dynamic range and availability. Although there are many FRET CN or PKA specific reporters described in literature; here I will only discuss the reporters relevant to this study.

The cAMP reporter is mTurquoiseΔ-Epac(CD, ΔDEP)-cp173- Venus-Venus. This sensor contains several modules (Figure 5C): 1) a truncated mTurquoise donor fluorophore, 2) an Epac based binding domain for cAMP that is catalytically dead (CD) and does not contain its native membrane targeting domain Dishevelled-Egl-10-Pleckstrin (DEP), 3) two Venus acceptor fluorophores which have been circularly permuted at amino acid 173 (cp173) to enhance their fluorescence properties[290]. mTurquoiseΔ and Venus are CFP and YFP based fluorophores, respectively, with improved quantum yields and acceptor extinction coefficient. The C-terminal truncation of mTurquoise has previously been shown to improve FRET efficiency[285]. This reporter is the newest Epac based cAMP reporter with the highest dynamic range in a line of cAMP reporters[285,291].

The PKA reporter dubbed AKAR4 is the fourth FRET reporter designed by Zhang and colleagues[289]. To date, all PKA FRET biosensors are based on the same principle as the AKAR reporters[292,293]. A SRS and an LBD are sandwiched between the donor and acceptor fluorophore. The SRS is specific for PKA, therefore when PKA becomes active it will phosphorylate the SRS. Subsequently, the SRS is recognised by the LBD. Upon binding of the LBD to

the SRS, the conformation of the sensor changes in a way that the fluorophores come into close proximity and energy can be transferred between donor and acceptor fluorophores upon excitation. In time, the different AKARs have been adapted by changing the donor-acceptor fluorophores to improve their FRET efficiency. AKAR4 is the newest version and contains a circularly permutated Venus (cp172) and a CFP based Cerulean[289].

The Cygnet2.1 sensor is specific for cGMP and based on PKGIα[286]. All available cGMP reporters have a small dynamic range compared to the newest cAMP sensor. We chose Cygnet2.1 based on its high specificity for cGMP, compared to other available cGMP sensors[288]. The first Cygnet was designed and constructed by Honda and co-workers[287]. They inserted the PKGIα sequence between ECFP and EYFP. They tested several PKGIα deletion mutants and found the N-terminal Δ1-77 construct to respond to cGMP. This yielded Cygnet1. In addition they rendered the PKG sequence catalytically dead by insertion of a T516A point mutation. This sensor was named Cygnet2. Finally, Cygnet2.1 was obtained by substituting EYFP with Citrine, an YFP based acceptor fluorophore that is pH insensitive[287]. pH sensitive fluorophores can undergo conformational changes under changing pH conditions, which can decrease their inherent properties and thus ultimately FRET sensor efficiency. For a complete review of cGMP FRET sensors refer to ‘cGMP: generators, effectors and therapeutic implication’, by Harald H. H. W. Schmidt et al[294].

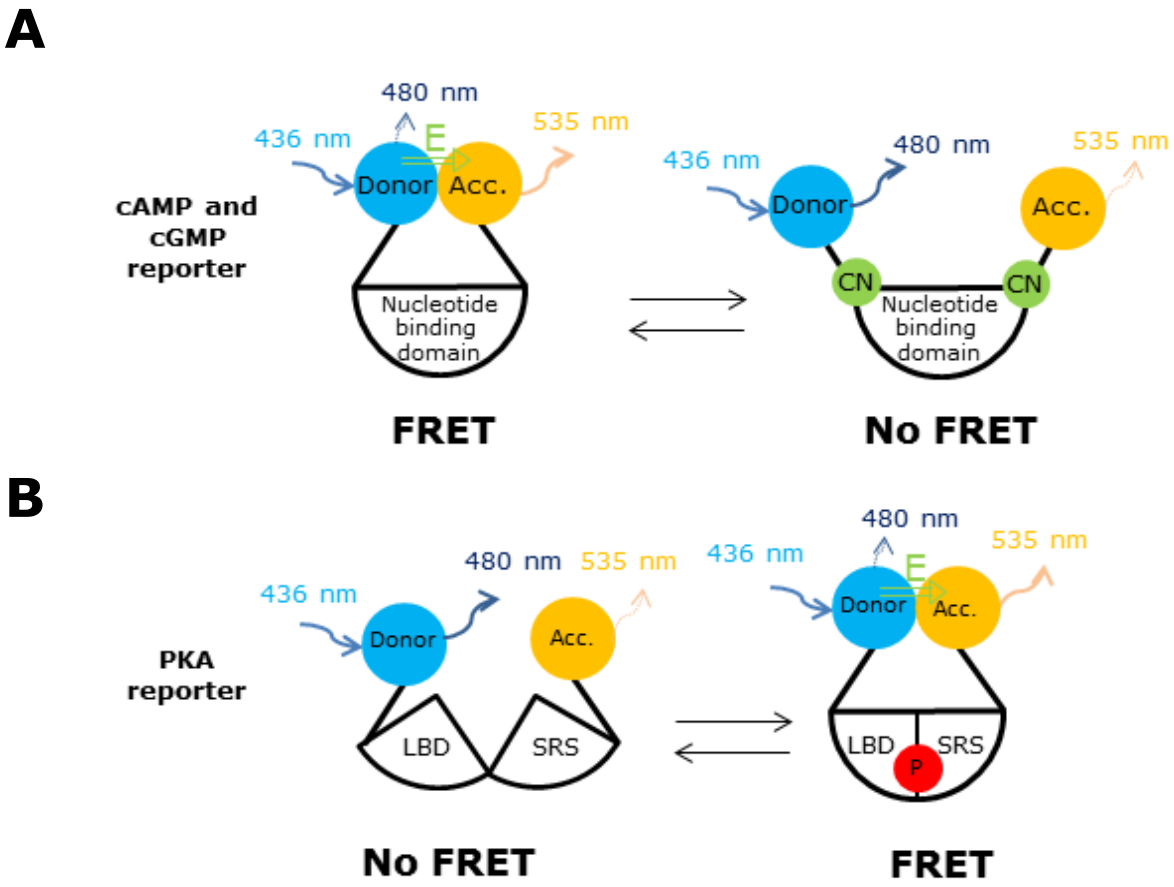

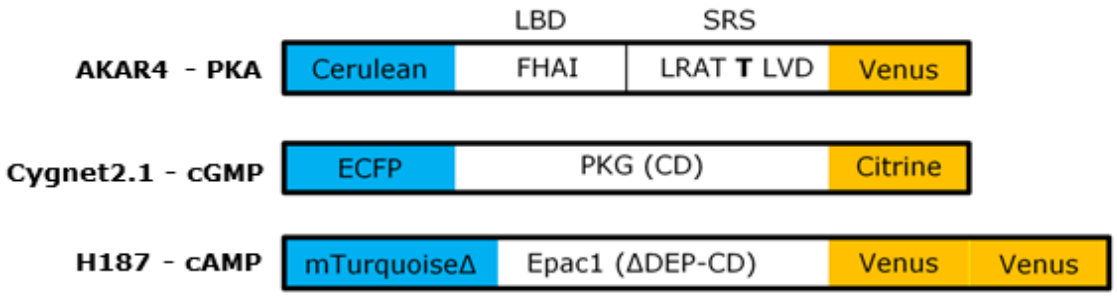

Figure 5: Schematic overview of the FRET principle of the two types of sensors employed in this study. A) Depicted is a so called “loss of FRET” sensor. The energy transfer (green arrow) between donor and acceptor fluorophore upon donor excitation (blue arrow; wavelength 436 nm) allows for an increase in FRET. Binding of CN (green circles) alters the biosensor conformation and decreases FRET. This is characterised by an increase in donor emission signal (dark blue arrow; wavelength 480 nm) and a decrease in acceptor emission signal (yellow arrow; wavelength 535 nm). B) A scheme of a "gain of FRET” sensor. The

schematic shows the change in conformation occurring upon phosphorylation of SRS (red circle) and LBD-SRS binding. The conformational change enables an increase of FRET upon donor excitation (blue arrow; wavelength 436 nm). This increase is characterised by a decrease in donor emission signal (dark blue arrow; wavelength 480 nm) and an increase in acceptor emission signal (yellow arrow; wavelength 535 nm). C) Structure of DNA encoding the three FRET reporters employed in this study. In the schematic of the PKA sensor, the Forkhead Associated Domain I (FHAI) corresponds to the LBD depicted in Figure 5B, whereas the amino acid sequence LRATTLVD is the Substrate Recognition Sequence (SRS) for PKA which phosphorylates the second Threonine enabling binding of the LBD. The PKG and Epac domains, or nucleotide binding domains, of the cAMP and cGMP sensors allow for nucleotide binding induced conformational change and subsequently a decrease in FRET. Both domains are catalytically dead (CD) and the Dishevelled-Egl-10-Pleckstrin (DEP) domain was deleted from Epac to avoid membrane localisation. The donor fluorophore regions are depicted in blue and those of the corresponding acceptor fluorophores in yellow.

1.8 Relevance and aims

Specificity within signal transduction is achieved by expression of various signalling protein isoforms in distinct tissues, but also by assembly of macromolecular complexes. In the context of CN signalling, such complexes can consist of A/GKAPs, PDEs and other regulatory proteins. This regulatory compartmentalisation of CNs, via PDEs, makes PDEs interesting drug targets. In fact PDE inhibitors have been suggested for use in drug treatment of pathologies relating to endothelial barrier dysfunction including pulmonary oedema and asthma.

Increased cellular cAMP levels have been shown to improve barrier function, mostly based on cAMP accumulation assays. However, it remains to be

investigated how cAMP compartmentalisation, specifically in human pulmonary endothelial cells, affects barrier function. Recent evidence indicates that cAMP accumulation in the cytosol of rat pulmonary endothelial cells increases monolayer permeability, whereas cAMP increase at the membrane decreases permeability, suggesting similar cAMP compartmentalisation within human pulmonary endothelial cells.

Furthermore, PDE mediated cross-talk between cGMP and cAMP has been suggested; however, the spatiotemporal role of cGMP and PDEs in cellular permeability remains to be elucidated (refer to Figure 6). Therefore, this report aims to take initial steps towards uncovering the presence of CN compartmentalisation in human pulmonary microvascular endothelial cells (hPMEC) and its relation with barrier function (refer to Figure 3 and 6).

There are several different approaches to measure barrier function. Both *in vitro* and *in vivo* methodologies are crucial to give a more physiological representation of the effect that drugs can have on endothelial permeability. Our elaborations on different methods to assess intracellular cAMP show that there is no available method better suited to assess compartmentalisation and subcellular changes of intracellular cAMP in live cells than FRET. Investigations into the molecular CN mechanisms behind barrier function necessitate measurements employing FRET methodology as well as in vitro barrier function approaches. This body of work is aimed at laying the foundations and establishing tools to investigate the relation between CN compartmentalisation and endothelial barrier function for the first time in parallel within the same living cell.

This combinatorial approach would be the first of its kind and allow for unique

insight into the cAMP compartmentalisation-endothelial barrier dysfunction association. Improving the understanding of underlying mechanisms could ultimately allow for development of novel drug therapies that focus on subcellular cAMP redistribution. One such approach would be inhibition of specific PDEs expressed in hPMEC, which could re-establish a balance between cytosolic and membranous cAMP pools, or selectively increase cAMP in the microcompartment that is involved in strengthening the endothelial barrier.

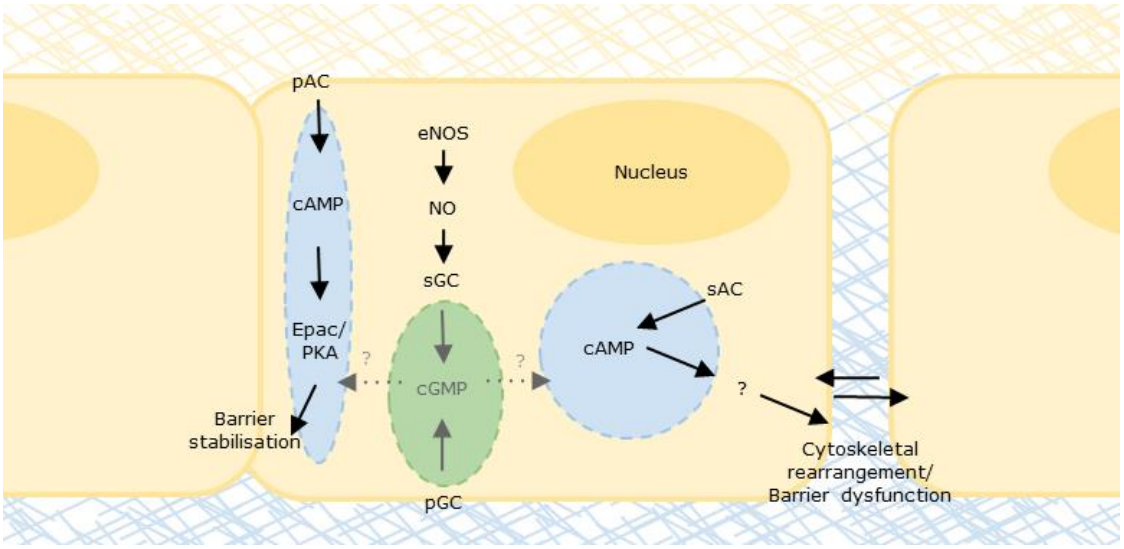

Figure 6: Suggested pools of specifically localised cyclic nucleotides regulating barrier function in pulmonary endothelial cells. Increasing cAMP levels at the membrane is thought to increase barrier function via Epac and PKA signalling, whereas cytosolic cAMP increases cellular permeability through unknown mechanisms (proposed cAMP pools shown in blue). A specific cGMP pool, produced by pGC/sGC, may regulate cAMP pools on the subcellular level (suggested cGMP pool shown in green).

2. Materials and methods

2.1 Reagents and materials

Restriction enzymes were purchased from New England Biolabs (Ipswich, MA). Thrombin was purchased from Enzyme Research Laboratories, Swansea, UK. Bay 41-2272 was purchased from Tocris Bioscience, Biotechne, Minneapolis, MN. Chemicals were purchased from Sigma Aldrich (St. Louis, MO) or Tocris Bioscience (Biotechne, Minneapolis, MN) unless otherwise stated. Cell culture reagents were obtained from (Gibco) Life Technologies Ltd, Paisley, UK, unless otherwise stated.

2.2 FRET imaging

FRET images were taken of HEK or hPMEC cells expressing FRET biosensors. Cells were imaged with an inverted microscope (IX71; Olympus, Tokyo, Japan) equipped with a 40x numerical aperture (NA) 1.30 or 60x NA 1.42 oil immersion objective lens (Olympus) or a 40x NA 0.6 long distance objective air lens, a cooled CCD camera (CoolSNAP HQ2; Roper Scientific, Tucson, AZ), and an LED illumination system (OptoLED, Cairn research, Faversham, Kent, UK). The following filters used for the dual-emission imaging studies were obtained from Chroma Technology (Bellows Falls, VT): for the excitation a CFP excitation filter (ET436/20x) and a dichroic mirror (455DCLP).

The beam splitter was equipped with a dichroic mirror (505DCLP) an YFP emission filter (ET535/30m) and a CFP emission filter (ET480/40m). For an overview of the FRET setup and light path, please refer to Figure 7. Donor and acceptor fluorophore emission intensities were measured and cells were imaged with MetaFluor Fluorescence Ratio Imaging Software (Molecular Devices, Sunnyvale, CA).

For the quantification, the average donor and acceptor fluorophore intensities over the whole cell area were measured in MetaFluor and exported to Excel software (Microsoft Corporation, Redmond, WA). In Excel background values were subtracted from the intensities and the FRET ratio, YFP/CFP (for "gain of FRET" sensors) or CFP/YFP (for "loss of FRET" sensors) from T=0 s until the time of stimulation was averaged and used as the reference. The background subtracted FRET ratio divided by the reference value was defined as the normalized ΔR/R0 value (for an overview of the analysis of imaging data, please refer to Figure 8).

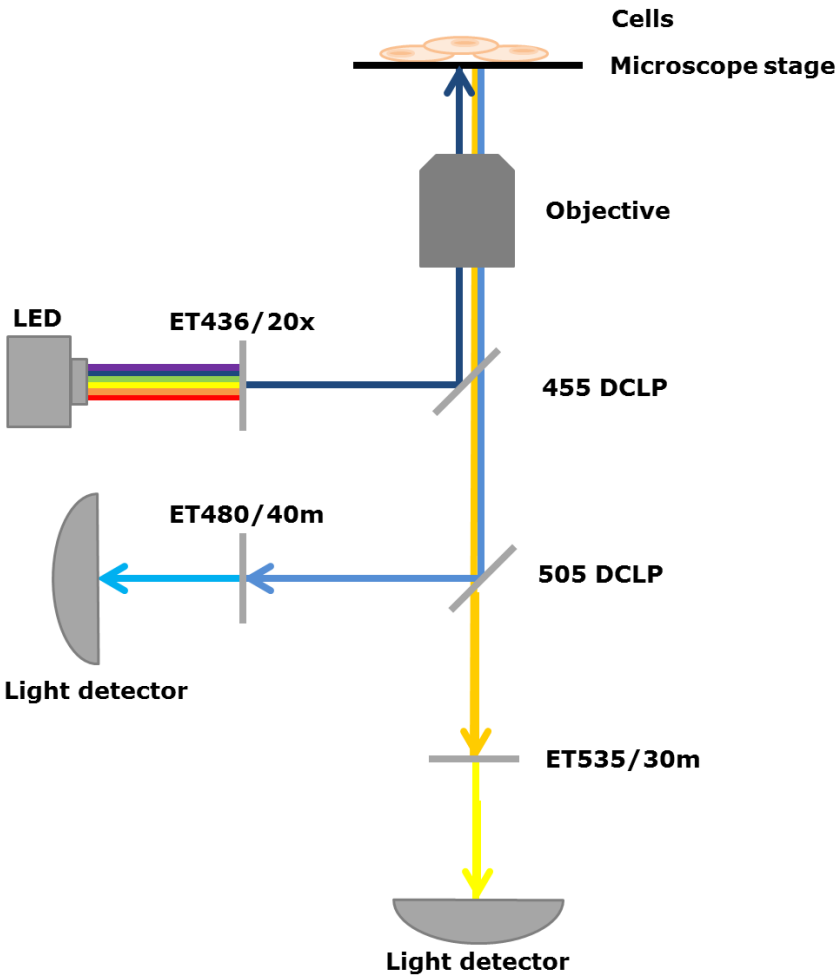

Figure 7: Schematic representation of FRET-setup and corresponding light path. Blue light of ~436 nm wavelength can pass through the ET436/20x filter. The light is then reflected by the 455DCLP dichroic mirror, which lets only light of 455 nm and higher through. The blue light then travels through the objective and onto cells expressing the FRET reporter. The reporters emit both blue and yellow light with emission spectra peaks of around 480 and 535 nm, respectively. The emitted light is now above the 455DCLP's cut off value, allowing it to pass through onto the 505DCLP dichroic mirror. Light above 505 nm can travel through this mirror. Therefore, blue light of about 480 nm will be reflected and yellow light of ~535 nm passes straight through. Both light beams fall onto their emission filters: ET480/40m and

ET535/30, respectively. The filtered light is collected by light detectors from which we obtain the intensity values for both donor and acceptor fluorophores.

2.3 FRET image data analysis and regions of interest

To assess changes in FRET emission intensity, we collected the light emitted from the donor and acceptor fluorophores through channels that only passed light of the wavelength specific to donor or acceptor, respectively (for a more detailed description, please refer to Figure 7 in the materials and methods section). This enabled us to obtain images of cells specific for the donor and acceptor emission signals. Upon addition of stimuli, changes in emission intensity over time became apparent, which correlated with a change in FRET. As mentioned before, background values were subtracted from the intensities and the FRET ratio, YFP/CFP (for "gain of FRET" sensors) or CFP/YFP (for "loss of FRET" sensors), respectively, was calculated after this subtraction. To do these calculations regions of interest (ROI) were selected in both sets of donor and acceptor intensity images. For cells expressing a cytosolic sensor, the entire cell was selected as a ROI. ROIs were duplicated in donor and acceptor images. MetaFluor could then extract the average intensity value of the selected ROI. To assess the average background value, a ROI was selected where there were no cells on the image. When assessing changes in FRET in cells that expressed a membrane targeted reporter, a ROI specific to the membrane (excluding the cytosol) could have been drawn. However, for general ease of analysis it was favourable to draw and area of interest around the entire cell, rather than only selecting the membranous region (compare

Figure 8A right and left panel). To assess whether whole cell ROI selection would affect our FRET read-out when working membrane-targeted reporters, we analysed a dataset of a cell expressing a membrane targeted cAMP FRET reporter, using both types of ROI.

The observed baseline intensity values for both donor and acceptor fluorophores were slightly increased, when working with a ROI including plasma membrane only (Figure 8B). The signal intensity at the membrane was higher than in the cytosol, therefore it was not surprising that the baseline intensities were increased. We found that the FRET ratio traces were not different when analysing the data with either ROI (Figure 8C and D). Therefore, we concluded that the choice of ROI did not affect the final FRET trace read-out. Based on these results, the analysis of FRET reporter data in the remainder of this study was carried out by selecting whole cell ROIs irrespective of the localisation of the expressed sensor.

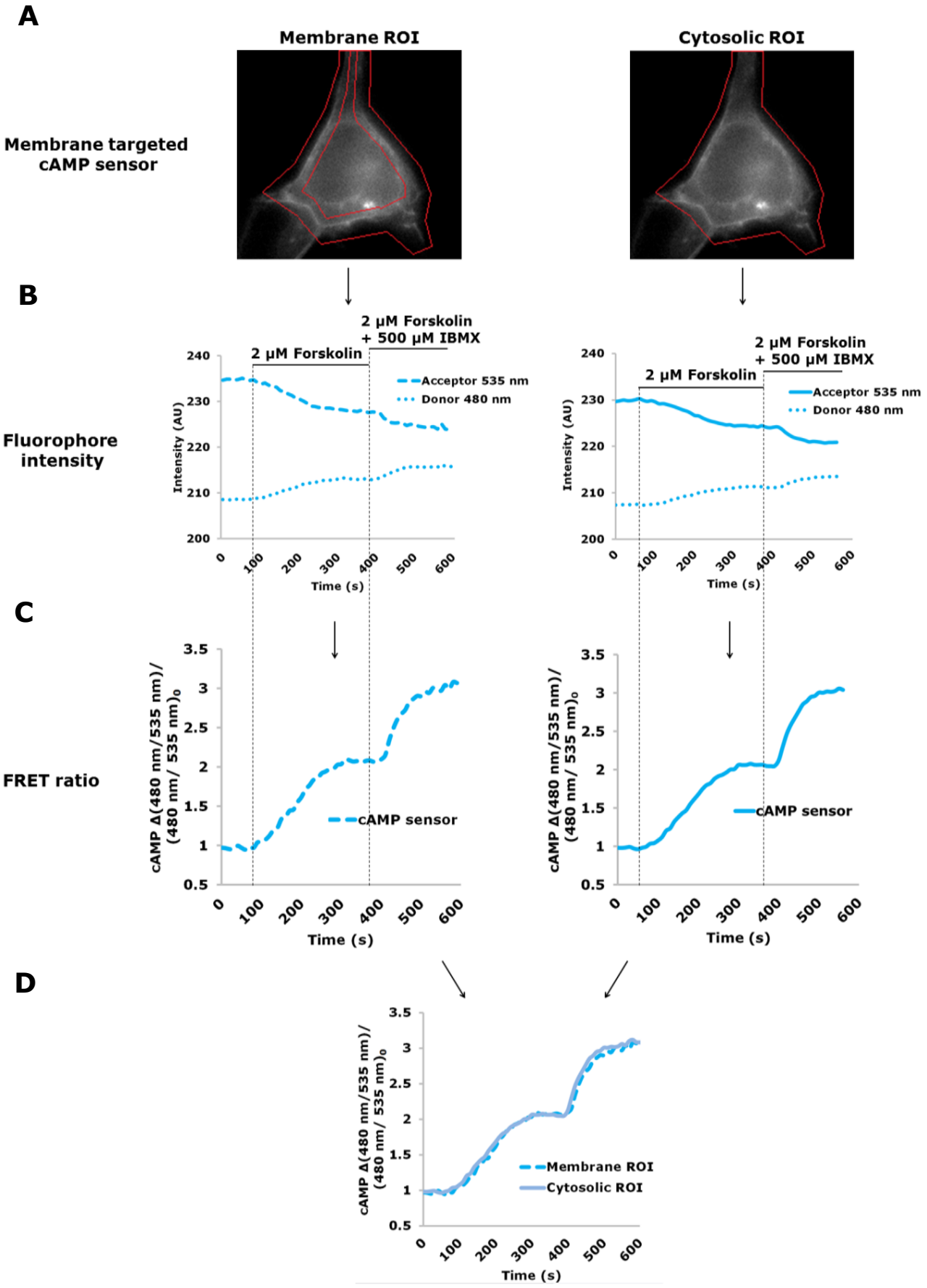

Figure 8: Comparison of application of different ROIs in the analysis of FRET images from membrane-targeted reporters. A) Delineation of whole cell ROI or membrane specific

ROI selection for cells expressing the membrane targeted FRET cAMP sensor. B) Donor and acceptor fluorophore emission intensity traces over time for each of the selected ROIs. Signal emission shifts after addition of intracellular cAMP increasing stimuli are shown. C) Normalised FRET ratio changes calculated using the traces shown in B. Note that for convenience the cAMP FRET ratio traces were calculated as donor emission divided by acceptor emission intensity, to represent the increase in cAMP concentration as an increase of the FRET ratio, even though FRET actually decreases, when the sensor binds more cAMP. D) Overlay of the FRET traces shown in C), for the membrane and cytosolic ROIs, respectively.

2.4 FRET reporter generation

Cytosolic reporters which were membrane targeted were designated H187-PM, AKAR4-PM and Cygnet2.1-PM. The membrane targeting sequences inserted were adapted from the original sequence of Depry et al.[289]: 3' KKKKKKSKTKCVIM 5' derived from K-Ras kinase with CaaX box (C = cysteine, a = aliphatic amino acid, and X = any amino acid) sequence along with a polylysine motif. The amino acid targeting sequence employed in this project is 3' MDELYKKKKKSKTKCVIM 5'. For the cDNA sequence and oligos refer to Table 1. The plasma membrane targeting sequence was introduced at the C-terminus of all three sensors by an EcoRI restriction site. The membrane targeting sequence oligos were synthesised in an already 'cut' state, annealed dephosphorylated by alkaline phosphatase and ligated into the target vectors, with the Rapid DNA Dephos and Ligation kit (Roche, Corning, Acton, MA), which were cleaved by EcoRI enabling insertion of the annealed primers. The Cygnet2.1-PM and H187-PM sensor sequences were excised from the backbone vectors and inserted into a designated vector for adenoviral particle

production, called pDual. AKAR4-PM was already in pDual. H187-PM was excised with PspXI and XhoI and ligated into the pDual backbone which was cut with XhoI and HindIII. Cygnet2.1-PM was excised with ScaI and NheI and ligated into the pDual backbone cut with the same enzymes. Vectors containing the membrane targeted biosensors were sequenced using primers depicted in Table 2. Finally, mutagenesis primers were designed to obliterate the STOP codons between the C-terminus of the Cygnet or AKAR4 and the membrane targeting sequence (Table 3).

Table 1: the different oligonucleotides which were used for construction of three membrane targeted FRET biosensors.

Insert	Sequence
Membrane targeting sequence H187 forward	5’ AAT TCA ATG GAC GAG CTG TAC AAG AAG AAG AAG AAG TCT AAG ACT AAG TGT GTT ATT ATG TAA G 3’
Membrane targeting sequence H187 reverse	5’ AAT TCT TAC ATA ATA ACA CAC TTA GTC TTA GAC TTC TTC TTC TTC TTG TAC AGC TCG TCC ATT G 3’
Membrane targeting sequence AKAR4 and Cygnet2.1 forward	5’ AAT TCG GCG GCG GCA GCG GCG GCG GCG GCA GCA TGG ACG AGC TGT ACA AGA AGA AGA AGA AGT CTA AGA CTA AGT GTG TTA TTA TGT AAA GTA CTG 3’
Membrane targeting sequence AKAR4 and Cygnet2.1 reverse	5’ AAT TCA GTA CTT TAC ATA ATA ACA CAC TTA GTC TTA GAC TTC TTC TTC TTC TTG TAC AGC TCG TCC ATG CTG CCG CCG CCG CCG CTG CCG CCG CCG 3’

Table 2: sequencing primers employed to validate the membrane targeted constructs.

Region	Sequence
Forward primer for H187	5' AGC GCA TGA GCT GAT CCC AC 3'
Reverse primer for H187	5' CCA CCT GGT GGA TAC TGT TGA AG 3'
Forward primer for AKAR4	5' TAC TAG GAG AAG ACG GTA ACC 3'
Reverse primer for AKAR4	5' ATT CCA CGC CTA CAC CAA CGG 3'
Forward primer for Cygnet2.1	5' TTC GCC AAC CTG AAG CTG TCT G 3'
Reverse primer for Cygnet2.1	5' GCT TCT CCG AGC GGA TGT G 3'
Forward primer for pDual	5' GAC GCA AAT GGG CGG TAG 3'
Reverse primer for pDual	5' TAG TTG TGG TTT GTC CAA ACT C 3'

Table 3: mutagenesis primers employed to delete the C-terminal STOP codons from the cytosolic AKAR4 and Cygnet2.1.

Region	Sequence
Forward mutagenesis primer for AKAR4	5' CCG CCA CAA CAT CGA GGG AGA ATT CGG CGG CGG CAG 3'
Reverse mutagenesis primer for AKAR4	5' CTG CCG CCG CCG AAT TCT CCC TCG ATG TTG TGG CGG 3'
Forward mutagenesis primer for Cygnet2.1	5' GGA CGA GCT GTA CAA GGG AGA ATT CGG CGG CGG CAG 3'
Reverse mutagenesis primer for Cygnet2.1	5' CTG CCG CCG CCG AAT TCT CCC TTG TAC AGC TCG TCC 3'

2.5 Cell culture

hPMEC (Promocell, Heidelberg, Germany) were routinely cultured in T25 flasks in Endothelial Cell Growth Medium MV (Kit from Promocell, Heidelberg, Germany) medium supplemented with and incubated at 37 °C in 5% CO2. Medium was refreshed every second day. Cells were plated on glass coverslips which were coated with 0.02% gelatin/ 0.005% fibronectin solution. Before passaging or seeding, cells were grown to 90-100% confluence. Cells were passaged after washing with calcium and magnesium free Phosphate Buffered

Saline (PBS -/-) and trypsinization with 0.05% trypsin-EDTA. Hereafter cells were resuspended in the required amount of growth medium and distributed to new flasks and/or plates.

For FRET experiments cells were seeded on 12 well plates containing gelatin/fibronectin coated coverslips. hPMEC were infected 24-48h before FRET experiments with cAMP or PKA reporter adenoviral particles. Medium was replaced after 6 hours. Cells were transferred to phenol red free serum free medium containing 28 mM HEPES with or without serum as stated for experiments. Stimuli were added to the cells in the same medium unless otherwise stated.

For HEK and HBE cells, transfection was carried out with Opti-MEM serum-free medium (Life Technologies Ltd, Paisley, UK) and Lipofectamine2000 (Life Technologies Ltd, Paisley, UK). Transfections were carried at the ratios Lipofectamine2000 Lipofectamine2000 (µl): DNA (µg) 3:1 for cells transfected with the cytosolic or membrane targeted cAMP, PKA or cGMP bioreproters, respectively. Briefly, DNA and Lipofectamine were separately mixed into a 75 µl Opti-MEM serum-free medium (Life Technologies Ltd, Paisley, UK) containing eppendorf tube. The solutions were briefly vortexed and incubated for 5 minutes at room temperature. Hereafter, the solutions were combined, briefly vortexed and incubated for 15 minutes at room temperature. After the incubation period, the solution was gently mixed by pipetting up and down and added to the cells. Medium was exchanged after 6 hours. 24 hours post-transfection FRET experiments were conducted. Stimulants were added to the cells in physiological FRET salina (125 mM NaCl, 5 mM KCl, 1mM $NaPO_4$, 1mM $MgSO_4$, 20 mM HEPES, 5.5 mM glucose, 1 mM $CaCl_2$, pH 7.4).

2.6 Permeability assay

hPMEC (4 x 10^4 seeding density) were cultured for indicated times on GF coated transparent PET Transwell inserts of 0.4 µm pore size (Falcon, Tewksbury, MA). 500 µl FITC-dextran (2 µg/ml initial concentration in the upper chamber, minimal calculated molecular mass 40 after 30 kDa) in phenol red and serum free medium were added to the upper compartment. After 30 minutes of incubation, 100-µl samples were withdrawn from the lower compartment and assayed photometrically for their absolute fluorescence signal.

2.7 Immunostaining

Endothelial cells grown on gelatinized coverslips were rinsed with PBS with calcium and magnesium, fixed in 3.7% paraformaldehyde for 10 min, and permeabilised with 0.1% Triton X-100 in PBS for 10 min. Cells were then washed briefly with PBS (5 min each x3), blocked with PBS containing 2% BSA for 1h, and incubated with primary VE-cadherin antibody (Santa Cruz biotechnology, Texas, USA) 1:500 for 1h, washed with PBS (5 min each x3) and incubated with secondary goat-anti mouse Alexa488 (Life Technologies Ltd, Paisley, UK) 1:1000 for 1 h. Alternatively cells were incubated with 1:5000 of Alexa658 phalloidin (Life Technologies Ltd, Paisley, UK) diluted in PBS with 2% BSA for 20 min. After being washed three times with 2% BSA PBS (5 min each), coverslips were mounted on slides with SlowFade mounting medium

(Life Technologies Ltd, Paisley, UK). Images were captured using a 60x oil objective with a Confocal Olympus FV1000 setup.

2.8 Soluble adenylyl cyclaseI/II experiments

Human Bronchiolar Epithelial (HBE) cells were transfected with the sACI/II and cytosolic H187 cAMP FRET reporter. Cells were transfected in ratios sACI/II:H187 0:1 (control), 1:1 and 1:3, respectively. Cells were grown to 70-80% confluence on 15 mm glass coverslips (Sigma Aldrich, St. Louis, MO) in 12 well dishes. At 70-90% confluence, cells on each coverslip were transfected with a ratio of 1:3 DNA (µg):Lipofectamine2000(µl) (Life Technologies Ltd, Paisley, UK). Cells were transfected following the standard Lipofectamine2000 protocol. Briefly, DNA and Lipofectamine were separately mixed into a 75 µl Opti-MEM serum-free medium (Life Technologies Ltd, Paisley, UK) containing eppendorf tube. The solutions were briefly vortexed and incubated for 5 minutes at room temperature. Hereafter, the solutions were combined, briefly vortexed and incubated for 15 minutes at room temperature. After the incubation period, the solution was gently mixed by pipetting up and down and added to the cells. Medium was exchanged after 6 hours. 24 hours post-transfection FRET experiments were conducted. Glass coverslips were mounted onto an RC-25F open diamond bath imaging chamber (Warner Instruments, Harvard Apparatus, Holliston, MA) with a small amount of silicon grease (various suppliers). Cells were covered with 400 µl of FRET salina. The RC-25F was placed onto a PH-4 chamber platform, which was then clipped

onto the stage adapter (Warner Instruments, Harvard Apparatus, Holliston, MA). The stage adapter was compatible with the microscope stage, allowing us to image the cells during FRET experiments. sACI/II and/or H817 expressing cells were imaged during 5 minutes before starting stimulation. During the course of the experiment cells were imaged every 10 seconds. Intracellular cAMP levels were increased by treatment with forskolin, a direct activator of mtACs, and 3-isobutyl-1-methylxanthine (IBMX), a general PDE inhibitor. Cells were stimulated with increasing doses of forskolin at 100 nM, 1 µM, and 10 µM with 100 µM IBMX, respectively (sensor saturating stimulus as determined by Dr. Stefania Monterisi; data not shown). The RC-25F was connected by a tube to a suction pump, allowing for washing the cells with FRET salina in between stimulations.

2.9 Infrared light-activated adenylyl cyclase experiments

Human Embryonic Kidney 293 (HEK293) or HEB cells were transfected with the IlaC and cytosolic H187 cAMP FRET reporter. Cells were transfected in ratios IlaCI:H187 0:1 (control) or 1:1. Cells were grown to 70-80% confluence on 15 mm glass coverslips (Sigma Aldrich, St. Louis, MO) in 12 well dishes. At 70-90% confluence, cells on each coverslip were transfected with a ratio of 1:3 DNA(µg):Lipofectamine2000(µl) (Life Technologies Ltd, Paisley, UK). Cells were transfected following the standard Lipofectamine2000 protocol and as described in the material and methods section for the sACI/II experiments. Medium was exchanged after 6 hours. 24 hours post-transfection FRET

experiments were conducted. Glass coverslips were mounted onto an RC-25F open diamond bath imaging chamber (Warner Instruments, Harvard Apparatus, Holliston, MA) with a small amount of silicon grease (various suppliers). Cells were covered with 400 µl of FRET salina. The RC-25F was placed onto a PH-4 chamber platform, which was then clipped onto the stage adapter (Warner Instruments, Harvard Apparatus, Holliston, MA). The stage adapter was compatible with the microscope stage, allowing us to image the cells during FRET experiments. During the course of the experiment cells were imaged every 10 seconds. Two types of experiments were conducted that differed in regard to the red light illumination devices to activate the IlaC. One experimental setup employed white light (incorporated into imaging setup), which was passed through a 500 nm long pass filter and then onto the cells. In the other setup cells were illuminated directly with a 660 nm LED (Kingbright Electronic Co, Ltd, New Taipei City, Taiwan) IlaC and/or H817 expressing cells were imaged during 5 minutes before activating the IlaC with the respective light sources. Cells were illuminated with red light during 5 minutes, whilst FRET data and images were acquired in parallel. After 5 minutes the red light source was switched off and FRET data and image acquisition continued. At the end of each experiment cells were treated with 25 µM and 500 µM IBMX to confirm that FRET reporters were responding appropriately.

2.10 FRET-TER chamber experiments

hPMEC were grown at 4×10^4 seeding density on 0.02% gelatin/ 0.005% fibronectin coated transparent PET 24 Transwell inserts of 0.4 µm pore size

(Falcon, Tewksbury, MA). hPMEC were infected with cAMP reporter adenoviral particles 24 h before FRET experiments. Medium was replaced after 6 hours in both upper and lower compartment of the transwell inserts hung in 24 wells plates. Cells were transferred to phenol red free serum free medium containing 28 mM HEPES without serum in the FRET-TER chamber. The FRET-TER chamber was made costum made by Dr. Andreas Koschinski (Department of Physiology, Anatomy and Genetics, University of Oxford, UK). The chamber consisted of a glass bottom 24 transwell plate, in which the transwell insert with infected hPMEC was placed. The lower electrode ring was permanently attached to the setup and placed below the 24 transwell insert. The upper electrode ring was lowered into the transwell insert by a mechanical arm that was stably positioned above the hPMEC and in the medium. Both electrodes were fully immersed in medium. The electrodes were connected to the EVOM^2 voltohmmeter (World Precision Instruments, Berlin, Germany), which allowed us to measure the transendothelial barrier resistance in Ohm. By connecting the EVOM^2 to an analogue to digital data translation board called CEBO-LC (Cesys GmbH, Herzogenaurach, Germany), which was attached to a computer, the electrical signal could be converted into a digital signal. Signals were recorded with CEBO-LC DataLogger Software (Cesys GmbH, Herzogenaurach, Germany) and then exported to Excel software (Microsoft Corporation, Redmond, WA). In Excel the background was subtracted from raw data in kΩ. The background was approximated to be 350 Ω based on previous EVOM^2 measurements (data not shown). After background subtraction the resistance was multiplied with the surface over which TER was measured, in

this case 0.3 cm^2, to obtain the TER in $\Omega \cdot cm^2$. Data was normalised to values of the first stable TER measurements obtained within the same experiment.

2.11 Mathematical and statistical analysis

Data are reported as mean plus minus standard deviation. We performed statistical analyses using the Student t test, one-way ANOVA or two-way, as appropriate. Statistical significance was defined as $P < 0.05$.

3. Results

To address our questions relating to CN regulation and compartmentalisation, we employed FRET microscopy, which allowed for live cell imaging of molecular interactions to monitor physiological responses at specific cellular sites. The principles behind FRET and the bioreporters used in this study are illustrated in Figures 4 and 5. These sensors were used for the first time in the hPMEC line, in which we optimized conditions specifically for this purpose. Next to assessing changes in CN levels by FRET, we wanted to investigate their association with endothelial barrier function. Therefore we established staining and FITC-dextran conjugate methods to assess barrier function. Furthermore, we aimed to combine FRET methodology with a unique and novel transendothelial resistance measurement setup which would enable us to monitor simultaneously cellular barrier function and changes in CN levels live at specific cellular regions. Finally, we used the tools describe above for preliminary investigations into the relation between CN changes and barrier function. The optimisation of the different approaches is described below. For a detailed description of methods please refer to the appendix.

3.1 FRET sensors: mechanism, types and image data analysis

This project combines FRET methodology with endothelial barrier function assessment to gain an understanding of CN regulated barrier function. The

FRET approach offers many advantages including high resolution imaging in live cell, flexibility through variety of FRET sensors to assess cellular changes of different molecules of interest in both space and time. In the following sections, we will discuss the reporters employed in this study and their different characteristics, as well as our approach to analyse data obtained with them.

3.1.2 Comparison of FRET reporters used in this study

The dynamic range of FRET reporters is dependent on the choice of donor-acceptor pair and appropriate positioning between the fluorophore[295]. The different reporters described in this study contained various donor-acceptor pairs all based on blue and yellow fluorescent proteins, which were connected by the sensor specificity domain(s) (Figure 9A).

Appropriate positioning of the fluorophores could be modulated by adapting the linker size and composition to allow for optimal proximity and interaction of the donor-acceptor pair of the unimolecular FRET sensor[295].

Cyan Fluorescent Protein (CFP), Cerulean and mTurquoise (Figure 9A) are all donor molecules, which in that order have ascending quantum yields[296]. The higher the quantum yield, the more energy the donor can transfer, thus increasing FRET efficiency. This suggests that choosing fluorophores with higher quantum yields could increase FRET efficiency, when paired with the appropriate acceptor molecule and a sensor domain that allows for optimal orientation of the donor-acceptor pair in regard to each other.

Another factor that determines the dynamic range of FRET sensor is the

extinction coefficient, or molar absorptivity of the acceptor fluorophore. This is a measure of how strongly the acceptor fluorophore absorbs light at its characteristic excitation wavelength. Yellow Fluorescent Protein (YFP) and its variant Venus are acceptor fluorophores, which are marked by an increased brightness and extinction coefficient. These can be employed used in conjunction with a high quantum yield donor, which would enable better overall FRET.

We compared the dynamic range of reporters employed in this study in Figure 9B. We found that the cAMP sensor had the highest dynamic range, as well as the fluorophore donor-acceptor pair with the highest quantum yield and extinction coefficient, respectively. Interestingly, in addition to containing two Venus fluorophores for enhanced energy absorption, the acceptor fluorophores of the cAMP sensor are also circularly permutated, rendering them even more efficient in energy absorption[290]. The PKA sensor had the second highest dynamic range, with Cerulean and Venus as the FRET fluorophore pair. The cGMP reporter had the smallest range in conjunction with the fluorophore donor-acceptor pair with the lowest quantum yield and extinction coefficient. Figure 9C shows the comparison of dynamic ranges of the cAMP reporters H187 and H30[297]. H187, the cAMP reporter we use in this study, is the next generation sensor based on H30. Therefore the design of H187 (refer to Figure 9A) is almost the same as for H30. The exception lies within the fluorophores of the sensors. Whereas H187 contains mTurquoise and a tandem Venus, the H30 reporter consists of a CFP and YFP, comparable to the cGMP reporter (Figure 9A). Figure 9C shows the difference in dynamic range that can be obtained by choosing a more favourable donor-acceptor fluorophore pair.

Interestingly, the H30 reporter has a higher dynamic range than the cGMP reporter (compare Figure 9B and C), indicating that the specificity domains of the reporters also play a key role in determining the overall efficiency of FRET sensors. This is due to position of the donor and acceptor to each other as defined by the connecting specificity module, or linker in between the donor-acceptor pair to allow for efficient FRET. Overall, the fluorophore quantum yield and extinction coefficient may contribute to the overall efficiency of a FRET reporter. However, it should be noted that the sensor confirmation and distance between the donor and acceptor fluorophores are also crucial factors for FRET efficiency.

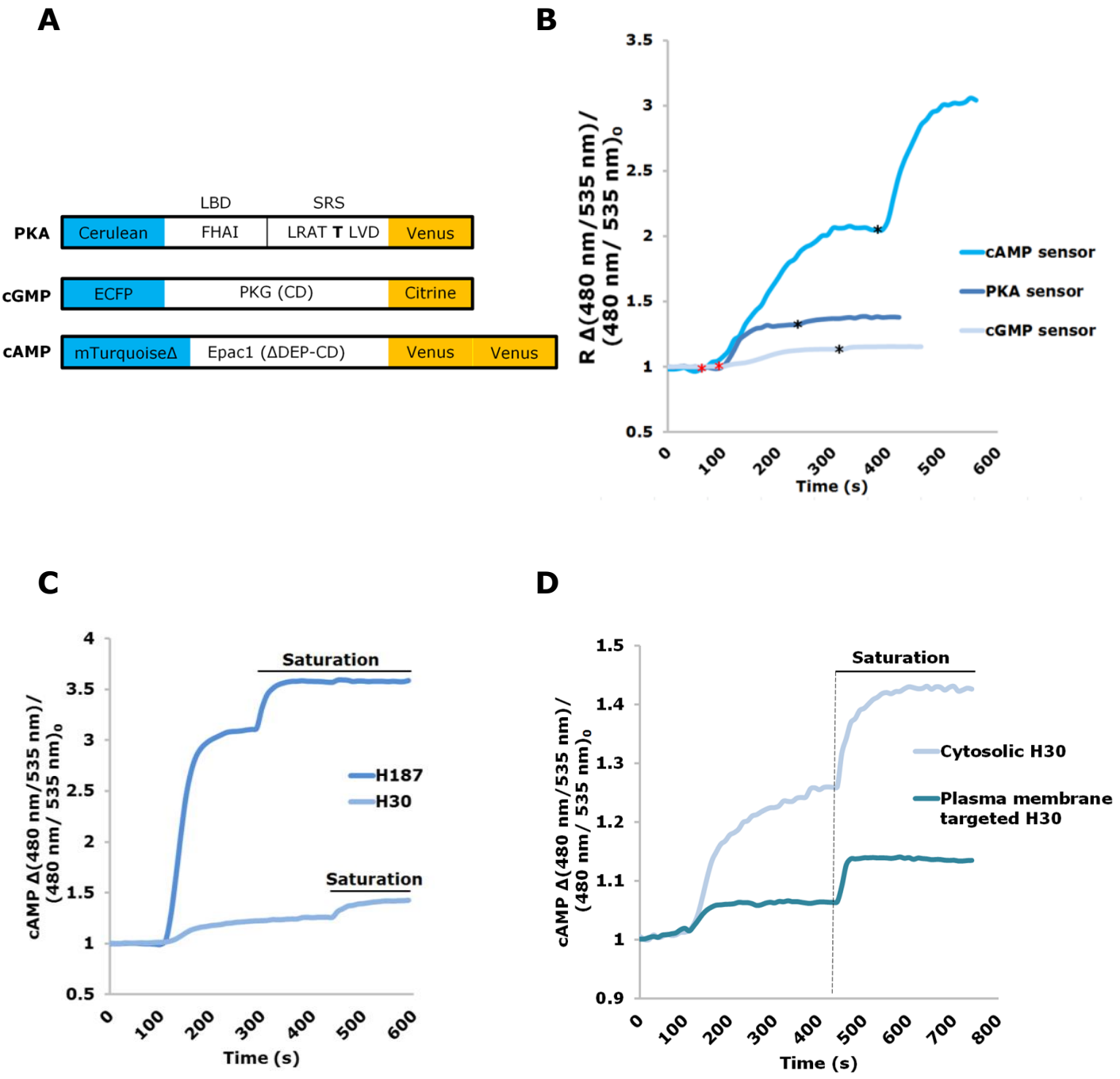

Figure 9: Comparison of characteristics of FRET reporters used in this investigation. A) Structure of DNA encoding the three FRET reporters employed in this study. In the schematic of the PKA sensor, the Forkhead Associated Domain I (FHAI) corresponds to the LBD depicted in Figure 3B, whereas the amino acid sequence LRATTLVD is the Substrate Recognition Sequence (SRS) for PKA which phosphorylates the second Threonine enabling binding of the LBD. The PKG and Epac domains, or nucleotide binding domains, of the cAMP and cGMP sensors allow for nucleotide binding induced conformational change and subsequently a decrease in FRET. Both domains are catalytically dead (CD) and the Dishevelled-Egl-10-

Pleckstrin (DEP) domain was deleted from Epac to avoid membrane localisation. The donor fluorophore regions are depicted in blue and those of the corresponding acceptor fluorophores in yellow. B) Comparison of normalised FRET ratio traces of membrane targeted reporters from Figure 9A. The cAMP reporter shows ~5 fold increase in maximal FRET response compared to the PKA and cGMP sensors. Red asterisks indicate addition of 2 µM forskolin, the time points of addition for the PKA and cGMP reporter overlap. Black asterisks indicated addition of the sensor saturating stimuli 20 µM forskolin and 500 µM IBMX. C) Comparison of the dynamic range of the cytosolic cAMP H30 FRET sensor and the next generation H187 reporter. A roughly 5 fold increase in maximal FRET change is observed when substituting the donor acceptor pair CFP and YFP in H30 by mTurquoise and double circular permutated Venus in H187[285,291,297]. Both sensors retained the same cAMP binding module. D) Comparison of the dynamic range of the cytosolic cAMP H30 FRET sensor and the same H30 reporter targeted to the plasma membrane. A roughly 3 fold decrease in maximal FRET dynamic range is observed when targeting the reporter to the cellular membrane. Note that for convenience the cAMP FRET ratio traces were calculated as donor emission divided by acceptor emission intensity, to represent the increase in cAMP concentration as an increase of the FRET ratio.

The dynamic range of FRET reporters can be altered by addition or modulation of domains that interfere with the structure of the specific sensor. An example of this is depicted in Figure 9D, where we applied a saturating stimulus to cells expressing the same reporter H30; however, cells were expressing the cytosolic or the plasma membrane targeted version. Cells expressing the membrane targeted sensor showed a lower maximal FRET ratio change compared to the cytosolic H30. The lower dynamic range of the membrane targeted H30 could be due to the addition of the membrane targeting sequence. The membrane targeting sequence was added to the N-terminus of the cytosolic H30 sensor[298]. Therefore the targeting sequence was directly

linked to the donor fluorophore, CFP. An explanation of decreased FRET efficiency would be the interference of the membrane targeting sequence with the conformation of CFP. It could also be that FRET between the donor and acceptor fluorophore would be sterically hindred by the added sequence. Another explanation for the decrease in dynamic range would be the re-localisation of the sensor to the membrane itself. As the sensor is bound to the membrane by the targeting sequence, it could not move as freely as it was able to do floating in the cytosol. This may decrease the proximity and optimal confirmation between the fluorophores that allow for FRET.

Ratiometric imaging allows for comparison between cells which express the same FRET bioreporter. However, when the maximal saturation plateau is significantly different, a direct comparison between both reporters is no longer possible. This is the case for the cytosolic and plasma membrane targeted H30 sensors shown in Figure 9D, as we cannot make any predictions as to how the relation between cAMP increase and degree of FRET change has been altered due to the modifications. When comparing experimental data from reporters with different dynamic ranges, it is essential to establish dose response curves for each individual reporter. This can be achieved by micro-perfusion patch-clamp methodology, which is briefly explained in the discussion of this report.

3.2 Generation of membrane targeted FRET reporters

Several lines of evidence have suggested that increases in cAMP, specifically in the cytosol, can lead to endothelial barrier dysfunction, whereas whole cell

cAMP increases, localized in the cytosol and at the membrane, stabilize barrier function[118,119,299,300]. This suggests compartmentalisation in endothelial cells. CN compartmentalisation can be investigated by using FRET reporters localised to different sites within living cells. Upon addition of stimuli that increase CN levels, changes can be monitored by these FRET sensors. Previous studies have never shown the cAMP-barrier function relationship in living cells. Therefore, we set out to assess changes in cyclic nucleotides at the membrane as well as in the cytosol to uncover possible compartmentalisation in endothelial cells. The generation of membrane targeted reporters from cytosolic sensors is discussed in this chapter (Figure 10–13).

In order to visualise CN activity at the plasma membrane, we targeted cytosolic FRET reporters specific for cAMP, cGMP and PKA to the plasma membrane using a lipid modification domain adapted from the protein K-Ras [289] (Figure 10A; more details regarding the method of sensor generation can be found in the materials and methods section). All reporters were chosen based on their specificity and superior dynamic ranges as compared to previous versions of the same reporters. In Figure 9 we discussed that targeting sensors to subcellular locations may interfere with their FRET efficiency and dynamic range, making it harder to observe smaller changes. As we wanted to compare cytosolic and membrane changes of cyclic nucleotides, we decided it was crucial to target FRET reporters that have the highest dynamic range available. Therefore we chose the cAMP reporter H187 over H30 and the PKA and cGMP reporters, AKAR4 and Cygnet2.1, respectively, over all other available reporters. A schematic overview of the membrane targeted reporters is depicted in Figure 10A.

Membrane targeted sensors were confirmed by sequencing analysis (data not shown). Plasma membrane localisation of the targeted reporters was confirmed visually by expression in transfected HEK293 cells (Figure 10B and 10C). The responsiveness of the membrane targeted reporters to CN changes was assessed by treatment of these sensors with the cyclic nucleotide increasing stimuli (Figure 11B, 12B and 13B). The changes in emission intensity could be clearly appreciated for all membrane targeted reporters in their respective emission intensity traces (Figure 11B, 12B and 13B; upper graphs). Notably, the intensity images show differences less clearly than the cAMP reporter intensity images (compare Figure 11A with 12A and 13A, respectively). As previously mentioned, this could be partially due to the inferior quantum yield and extinction coefficient of the donor acceptor pairs of the PKA and cGMP sensors.

All three reporters showed marked FRET ratio increases upon addition of CN increasing stimuli (Figure 11B, 12B and 13B; lower graphs), thus we concluded that the plasma membrane targeted versions of the FRET sensors were able to detect CN changes or PKA activity and could be employed to monitor CN changes at this site.

It should be noted that some cytosolic signal was detected in cells expressing membrane targeted reporters. This may have been due to mistargeting, but could have also resulted from signal collection below and above the focal plane, which is attributable to the nature of epifluorescence microscopy.

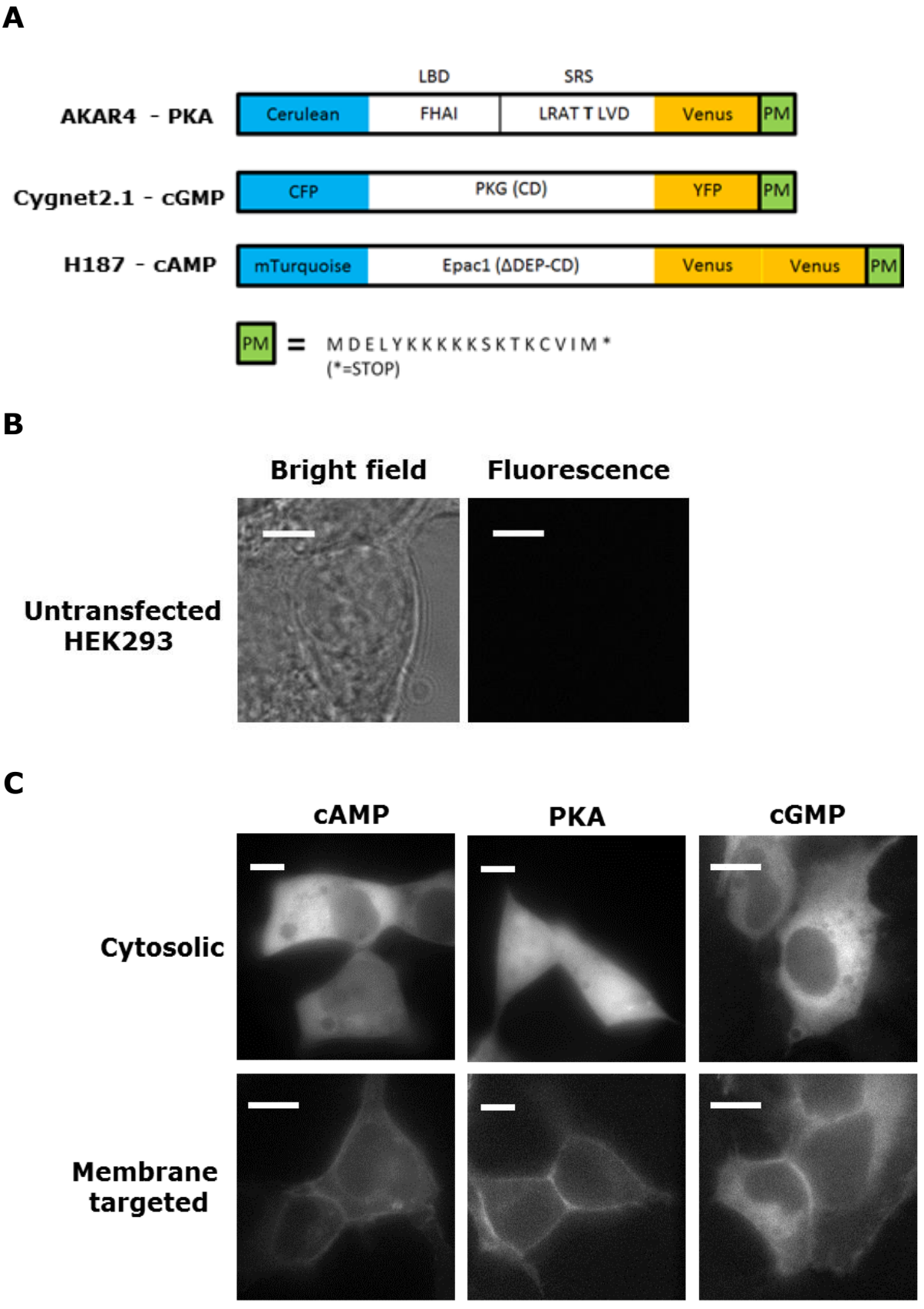

Figure 10: Generation of membrane targeted FRET reporters. A) Structure of DNA encoding the three FRET reporters to which a plasma membrane anchoring site (indicated by PM in green) adapted from the K-Ras protein sequence was added at the C-terminus. The

donor fluorophore regions are depicted in blue and those of the corresponding acceptor fluorophores in yellow. B) Depiction of untransfected HEK293 cells under bright field illumination (left panel) or fluorescent illumination with excitation/emission wavelengths of 436 nm and 535 nm respectively (right panel). For both conditions the exposure time was 150 ms. Scale bars represent 10 µm. C) HEK293 cells transfected with plasma membrane targeted or cytosolic cAMP, cGMP and PKA reporters. Cells were exposed to fluorescent light with excitation/emission wavelengths of 436 nm and 535 nm respectively. The exposure time was 150 ms. Scale bars represent 10 µm.

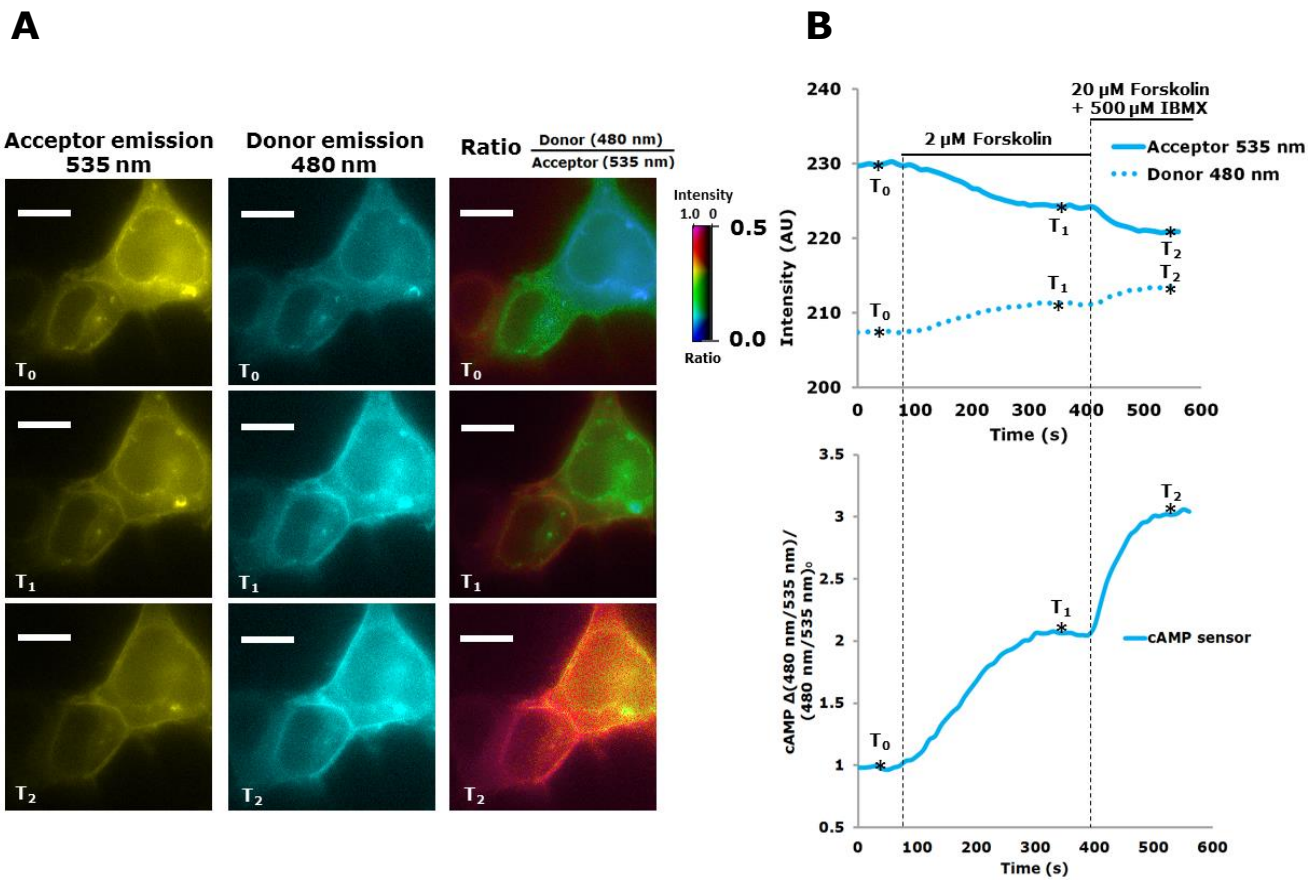

Figure 11: Representative emission and FRET ratio images of cAMP membrane targeted reporters with the corresponding emission intensity and FRET ratio traces. A) HEK293 cells transfected with the cAMP membrane targeted reporter, before application of the stimulus (T_0) and over time after addition of cAMP increasing stimuli (T_1 and T_2). 2 µM forskolin followed by 20 µM forskolin and 500 µM IBMX, to saturate the sensor, were applied as indicated. Shown are the cells imaged at emission wavelengths of 535 and 480 nm and the matching ratio

images. Note that no background subtraction was performed for these images. Scale bars represent 10 µm. B) Donor and acceptor fluorophore emission intensity traces (upper panel) and representative normalised and background subtracted FRET ratio trace (lower panel). The fluorescence intensity traces represent the average fluorescence values measured over the entire cell over time. The time point at which images shown in A were acquired is indicated by the asterisks (T_0-T_2). Data shown confirms the response of membrane targeted cAMP reporters to cAMP increasing stimuli in HEK293 cells expressing these sensors (representative trace of N=16 showing comparable results). Forskolin is known to stimulate cAMP production via mtACs and IBMX is a general PDE inhibitor. Note that for convenience the cAMP FRET ratio traces and images were calculated as donor emission divided by acceptor emission intensity, to represent the increase in cAMP concentration as an increase of the FRET ratio.

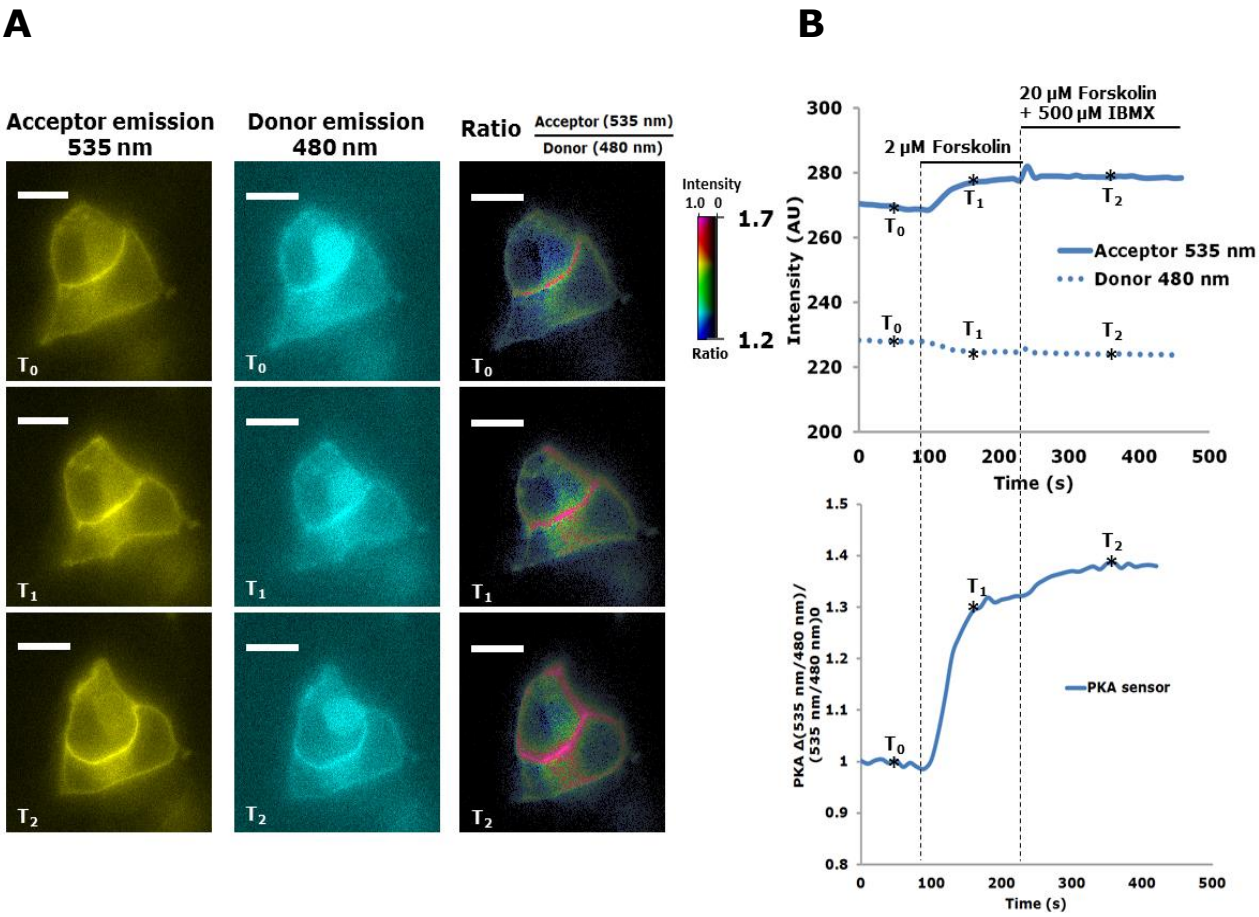

Figure 12: Representative emission and FRET ratio images of PKA membrane targeted reporters with the corresponding emission intensity and FRET ratio traces. A) HEK293 cells transfected with the cAMP membrane targeted reporter before the application of the

stimulus (T_0) and over time after addition of cAMP increasing stimuli (T_1 and T_2). 2 µM forskolin followed by 20 µM forskolin and 500 µM IBMX, to saturate the sensor, were applied as indicated. Shown are the cells imaged at emission wavelengths of 535 and 480 nm and the matching ratio images. Note that no background subtraction was performed for these images. Scale bars represent 10 µm. B) Donor and acceptor fluorophore emission intensity traces (top panel) and representative normalised and background subtracted FRET ratio trace (lower panel). The fluorescence intensity traces represent the average fluorescence values measured over the entire cell over time. Asterisks (T_0-T_2) indicate time points at which images shown in A were acquired. Data shown confirms the response of membrane targeted PKA reporters expressed in HEK293 cells, to cAMP increasing stimuli (representative trace of N=16 showing comparable results).

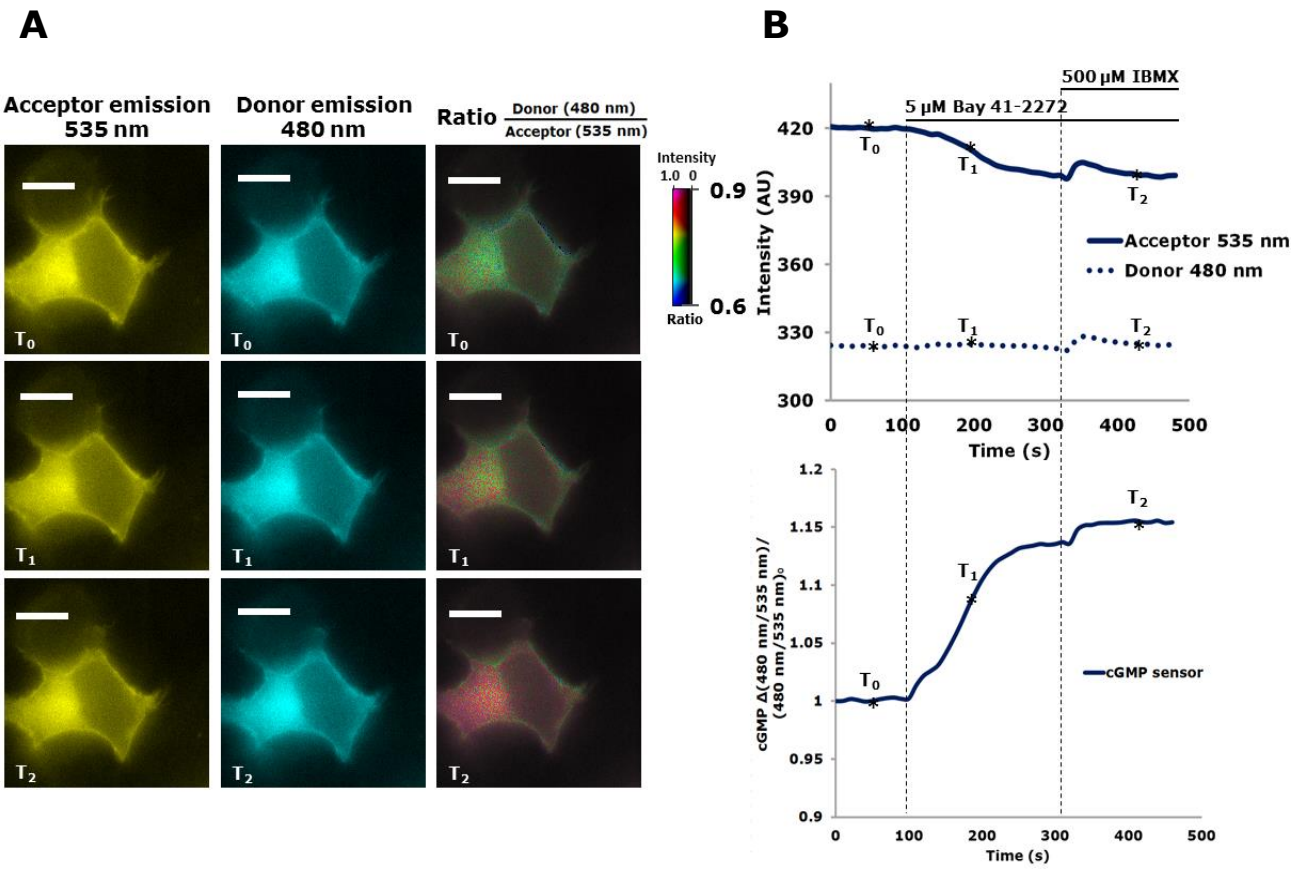

Figure 13: Representative emission and FRET ratio images of cGMP membrane targeted reporters with the corresponding emission intensity and FRET ratio traces. A) HEK293 cells transfected with the cGMP membrane targeted reporter before application of the stimulus

(T_0) and over time after addition of cGMP increasing stimuli (T_1 and T_2). 5 µM Bay 41-2272 followed by 5 µM Bay 41-2272 and 500 µM IBMX, to saturate the sensor, were applied as indicated. Shown are the cells imaged at emission wavelengths of 535 and 480 nm and the matching ratio images. Note that no background subtraction was performed for these images. Scale bars represent 10 µm. B) Donor and acceptor fluorophore emission intensity traces (top panel) and representative normalised and background subtracted FRET ratio graph (lower panel). The fluorescence intensity traces represent the average fluorescence values measured over the entire cell over time. The time point at which images shown in A were acquired is indicated by the asterisks (T_0-T_2). Data shown confirms the response of membrane targeted cGMP reporters expressed in HEK293 cells, to cGMP increasing stimuli (representative trace of N=7 showing comparable results). Bay41-2272 is a direct activator of sGC. Note that for convenience the cGMP FRET ratio traces and images were calculated as donor emission divided by acceptor emission intensity, to represent the increase in cGMP concentration as an increase of the FRET ratio.

3.3 Optimizing human pulmonary microvascular endothelial cell culture conditions for FRET microscopy

We wanted to express the membrane and cytosolic FRET sensors (refer to 3.2) in endothelial cells, to increase our understanding of the relation between CN compartmentalisation and endothelial barrier function.

In its early stages, this project was a collaboration between Novartis and the Zaccolo group. The interest of Novartis in this project lay in the premise of uncovering new GPCRs in the human pulmonary microvasculature, which could be investigated as potential drug targets. Novartis wanted to determine the GPCRs expressed by hPMECs and obtain a better understanding of how these GPCRs may regulate barrier function, by for example affecting cellular

cAMP. This knowledge would finally enable identification GPCRs who's function could be modulated, to ameliorate endothelial barrier dysfunction[301,302]. We wanted to express our FRET sensors in human pulmonary microvascular endothelial cells to gain a better understanding of subcellular cAMP regulation in endothelial cells and the possible relation to endothelial barrier function, as part of the Novartis collaboration. In addition, cAMP compartmentalisation within lung endothelium and more specifically within hPMEC has never been shown. As the hPMECs had never before been used in FRET experiments, we set out to optimize cell culture conditions in order to obtain reproducible and reliable results.

3.3.1 Cell culture conditions optimisation for the human pulmonary microvascular endothelial cell line

The Zaccolo group had no previous experience with the hPMEC cell line. Therefore, we initially adapted the same approach towards FRET experiments in hPMEC as we would have done for other generally used cell lines.

Generally, cells were kept in a physiological HEPES-buffered salt solution during FRET experiments. However, hPMEC expressing FRET biosensors were shown to have very slow kinetics of FRET shift and drastic shrinkage when kept in this physiological solution (data not shown). We therefore assessed how hPMECs performed if kept in the medium recommended by the supplier for this cell type.

From the start, we omitted the pH indicator phenol red in medium used for

FRET experiments. We did this because phenol red has been shown to autofluoresce. This autofluorescence would interfere with our FRET measurements.

The basal cell culture medium was bicarbonate buffered and designed to maintain a physiological pH under cell culture conditions at 37°C and 5 % CO_2. Under normal atmospheric conditions this buffer alkalizes, thus we compared it to the same medium supplemented with 28 mM HEPES, as suggested by the supplier. The HEPES buffering system is not affected by atmospheric CO_2 levels and should be more able to maintain a physiological pH under atmospheric CO_2 concentrations. As FRET experiments usually took about half an hour we investigated the effect of HEPES or bicarbonate buffered medium on hPMEC cell morphology and medium pH, under atmospheric (0.04% CO_2 and room temperature) or cell culture conditions (5 % CO_2 at 37°C; Figure 14A). We pooled three samples for each of the four conditions and measured the pH. After 0.5 and 1 h we observed an increase in shrunken and floating cells in bicarbonate buffered medium, suggestive of decreased cell viability. We confirmed that the pH of bicarbonate buffer medium kept under atmospheric conditions increased over time, whereas the HEPES buffered medium maintained the physiological pH around 7.4, comparable to hPMECs kept under cell culture conditions without HEPES.

As we ultimately wanted to image hPMEC using the FRET reporters, we next tested the effect of sources of variability, including addition of HEPES to basal medium, on the reproducibility of FRET experiments. Another factor that we took into account was the presence of serum, which the basal hPMEC medium contained. Although serum is a commonly used additive in cell culture media,

the concentrations and specific substances in serum have not been defined accurately, because it is directly drawn from bovine foetus blood and thus its composition can vary among different batches[303]. As we had no knowledge of the exact components of foetal bovine serum, we could not exclude the possibility of auto fluorescence. Furthermore, serum could contain components that could act as ligands for hPMEC expressed receptors. Triggering undesired signalling cascades by serum could have falsified our FRET experimental data or interfered with the reproducibility of experiments.

To assess the effect of serum and HEPES on FRET measurements, we tested different conditions, with or without HEPES and serum, respectively. This approach enabled us to tease out whether omission of serum or HEPES altered our FRET measurements. Figure 14B (upper and lower panel) depicts our findings in terms of kinetics and the reproducibility of FRET responses upon addition of CN increasing stimuli.

We found no significant differences in FRET ratio shifts or traces between conditions with or without serum or HEPES, respectively, in hPMEC (Figure 14B). As depicted by representative curves in Figure 14B, HEPES and/or serum omission did not affect the sensor kinetics or the FRET change upon addition of cAMP-increasing agents, forskolin and IBMX. Regardless, as variability between experiments should be kept to a minimum and we did not know how serum may interfere with other stimuli, we decided to perform all further experiments in hPMEC in phenol red free basal medium without serum. We also added 28 mM HEPES to cell culture medium that we used in FRET experiments, because it maintained the physiological pH and significantly improved cell morphology.

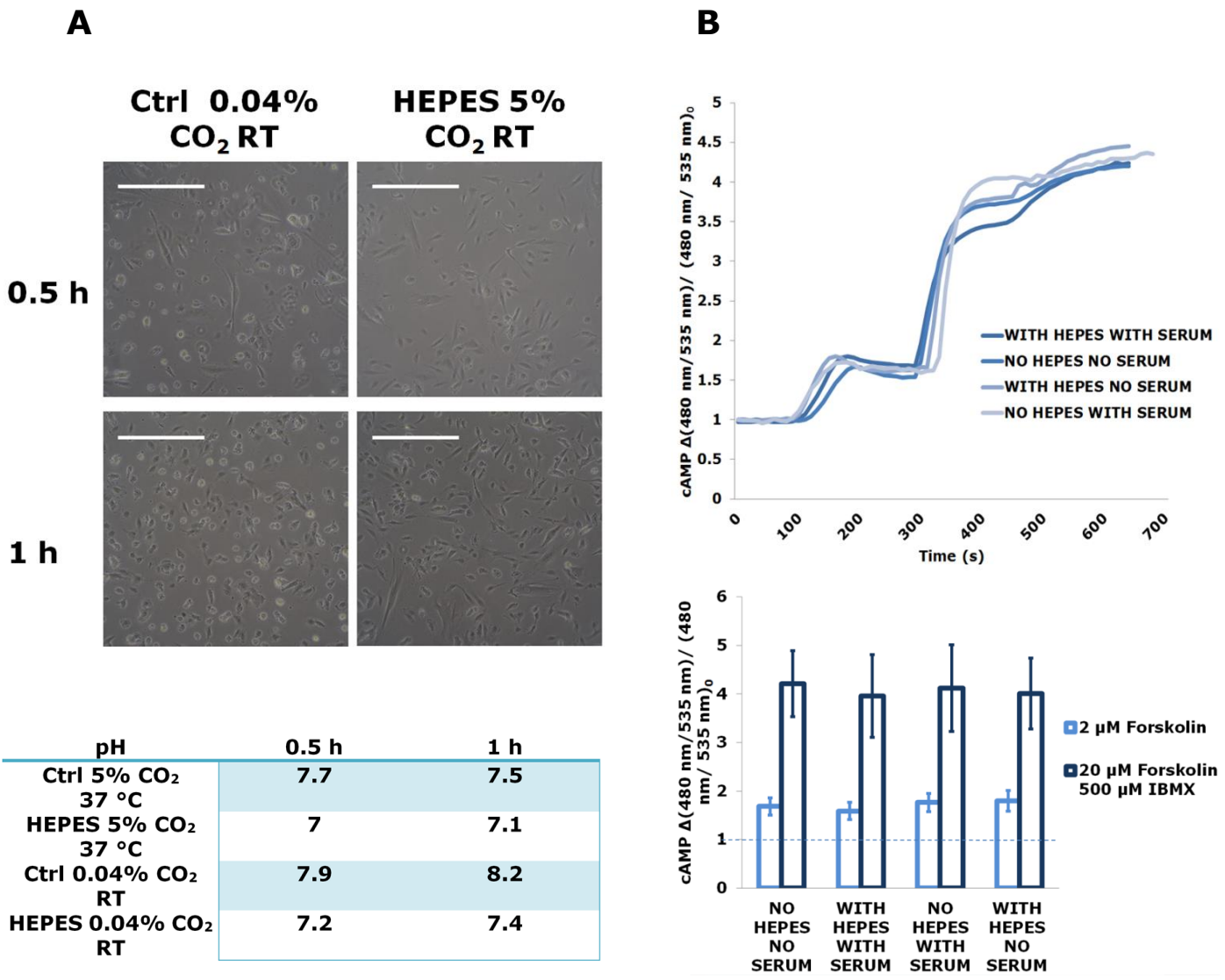

pH	0.5 h	1 h
Ctrl 5% CO_2 37 °C	7.7	7.5
HEPES 5% CO_2 37 °C	7	7.1
Ctrl 0.04% CO_2 RT	7.9	8.2
HEPES 0.04% CO_2 RT	7.2	7.4

Figure 14: Optimisation of culture conditions for the hPMEC cell line. A) hPMEC in basal medium at room temperature (RT) without HEPES, were compared to cells in basal medium with 28 mM HEPES at RT, as recommended by the supplier of the hPMEC line. Addition of HEPES improved the buffering capacity of the control bicarbonate buffer under RT experimental conditions. Scale bars represent 100 µm. B) FRET cAMP sensor response to stimuli in basal media containing serum or HEPES showed no significant differences between conditions (n≥13). The composition of serum is not well defined; therefore, omission of serum was tested as it may affect FRET changes. Error bars indicate s.d.

3.3.2 Dynamic range assessment of FRET sensors in human pulmonary microvascular endothelial cells

Once we had established culture conditions adequate for FRET experimentation, we needed to assess the maximal FRET change of the reporters in hPMEC. This was necessary because the maximal change of FRET, characteristic for the specific reporter and cell line, enables us to compare data from different cells. In addition, the maximum FRET ratio shift at the end of an experiment is a positive control for FRET reporter responsiveness.

In order to establish the stimuli required to achieve saturation of the sensors, increasing concentrations of forskolin and IBMX were added to hPMEC expressing cAMP or PKA reporters (Figure 15), to attain maximal cellular cAMP production through forskolin and minimal degradation of cAMP by PDEs by addition of IBMX.

Previously, it was found that 30 µM forskolin did not increase the FRET response any further in both sensors as well as 1 mM IBMX did not increase the FRET change above 500 µM IBMX (Data not shown). Therefore we chose 30 µM forskolin and 500 µM IBMX as maximal stimuli and investigated the effect on FRET ratio shift after addition of increasing doses of forskolin and IBMX together. Application of 20 µM forskolin and 500 µM IBMX to hPMEC cells expressing the cAMP reporter (Figure 15A) and 20 µM forskolin and 100 µM IBMX to cells expressing the PKA reporter (Figure 15B) was shown to be sufficient to achieve the maximal FRET change.

Overall, optimal conditions for further FRET experiments with hPMEC included

addition of 28 mM HEPES and the omission of serum. In addition, the concentration to saturate cAMP and PKA sensors was determined to be 20 µM forskolin and 500 µM IBMX. The same types of experiments would need to be done to assess the maximal saturation of the cygnet sensor albeit forskolin would be substituted by the direct activator of sGC, Bay41-2272.

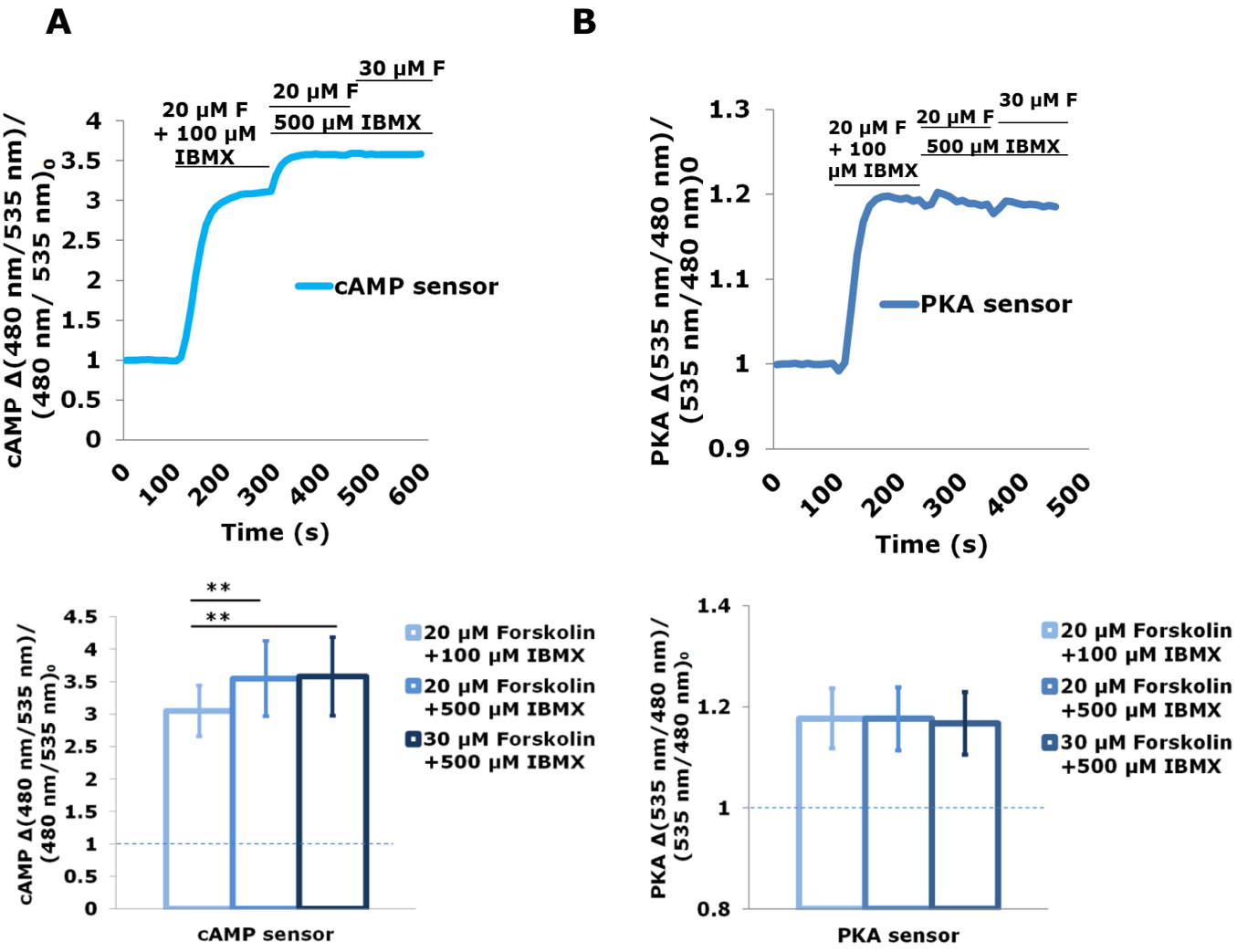

Figure 15: Assessment of the cytosolic FRET reporter saturation stimuli. A) Increasing doses of cAMP generating stimuli were added to hPMEC cells expressing the cAMP FRET sensor as shown in the bar graph and representative FRET ratio trace (n=16). ** P<.01 B) Increasing doses of cAMP generating stimuli were added to hPMEC cells expressing the PKA FRET reporter as shown in the bar graph and representative FRET ratio trace (n=17). Error bars indicate s.d.

3.4 Approaches to manipulate intracellular cytosolic cAMP

Once we established the FRET reporters and optimal cell culture conditions, we aimed to assess CN compartmentalisation in hPMEC and its effect on endothelial barrier function. As previously mentioned, several studies have reported that an increase in cytosolic cAMP reduced barrier function[118,119,299]. However, this correlation has never been shown in parallel in live hPMEC. We hoped, by using tools validated in previous studies, to be able to a) increase cytosolic cAMP and b) assess its effect on barrier function. We explored two such tools: the soluble adenylyl cyclase chimera (sACI/II)[119,261] and the near infra-red light activatable adenylyl cyclase (IlaC)[304]. First, we set out to prove that both the sACI/II and the IlaC were able to increase cytosolic cAMP concentrations.

3.4.1 The soluble adenylyl cyclase

In a previously published study a genetically engineered soluble adenylyl cyclase (sACI/II) was expressed in rat pulmonary microvascular endothelial cells[119]. The employed sACI/II chimera was generated by fusing the amino-terminal portion of the catalytic loops of mammalian transmembrane AC type I (C1a) and II (C2a) with an amino acid linker[119] (Figure 16A).

Sayner et al.[119] showed that after treatment of sACI/II expressing cells with 100 µM forskolin, a small yet significant increase in the cytosolic cAMP pool was observed, as assessed by a radioimmunoassay. The cAMP concentration at

the cellular membrane showed no change. This localised shift in cAMP led to interendothelial gap formation, indicative of barrier dysfunction and epithelial lung compartmentalisation. In their studies, Sayner et al. indirect evidence of compartmentalisation directly demonstrated compartmentalisation and its effect on barrier function[118,119]. Therefore, we aimed to directly test presence of compartmentalisation by employing the sACI/II and FRET methodology.

We set out to co-transfect sACI/II with the cAMP FRET reporter into human bronchiolar epithelial (HBE) cells. Then we stimulated cells with increasing doses of forskolin to monitor cytosolic FRET ratio changes. Compared with HBE only expressing the cAMP reporter, we expected to see an increase in FRET shift.

HBE cells co-transfected with the cAMP reporter and sACI/II (ratio 1:1 and 1:3, respectively) showed no significant differences in the FRET ratio changes compared to cells only expressing the cAMP reporter (Figure 16B). This suggested that the sACI/II did not increase the cytosolic cAMP generated in HBE. The levels of cytosolic cAMP produced seemed wholly attributable to the endogenously expressed membrane-bound ACs, also stimulated by treatment with forskolin.

We tested the sACI/II in HBE cells, because unlike hPMEC, they were transfectable. In addition, compartmentalisation had previously been shown in HBE cells[305]. This was interesting to us, as the follow up experiment would have been a co-transfection with sACI/II and the membrane targeted cAMP reporter. We expected to see no difference in FRET shift between cells with only the reporter or the reporter and sACI/II upon stimulation with increasing doses of forskolin.

Unfortunately, we found no significant increase in cytosolic cAMP due to sACI/II expression in HBE. We concluded that his method could not be used to generate increased levels of cAMP at specific cellular localisations (Figure 16B). Therefore, we moved on to investigate the IlaC's potential to specifically increase cytosolic cAMP pools.

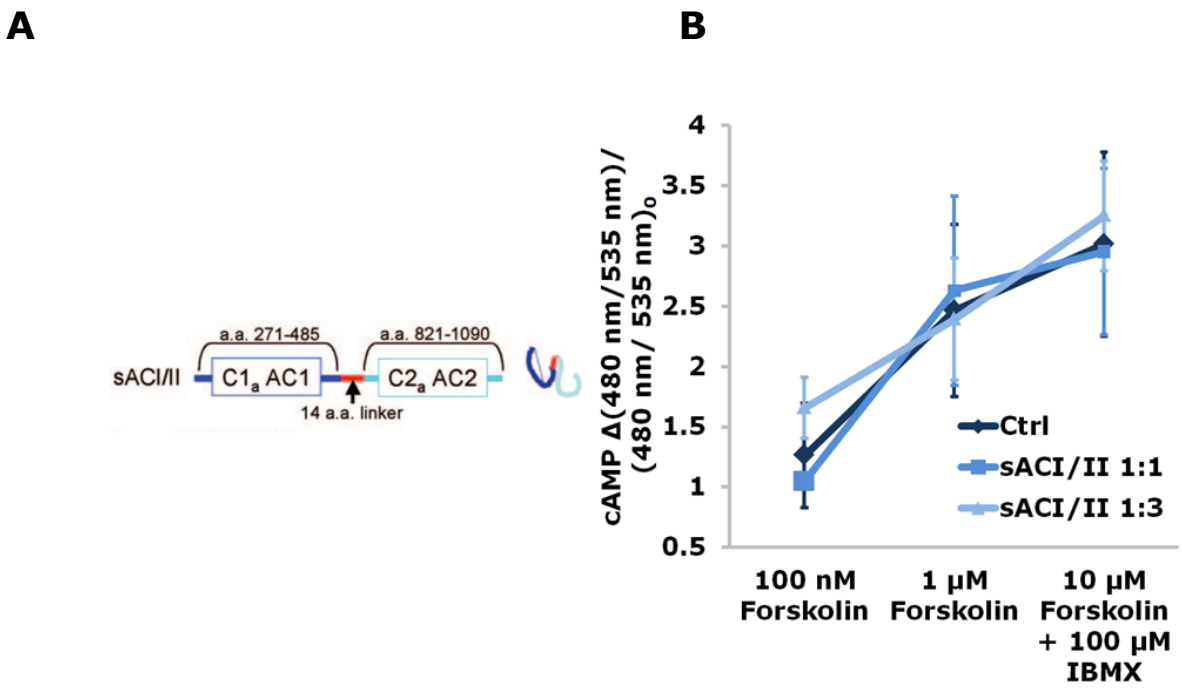

Figure 16: Assessment of sAC as a tool to investigate compartmentalisation within cells. A) Schematic overview of the DNA sequence of the sACI/II, comprised of the two catalytic loops $C1_a$ and $C2_a$ of the ACs 1 and 2, respectively. The two catalytic loops were joined by a 14 amino acid long linker and lacked the AC membrane targeting domains, which enabled it to remain in the cytosol. Image adapted from Sayner et al[119]. B) HBE cells were double-transfected with the cytosolic cAMP, sensor to have a readout for the cAMP-levels, and with sACI/II at a ratio of 1:1 and 1:3 (µg DNA), respectively. Control cells were only transfected with the cytosolic cAMP sensor. To see the expected differences in pool specific cAMP increase, the cells were treated with different concentrations of forskolin. One-way ANOVA showed no significant differences in FRET change between control cells and cells expressing sAC. n≥7 cells for both experimental and control conditions (transfected sACI/II 1:1, 1:3, and untransfected, respectively)

3.4.2 Infrared light-activated adenylyl cyclase

In the context of this project, we intended to explore the possibility of using a IlaC to generate specific cAMP pools in cells expressing cytosolic or membrane targeted FRET-reporters. Generation of cytosolic cAMP in combination with the FRET-TER chamber could enable us to assess whether increases in cytosolic cAMP induce permeability as suggested by Sayner et al[119]. By photo activating the IlaC and monitoring cAMP concentrations at different subcellular locations, with targeted FRET reporters, we would aim to determine the presence of cAMP compartmentalisation in hPMEC. The IlaC could also be targeted to different subcellular compartments via genetic tagging to generate local increases in cAMP. Targeted IlaCs could be used to investigate the effect of increased differentially localised cAMP pools on barrier function in the FRET-TER chamber.

The IlaC is a fusion protein comprised of a photosensory module (absorption maximum at 700 nM and general excitation spectrum between 600-750 nm) and a catalytic cAMP generating module, which form homodimers yielding the photoactivatable adenylyl cyclase (Figure 17)[304]. Excitation of the IlaC with light of approximately 700 nm in wavelength induces the IlaC to produce cAMP. Mammalian cells do not have proteins that absorb near-infrared light wavelengths, making near-infrared light harmless to mammalian tissue[304].

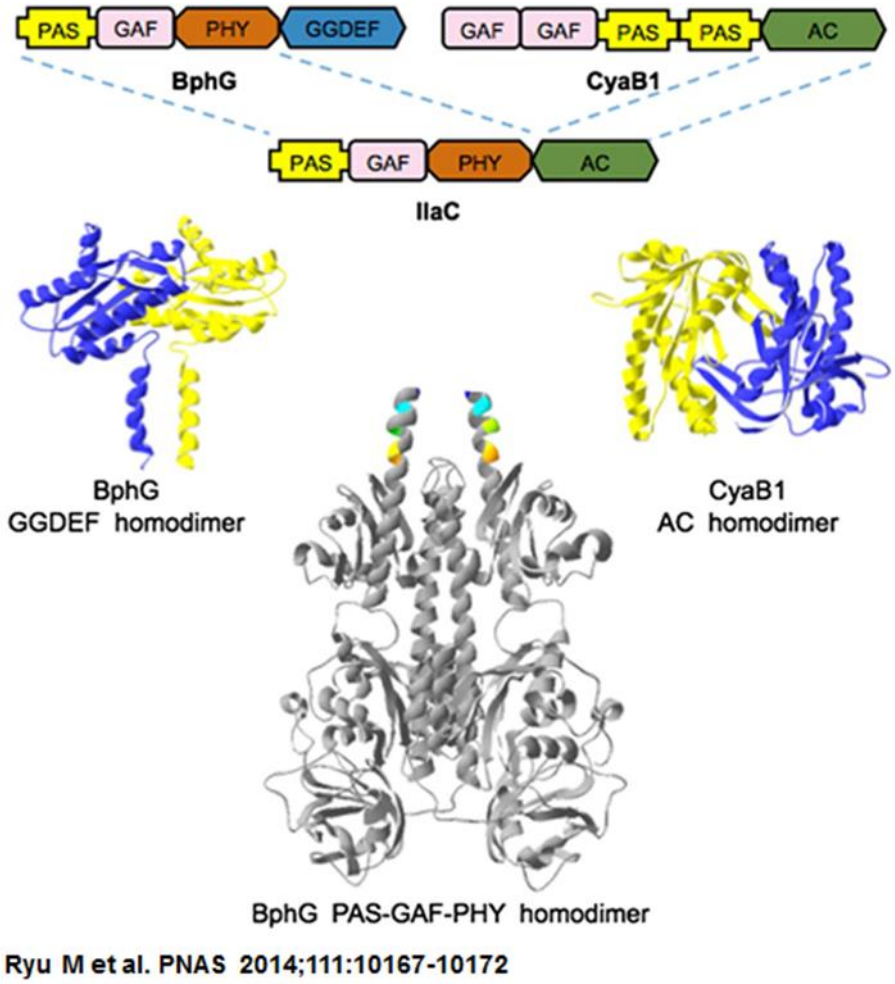

Figure 17: Domain architectures and 3D models of the components used in IlaC engineering. The PAS-GAF-PHY photosensory homodimer and the CyaB1 catalytic cAMP generating homodimer, which substituted the GGDEF module, make up the IlaC. The GGDEF homodimer is responsible for cyclic dimeric GMP production. *R. sphaeroides* BphG is bacteriophytochrome DGC; *Nostoc* sp. CyaB1 is homodimeric AC.

Additionally, the excitation wavelength of the IlaC does not overlap with the wavelengths necessary to work with our FRET reporters. This would have been a problem with a previously published photoactivatable AC, named bPAC[306]. bPAC's activation requires a wavelength that would also excite the donor chromophores of our FRET reporters. Thus, FRET imaging would result in

continuous production of cAMP, making experiments impossible.

The photosensory module from the *Rhodobacter sphaeroides 2.4.1* bacterophytochrome is a bacterial photoreceptor that is able to sense red/far red light using the biliverdin chromophore, which is naturally present in mammalian cells. The C-terminus of the *Rhodobacter sphaeroides 2.4.1* red light photosensory module was linked to the adenylyl cyclase catalytic domain. The catalytic site for cAMP production was taken from a bacterial adenylyl cyclase type III of the *Nostoc sp. PCC 7120* (for an overview refer to Figure 17)[304]. Upon excitation of the photosensory module, conformational changes occur, which activate the catalytic adenylyl cylase module, leading to cAMP production.

The DNA sequence of the IlaC had been codon optimised by Dr. Lyuksyutova (University of Wyoming) to enable expression in mammalian cells (Figure 18A depicts the obtained mammalian expression vector). The IlaC vector was a kind gift from Dr. Lyuksyutova (University of Wyoming). This construct had never been tested before in mammalian cells. In this vector, both the IlaC and mCherry are under the control of a cytomegalovirus (CMV) promoter. Bicistronic expression was enabled by fusion of the two genes of interest by a 2A peptide sequence (Figure 18A)[307]. This results in co-expression of mCherry and IlaC.

To validate expression of IlaC in a mammalian system, we transfected HEK cells with the IlaC vector (Figure 18B). As IlaC was co-expressed with mCherry, we validated mCherry by fluorescence microscopy and indirectly confirmed IlaC expression in transfected cells (Figure 18B). To activate IlaC and monitor changes in cytosolic cAMP we co-transfected HEK or HBE cells with the cAMP

FRET reporter. After validating expression of both IlaC and cAMP sensor (as shown in Figure 18B), we set out to optimize conditions for IlaC activation. Previously, IlaC had been expressed in bacteria and *C. elegans* and activated by illumination with generally available standard 660-700 nm light emitting diodes (LEDs)[304]. Bacteria were transfected with an IlaC and a *lacZ* gene under a cAMP-dependent promoter containing vector. Ilac/*LacZ* co-transfected bacteria showed fewer blue colonies when grown in the dark, than under illumination with 660 nm LEDs. This suggested an increased cAMP production under illuminated conditions, validating that the IlaC worked[304].

Further validation of the IlaC was obtained from studies in C. elegans. C. elegans expressing IlaC in their cholinergic neurons were exposed to red light for 30 seconds. This increased locomotion suggested an association between increased neuronal cAMP and movement in the worms[304].

Based on these previously published experiments, we decided to activate the IlaC in mammalian cells with two different light sources. First, we co-transfected HEK or HBE cells with both IlaC and cAMP FRET sensor, to monitor changes in cAMP by FRET microscopy over the course of the entire experiment (Figure 18C-D). Then we illuminated the cells with two different sources. The first was the built-in brighfield light bulb of the microscope, passed through a 600 nm long pass (LP) filter (Figure 18C). The LP filter ensured that cells were only illuminated by light above 600 nm. The second light source was a 660 nm LED, directly placed above the cells. The LED light was passed through a Texas Red filter, which allowed passage of light at 660-680 nm (Figure 18D).

Both types of experiments were conducted in the dark to exclude interference of other light sources with the FRET measurements and IlaC excitation. As

excitation of the cells by light above 600 nm did not interfere with our FRET measurements, we were able to monitor FRET changes in parallel with stimulating the IlaC.

We validated adequate cAMP FRET sensor reaction to increasing intracellular cytosolic cAMP levels by sensor saturation after initial illumination (Figure 18C anc 18D). However, we did not observe an increase in cytosolic cAMP for either illumination approach (Figure 18C and D). In the initial experiments we took images of mCherry expressing cells, before starting the actual experimental protocol, which is depicted in Figure 18C. Therefore, we cannot exclude that the slight change in FRET ratio change in Figure 18C is due to preliminary excitation with the built-in LED of the microscope. We were not able to reproduce this small FRET change in cells that were not exposed to the red LED light of the microscope before commencing the experimental protocol (data not shown).

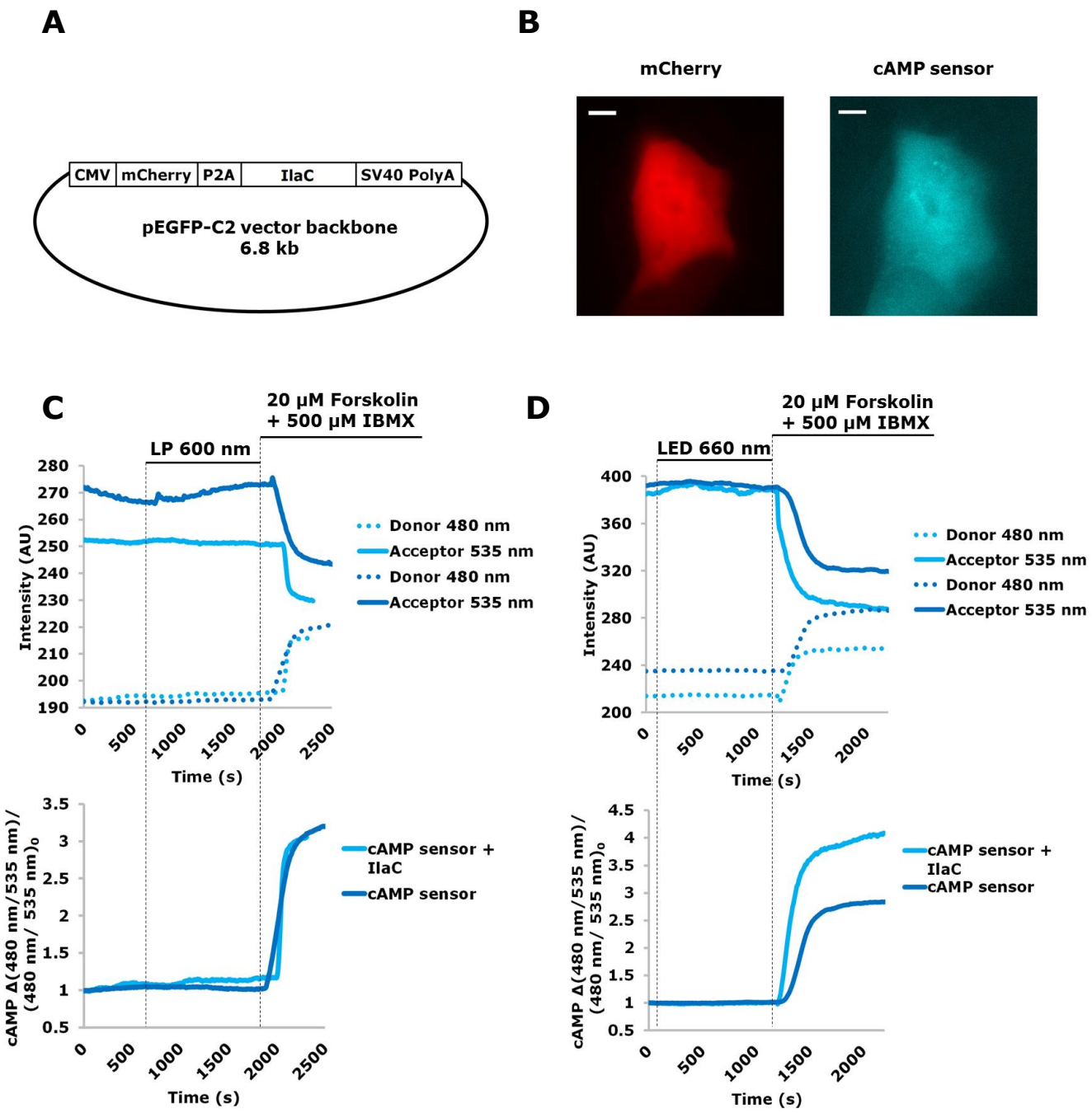

Figure 18: Assessment of IlaC as a tool to investigate compartmentalisation within cells. A) Schematic overview of the IlaC vector sequence comprised of the IlaC sequence, which is expressed in tandem with the mCherry fluorescent protein and cleaved via the peptide 2A in between the two sequences. The proteins were expressed under the mammalian cytomegalovirus (CMV) promoter. B) Cells were transfected with the cytosolic cAMP sensor to have a read-out for the cAMP levels, and with the IlaC vector at a DNA ratio of 1:1. Due to the mCherry and reporter fluorophores we were able to check for adequate co-transfection by fluorescence microscopy. Scale bars represent 10 µm. C) HBE cells transfected with the IlaC

and cAMP FRET reporter or only the cAMP reporter (control) were subjected to white light, passing through a 600 nm long pass (LP) filter as well as FRET microscopy to monitor changes in intracellular cAMP induced by light activation of the IlaC. At the end of each experiment the reporter was saturated with 20 µM forskolin and 500 µM IBMX to confirm adequate sensor function. The upper panel depicts emission intensity traces of the donor and acceptor fluorophores for the control (dark blue) and IlaC transfected cells (light blue). The lower panel depicts the accompanying background subtracted normalised FRET ratio traces (representative traces of n=3 and n=4 for IlaC and controls, respectively, showing comparable results). D) HEK cells transfected with the IlaC and cAMP FRET reporter or only the cAMP reporter (control) were subjected to 660 nm (emission peak) LED illumination, as well as FRET microscopy to monitor changes in intracellular cAMP induced by light activation of the IlaC. At the end of each experiment the reporter was saturated with 20 µM forskolin and 500 µM IBMX to confirm adequate sensor function. The upper panel depicts emission intensity traces of the donor and acceptor fluorophores for the control (dark blue) and IlaC transfected cells (light blue) and the lower panel the accompanying background subtracted normalised FRET ratio traces (representative traces of n=22 and n=9 for IlaC and controls, respectively, showing comparable results).

3.5 Approaches to measure endothelial permeability

We now had established the tools to assess spatiotemporal CN changes in live hPMEC, by generating targeted FRET reporters and optimizing cell culture conditions. However, these methodologies only allowed exploration of one part of this project: CN compartmentalisation. The next question was: how does CN compartmentalisation affect endothelial barrier function? To investigate the effect of intracellular CN changes on endothelial barrier function, we needed to apply barrier measurement assays. We set out to optimise cellular

immunostaining and FITC-dextran permeability assays to assess monolayer integrity.

3.5.1 Immunocytochemistry

We optimised cellular immunostaining of the hPMEC plasmamembrane with VE-cadherin, a well-known AJ marker. Protocols were optimised in order to stain VE-cadherin, actin fibres and the nuclei of hPMEC (Figure 19). Under confluent conditions, VE-cadherin antibody clearly stained VE-cadherin mediated cellular adhesions in a cellular monolayer; the same was true for phalloidin mediated staining of actin fibres. When cultured cells were sub confluent, the appearance of the cortical actin ring shifted to stress fibres and the VE-cadherin showed an interrupted pattern at the cell membrane as compared to confluent conditions (indicated by red arrows in Figure 19). We expected that the (sub) confluent condition could be mimicked by application of barrier disruptive GPCR ligands, such as thrombin. Therefore both the actin and VE-cadherin staining could be employed to assess differences in barrier integrity upon application of drugs that modulate cAMP levels.

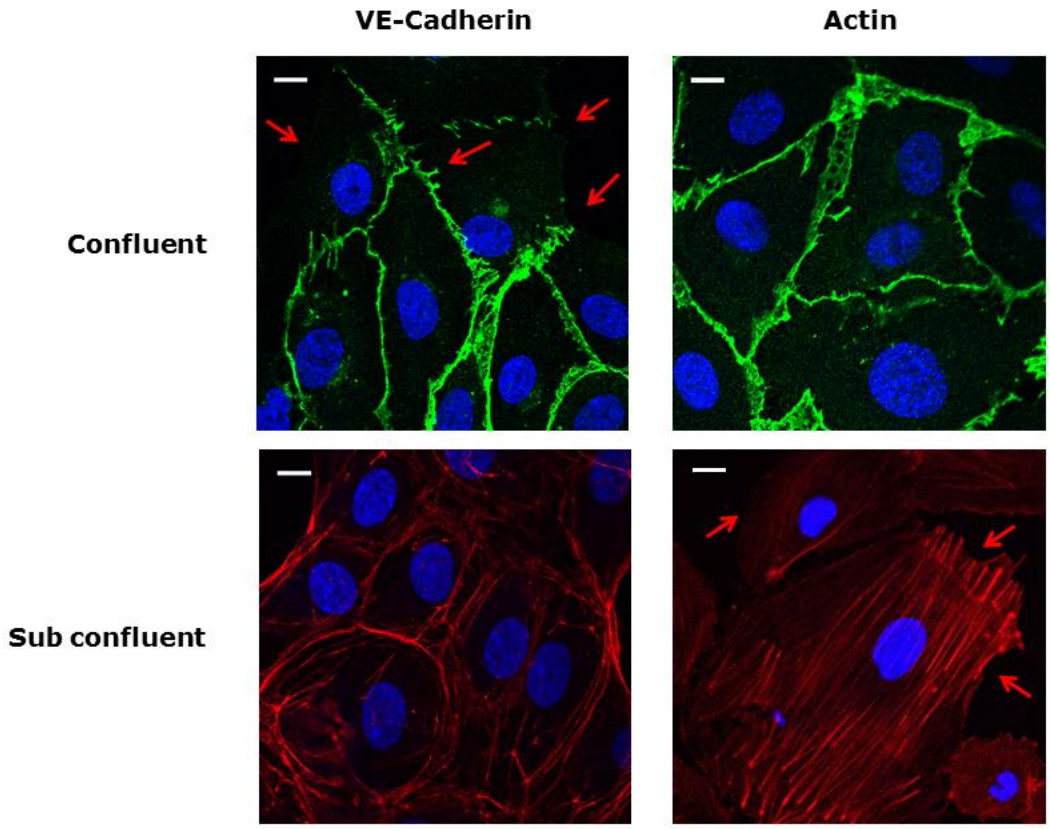

Figure 19: hPMEC fluorescently labelled for VE-cadherin and actin. hPMEC grown confluently or subconfluently on GF coated glass coverslips and stained with VE-cadherin antibody (green) or phalloidin against actin (red) and the nuclear DAPI stain (blue). Scale bars represent 10 µm.

3.5.2 FITC-dextran assays

Immunostaining would provide visual affirmation of changes in barrier function; however, it did not allow for a quantitative reading of cellular monolayer integrity. Therefore, we set out to optimise the FITC-dextran assay for hPMEC. Figure 20 illustrates the cell permeability for FITC-Dextran (40 kDa) of hPMEC seeded on coverslips uncoated or coated with a gelatin fibronectin (GF) mixture on 24 transwells over the course of 3 weeks. The permeability of cellular

monolayers grown on uncoated wells showed an increasing trend over 3 weeks, whereas the coated samples showed a decrease in permeability between week 1 and 2 and an increase in permeability after week 3. This would indicate that cellular barriers are most impermeable after 2 weeks, with a permeability of less than ~40% compared to control empty transwell inserts. Therefore, we assumed that experiments may be best performed within the first 2 weeks of seeding cells.

Notably, we compared the conditions to control samples, which were transwells without hPMEC grown on them, which may explain the 'high' cellular permeability under untreated conditions. Usually, in studies exploiting the FITC-dextran methodology, treatment conditions are compared to untreated cellular monolayers grown on transwells. Therefore, the permeability under basal conditions shown here may appear high; however, in publications the comparison with empty transwells is never made. Furthermore, the monolayer permeability is characteristic of the type of cells being investigated and their respective environments[16]. For example, studies have shown that brain barrier endothelial cells show higher endothelial resistance than microvascular endothelial cells[278,279,308,309]. Endothelial cell lines are known to form weaker junctions than endothelial beds *in vivo*, which may be due to the lack of shear stress and flow under cell culture conditions[308].

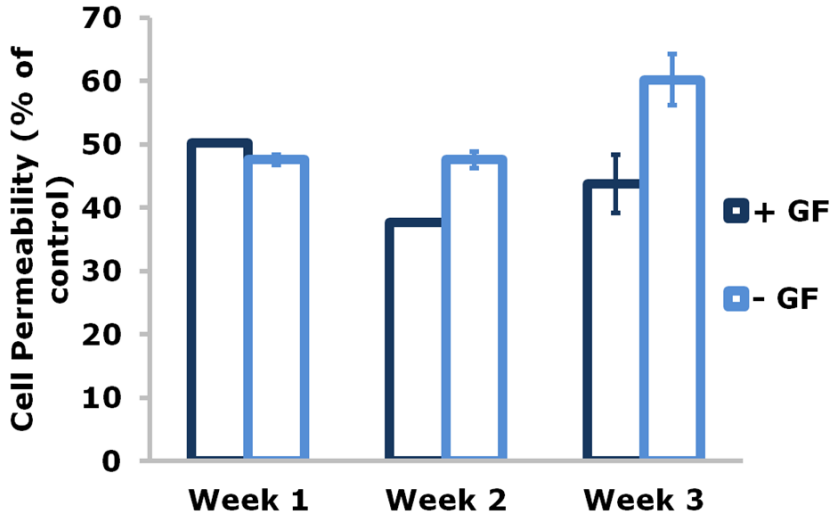

Figure 20: FITC-dextran assay optimisation for hPMEC. HPMEC seeded at a density of 4 x10^4 cells/well were grown on 24 transwell inserts with or without GF coating. Permeability was monitored over time by means of FITC-dextran assay. Samples were compared to control inserts that had no cells seeded on them N=1 with for each condition at least duplicate samples measurements.

3.6 Construction of a FRET-TER measurement chamber

The previous sections have discussed the establishment of several tools to investigate CN compartmentalisation in space and time in hPMEC, as well as the effect of CN modulation on barrier function. The established tools do not allow measurement of localised changes in CN in combination with barrier function changes. Until now, no methodology has been developed that allows simultaneous FRET measurements in addition to monitoring monolayer barrier function. Therefore, we set out to develop such an approach. We hoped to achieve this by monitoring simultaneously TER and FRET signals in one chamber.

3.6.1 Validation of FRET

The initial design of the FRET-TER chamber was based on a combination of methodologies: the FRET microscopy setup, the TER measurement probe EVOM^2 and FITC-dextran assays. As FRET experiments were usually conducted in a microscope setup that allowed for high resolution imaging, we needed to ensure clear visibility of the cells. This was provided by imaging of the cells through a glass plate and an appropriate objective. Usually cells for FRET experiments were grown on glass coverslips and imaged with a 40x oil immersion objective, which was in direct contact with the glass. However, this would not allow for TER measurements. TER is measured by placement of an electrode above and below the cells and measuring the current across the cells. However, cells grown on glass coverslips would not allow for placing an electrode below the cells, as the glass would obstruct any transendothelial resistance measurement. We solved this problem by using the general setup of a FITC-dextran permeability assay. We grew hPMEC on a transparent porous membrane of a 24 well insert, hung in a 24 well plate. Above and below the insert we placed the electrodes for TER measurements (refer to Figure 21A). Electrodes connected to the TER-measurement setup, were inserted into the chamber to measure cellular barrier function in living cells. The electrical signal of the resistance meter was then converted into a binary signal by the converter enabling us to obtain the read-out on a computer. Finally, the plastic bottom of the plate was substituted by a glass plate for imaging. In this design, the cells were further away from the objective than originally. The short distance, oil immersion objective that is normally used for FRET imaging was therefore not

fit to image the cells anymore. We acquired an air 40x long distance objective instead, that allowed us to bridge the distance between the glass plate and cells. A schematic overview of the final FRET-TER chamber is depicted in Figure 21A.

One of the challenges we encountered was poor visibility with brightfield microscopy of cells grown on transwell inserts (Figure 21B, left panels). This was at least in part due to the morphology of hPMEC, which are wide and very flat. We came to the conclusion that we needed to “colour” the cells somehow to see them better. As they were ultimately going to express FRET reporters, we decided to use the reporters as an indication of confluency, and thus establishment of barrier function of the monolayer (Figure 21B right panels). Therefore we seeded cells onto the transwells and infected them with cAMP reporter adenoviral particles to assess how long after seeding the cells, confluence was reached. We found seeding 4 $x10^4$ hPMEC cells yielded a confluent monolayer after 3 days in culture (Figure 21B). This was in line with the observation that experiments with hPMEC on transwell inserts were best conducted within the first two weeks of seeding hPMEC (Figure 20).

Another factor in cell growth was coating of the porous membranes. The hPMEC did not adhere well to the surface of the porous membranes (Figure 21B, upper panel), making growth of a cellular monolayer virtually impossible. Therefore we tried coating the porous membranes with a gelatin and fibronectin (GF) solution prior to cell seeding. This coating was also used for growing hPMEC on glass coverslips for FRET experiments. We found that the GF coating significantly improved monolayer formation of the hPMEC (Figure 21B, compare upper and lower panels).

Originally, we started measuring the TER of hPMEC grown on inserts with a probe called EVOM^2. The probe consisted of two small disc shaped electrodes, each mounted on a flexible prong. When measuring TER, it was crucial that the distance between the electrodes remained the same. Changes interfered with the resistance measured, as the resistance increased with the distance between the electrodes. Due to the flexibility of the prongs, which needed to be held by hand, and the small size of the electrodes, our measurements showed high variability (data not shown), which did not allow us to make any assessment of the barrier function of the cellular monolayer. Although measurements of the barrier function were highly variable, the TER did not seem to exceed 30 $\Omega \cdot cm^2$ (data not shown).

Therefore we amended the design of the electrodes in the FRET-TER chamber (refer to Figure 21A). In Figure 21A, the electrodes for TER measurements are depicted as two parallel rings, above and below the cellular monolayer. These electrode rings were connected to a rigid structure, minimizing the movement of the electrodes during TER measurements. In addition, the rings spanned the whole surface of the membrane, measuring TER over a larger surface than the two small electrodes of the EVOM^2. These adaptations allowed us to measure the TER of the hPMEC monolayer more accurately and consistently over time. To assess whether the 40x magnification long distance objective (40x LD) was suitable for the envisioned FRET setup, we used it to image hPMEC grown on a 24 transwell insert, coated with GF and expressing the cytosolic cAMP reporter (Figure 21C). Upon saturation of the sensor we obtained a response comparable to previous results (compare Figure 21C with Figure 8D and 11B). From these preliminary experiments we concluded that GF coated transwell

inserts in combination with the 40x LD objective were a satisfactory starting point to investigate presence of compartmentalisation in hPMEC. Further validation of the applicability of the complete setup for parallel FRET-TER measurements is presented in chapters 3.7.2 and 3.7.3.

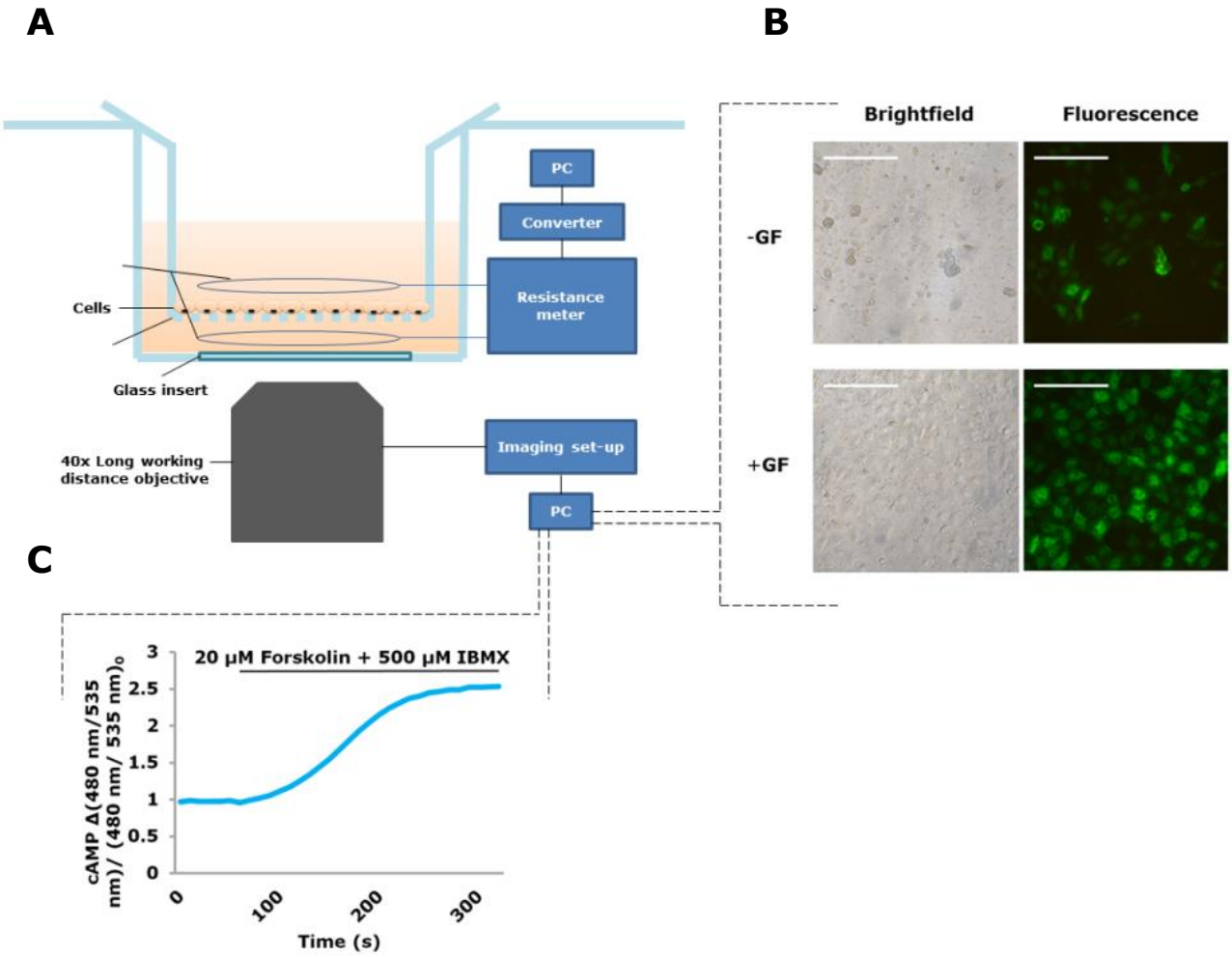

Figure 21: Validation of FRET ratio measurments in the FRET-TER measurement setup. A) Schematic overview of the chamber allowing parallel measurement of resistance in a cellular monolayer and live cell FRET imaging. B) Evidence for hPMEC growth expressing cytosolic cAMP sensor, on 24 transwell inserts with gelatin-fibronectin (GF) coating compared to cells grown on inserts without coating. C) Representative FRET trace confirming response of cytosolic cAMP reporter in hPMEC grown on GF coated inserts as monitored by the 40x LD

objective upon a saturating stimulus of 20 µM forskolin and 500 µM IBMX, which induced a 2.37± 0.36 (n=9) fold change increase in emission ratio.

3.7 Preliminary investigations into cAMP compartmentalisation in hPMEC

In the previous results chapters we demonstrated the tools that allowed us to monitor CN changes in space and time and endothelial barrier function in hPMEC, both separately and in parallel. With these tools and various GPCR ligands that have been shown to modulate endothelial barrier resistance, we set out to investigate the presence of CN compartmentalisation in hPMEC and the association with barrier function.

3.7.1 Adenosine

Adenosine is an endogenous GPCR ligand within many physiological functions. Within the context of endothelial lung barrier function, adenosine has repeatedly been shown to enhance barrier function, most probably by modulating intracellular cAMP concentrations[310–312]. As previously mentioned, evidence suggests that cAMP increase in the cytosol decreases barrier function, whereas membranous cAMP enhances it[118,119]. Intuitively, the barrier protective effect of adenosine would therefore result from a membranous cAMP increase. In order to assess whether adenosine would also affect cytosolic cAMP, we treated hPMEC expressing either the cytosolic cAMP or PKA FRET reporter with adenosine.

We treated hPMEC with adenosine and found a small but reproducible increase in FRET ratio of the cytosolic cAMP reporter in hPMEC (Figure 22A, lower panel, and 22C), following stimulation with 10 µM adenosine. This was confirmed by the observed decreases in donor emission intensity and increases in acceptor emission intensity and FRET ratio shift (Figure 22A, lower panel, and 22C). As one PKA protein can phosphorylate more than one target site, or in this case FRET sensor module, an amplification of FRET ratio shift for the PKA sensor would have been possible. However, we did not observe any change in FRET compared to baseline (Figure 22B and D). Repetition of experiments to validate these findings is necessary. Additional necessary experiments would include micro-perfusion to establish FRET dose-response curves for both cytosolic and membrane targeted reporters. This would allow for direct comparison between the targeted reporter responses and enable us to validate cAMP compartmentalisation in hPMEC, by observing differential responses.

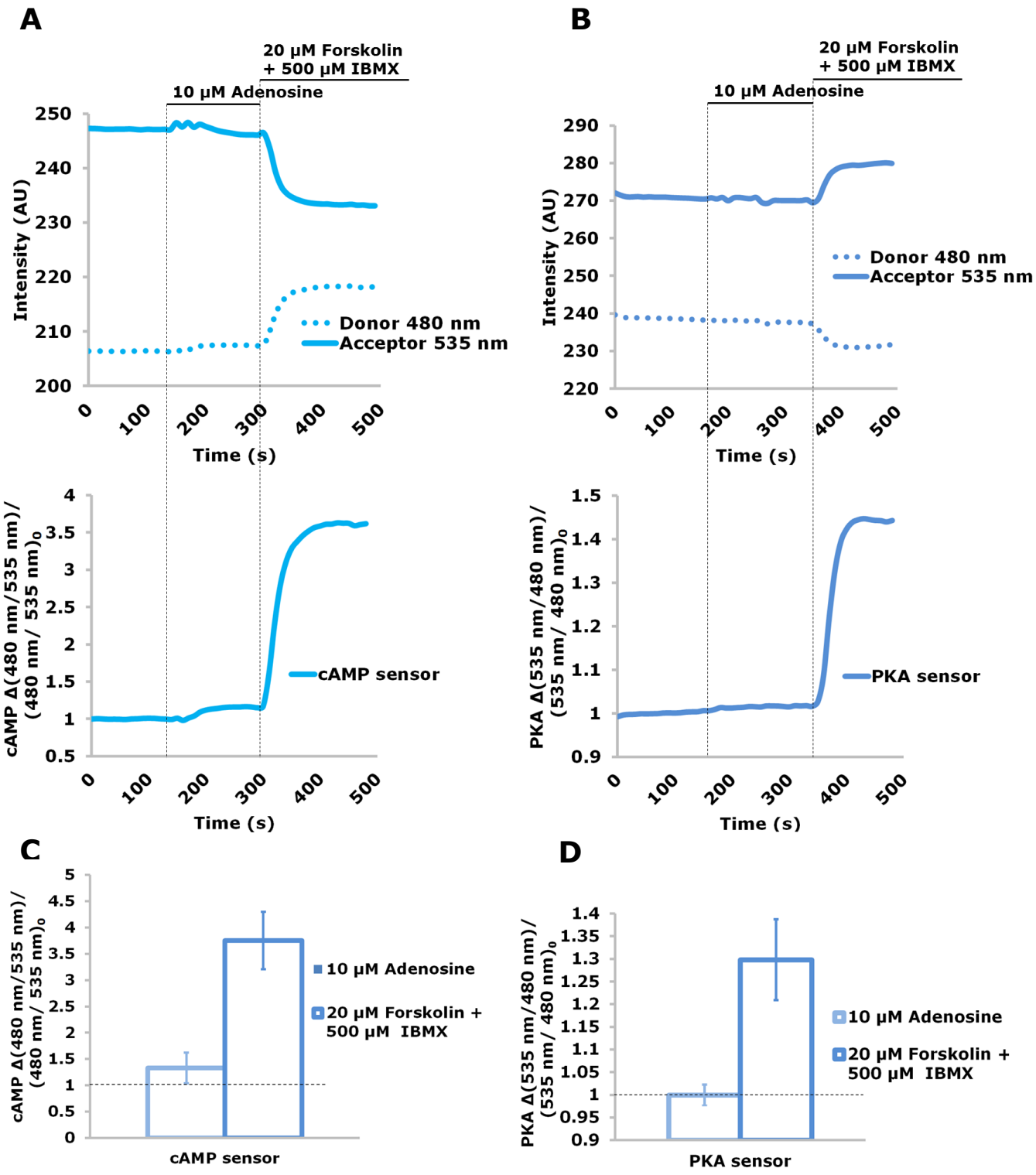

Figure 22: Assessment of cytosolic cAMP levels and PKA activation after hPMEC treatment with adenosine. hPMEC cells were infected with adenovirus particles of the cAMP or PKA cytosolic FRET reporters, respectively, and stimulated sequentially with 10 µM adenosine and 20 µM forskolin with 500 µM IBMX. A) Donor and acceptor fluorophore emission intensity shifts of the cAMP reporter over time, after addition of the indicated stimuli (upper

panel); the lower panel depicts a representative normalised and background subtracted FRET ratio trace (representative trace of n=21 showing comparable results). Note that for convenience the cAMP FRET ratio traces and images were calculated as donor emission divided by acceptor emission intensity, to represent the increase in cAMP concentration as an increase of the FRET ratio. B) Donor and acceptor fluorophore emission intensity shifts of the PKA reporter over time after addition of the indicated stimuli (upper panel); the lower panel depicts the accompanying representative normalised and background subtracted FRET ratio trace (representative trace of n=15 showing comparable results). C-D) Bar graphs depicting the findings from A and B; n=21 and n=15 for cAMP and PKA reporters expressed in hPMEC, respectively.

3.7.2 Histamine

Histamine is an endogenous GPCR agonist, most well-known for its role in immune modulation and allergic reactions. Additionaly, histamine has been shown to decrease barrier function and induce intercellular gaps in several vascular cell models and *in vivo*[32,225,313–315].

We were interested to see how histamine affected barrier function and cAMP production in hPMEC. We found no significant change in cytosolic cAMP production in hPMEC upon stimulation with 10 µM histamine after pre-stimulation with 2 µM forskolin in hPMEC (Figure 23A-C). Interestingly, we did observe sequential increases in endothelial monolayer resistance after addition of forskolin, histamine and the saturating stimulus, suggesting a cAMP independent increase in barrier function (Figure 23D; for the normalised trace refer to supplemental Figure S1). Immediately after forskolin and histamine

stimulation we observed a significant transient decrease and increase in resistance, respectively, which we identified as possible artefacts (Figure 23D).

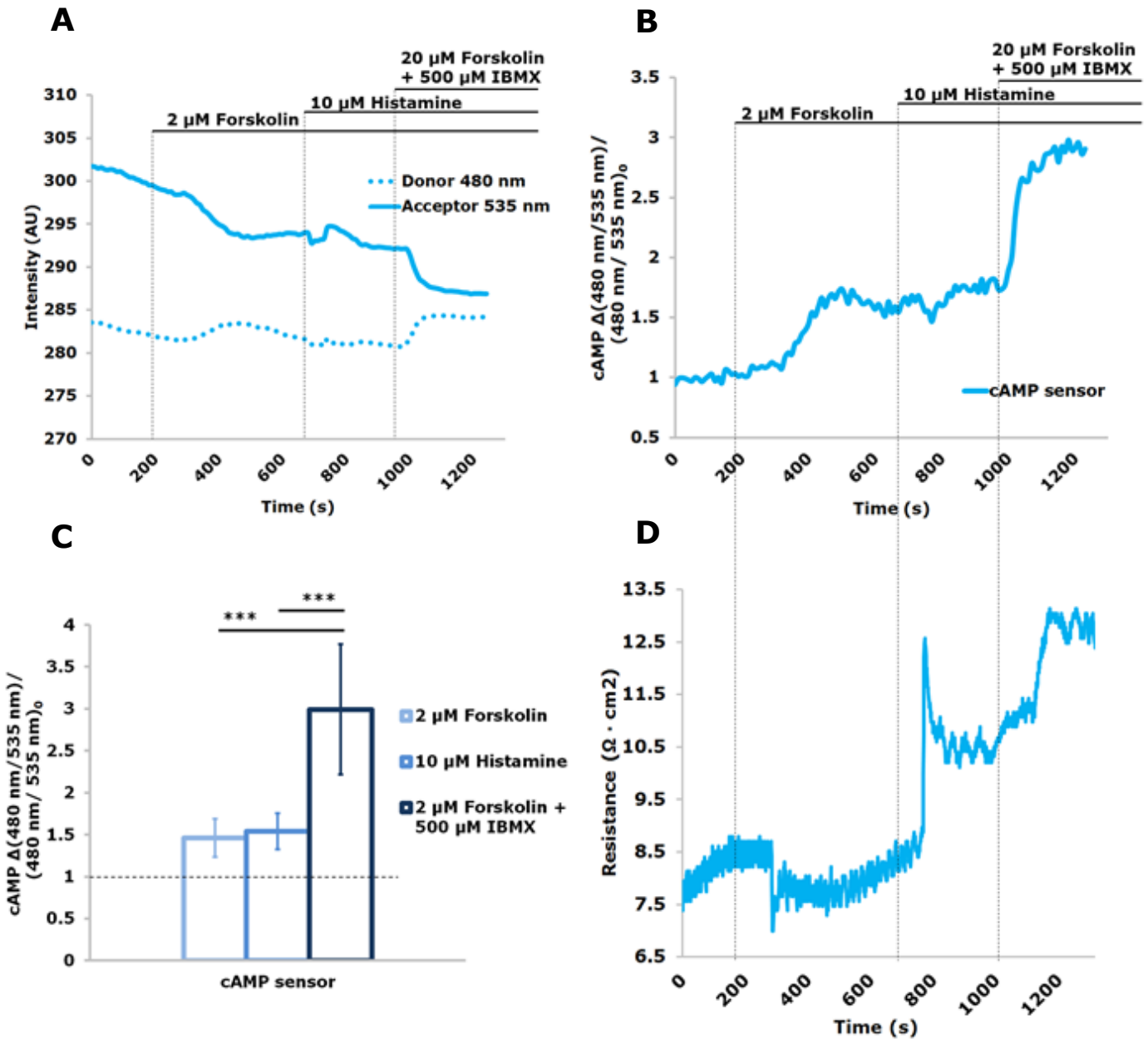

Figure 23: Assessment of barrier function and cytosolic cAMP levels after hPMEC treatment with histamine. hPMEC cells were infected with adenovirus particles of the cAMP cytosolic FRET reporter and stimulated with 2 µM forskolin, 10 µM histamine and 20 µM forskolin with 500 µM IBMX, respectively, whilst being monitored in the FRET-TER chamber. A) Donor and acceptor fluorophore emission intensity shifts over time after addition of indicated

stimuli. B) Representative normalised and background subtracted FRET ratio graphs stimuli (representative trace of n=6 showing comparable results). Note that for convenience the cAMP FRET ratio traces and images were calculated as donor emission divided by acceptor emission intensity, to represent the increase in cAMP concentration as an increase of the FRET ratio. C) Bar graph depicting the findings from A and B; n=6 and $P<0.001$. D) Representative trace of n=2, showing a comparable result of changes in TER over time after addition of 2 µM forskolin, 10 µM histamine and 20 µM forskolin with 500 µM IBMX, respectively.

3.7.3 Thrombin

Thrombin has been shown to increase permeability in endothelial cells[16,316]. The accompanying expected decrease in cAMP has not been firmly established. Several radio-immunobased assays have shown a cAMP decrease in endothelial cells after 5 minutes of thrombin treatment [317,318]. This is in stark contrast with more recent FRET based findings that indicate a thrombin induced transient cAMP decrease, followed by a cAMP increase in endothelial cells[319,320]. FRET and immono-assay findings cannot be compared directly because of their different underlying principles. Whereas immunobased approaches are representative of a single point in time of whole cell cAMP, the FRET methodology offers accurate measurements of small cAMP changes with high temporal resolution in single living cells. Due to these discrepancies in results, we set out to investigate the relationship between thrombin decreased barrier function and cellular cAMP in the FRET-TER chamber. Additionally, as thrombin has firmly been established as an endothelial permeability inducing agent, we used it as a control in our FRET-TER chamber to confirm adequate

resistance measurements.

hPMEC expressing the cAMP reporter were initially treated with 2 µM forskolin, as a previous report indicated that thrombin may couple to a G_i protein[321]. In this case we would expect to observe a cytosolic decrease in cAMP. The forskolin-mediated cAMP increase would enable us to observe the cAMP reducing effect of AC inhibition through G_i protein coupling. Unexpectedly, we found that 10 U/ml thrombin significantly increased the normalised FRET ratio, after an initial small transient decrease of cAMP, indicating a significant increase in cytosolic cAMP (Figure 24A-C). This finding coincided with a decrease in cellular monolayer resistance, reflected in a decrease of TER (Figure 24D; for the normalised trace refer to supplemental Figure S1). The TER trace showed the same continuous oscillations as previously observed in the histamine experiments. This apparent “noise” might be due to the fact that we are measuring resistance by applying a direct current, which is then transmitted to a PC that works on an alternating current. Notably, the TER baseline showed a decreasing trend before stimulation, which was stabilized after stimulation of the cells with 2 µM forskolin. We observed this repeatedly. In addition, immediately after thrombin stimulation we observed a significant transient peak in resistance (Figure 24D).

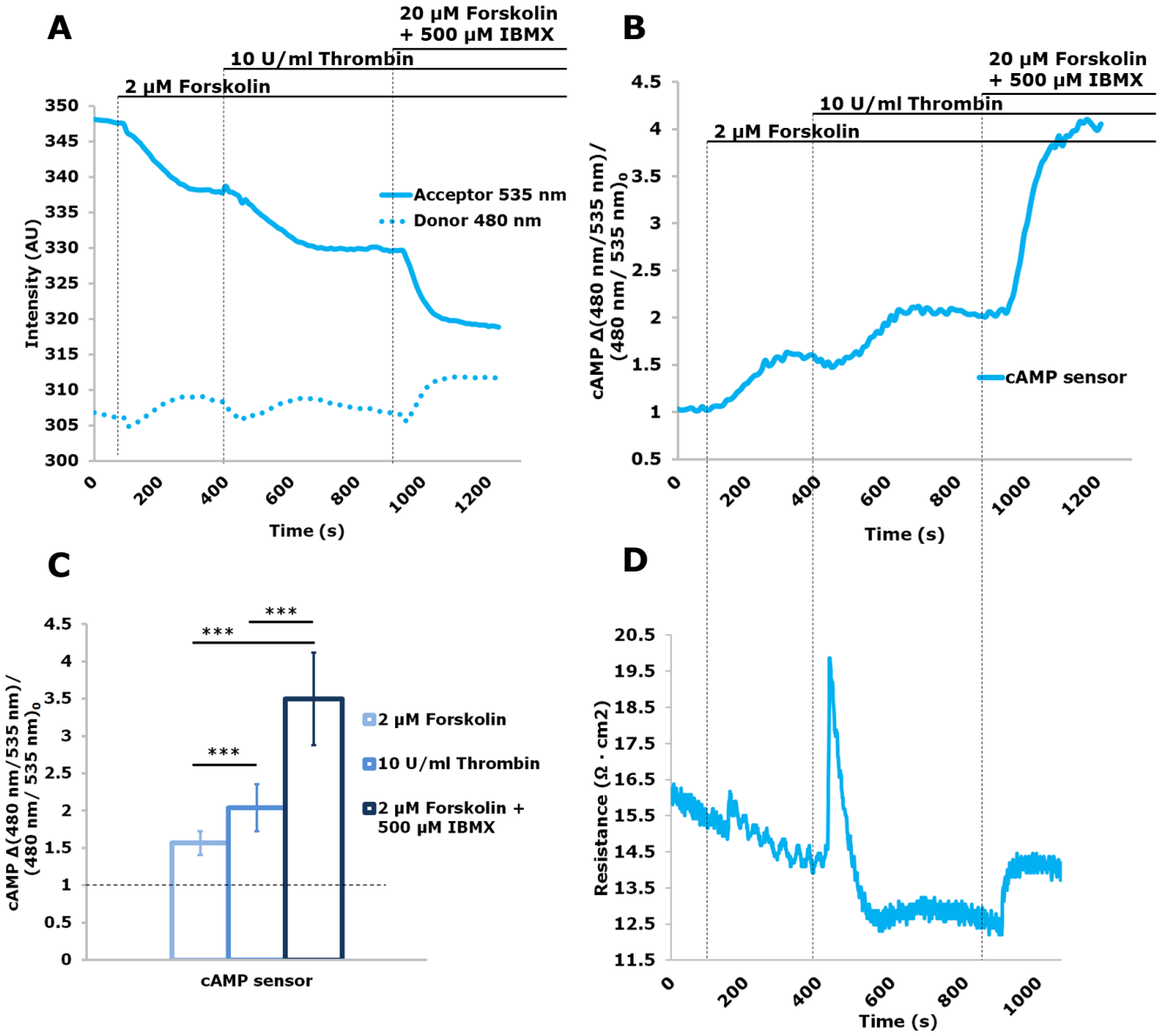

Figure 24: Assessment of barrier function and cytosolic cAMP levels after hPMEC treatment with thrombin. hPMEC cells were infected with adenovirus particles of the cAMP cytosolic FRET reporter and stimulated with forskolin, thrombin and forskolin with IBMX whilst monitored in the FRET-TER chamber. A) Donor and acceptor fluorophore emission intensity shifts over time after addition of indicated stimuli. B) Representative normalised and background subtracted FRET ratio graphs stimuli (representative trace of n=11 showing comparable results). Note that for convenience the cAMP FRET ratio traces and images were calculated as donor emission divided by acceptor emission intensity, to represent the increase in cAMP concentration as an increase of the FRET ratio. C) Bar graph depicting the findings

from A and B; n=11 and *P*<0.001. D) Representative trace of n=4, showing a comparable result of changes in TER over time after addition of 2 µM forskolin, 10U/ml thrombin and 20 µM forskolin with 500 µM IBMX, respectively.

4. Discussion

Endothelial barrier dysfunction can aid inflammation, a hallmark of several diseases, including acute respiratory distress syndrome, asthma, and chronic obstructive pulmonary disease. Barrier dysfunction is also associated with fluid extravasation, as observed in pulmonary oedema. Cellular barrier function has been shown to be enhanced by cellular increases of cAMP. However, recent evidence suggests that subcellular localisation of the increased cAMP pools may be an important determinant of the effect of this second messenger on barrier function.

Here the establishment of methods to investigate whether cAMP compartmentalisation is present in pulmonary endothelial cells and how it associates with cellular barrier function is described. Preliminary evidence supportive of barrier function regulation by cAMP compartmentalisation in hPMECs was also shown.

4.1 FRET reporters to assess localised CN regulation in space and time

FRET microscopy is a powerful tool that enables investigation into regulation of molecular interactions in living cells. To investigate spatiotemporal cAMP changes at different subcellular localisations, we employed FRET reporters targeted to different subcellular locations. As PKA is a downstream effector of cAMP and cGMP is known to crosstalk with cAMP, we decided to employ

sensors specific to these three targets to gain a better understanding of the regulatory processes behind localised CN signalling. We generated three membrane targeted FRET reporters, in addition to previously obtained cytosolic sensors. These reporters enabled us to monitor cAMP and cGMP levels, respectively, and PKA activation, both in the cytosol and at the plasma membrane. Successful targeting and ability to FRET of cAMP, cGMP and PKA specific FRET reporters was validated by fluorescence and FRET microscopy. These sensors will enable comparison of CN changes induced by drugs at the membrane and cytosol.

The FRET sensors were chosen based on their availability as well as their fluorophore superiority and improved ability to transfer energy through FRET. Introducing fluorophores with increasingly optimized characteristics has made the generation of a sensor with high dynamic range and photo stability (e.g. cAMP H187) possible. Sensors with characteristics comparable to H187 are favourable over our employed cGMP and PKA sensors, Cygnet2.1 and AKAR4, respectively. This is because, as we have shown, the shifts in CFP and YFP emission for a true FRET signal can be clearly visualized and measured. In contrast, sensors with a smaller dynamic range tend to show a smaller change in CFP and YFP emission, making it harder to distinguish between artefact and true signal. Therefore, one future approach could be to improve on the PKA and cGMP sensors by inserting their specificity domains into the H187 fluorophore backbone.

Another drawback of the Cygnet2.1 is that it contains the entire PKG sequence. Although PKG is mainly known to bind cGMP, PKG can in fact bind cAMP with lower affinity[322]. Therefore, the cGMP sensor FRET changes may be of mixed

specificity, and therefore distort measurements. It may be possible to assess which cGMP binding domains of the PKG protein bind cGMP with high specificity and consequently induce a substantial conformational change within the protein. This high specificity and significant conformational change would be desirable for a FRET reporter. Recent evidence suggests that of the Cyclic Nucleotide Binding Domains (CNBD) in the PKG sequence, the CNBD-A does not hold the cGMP specificity of the PKGI[323,324]. In fact, the CNBD-B was found to have a binding affinity for cGMP 240 times stronger than for cAMP and is able to induce a drastic conformational change. Future directions of investigation could include a cGMP specific FRET reporter based on the H187 sensor fluorescent domains and the CNBD-B.

Comparison of FRET ratio changes between cytosolic and membrane targeted sensors necessitates calibration and characterisation of each individual FRET sensor. This is because of the different structures and environment of individual sensors, which may alter their dynamic range. The calibration would be conducted by a micro infusion technique which allows the application of known concentrations of CN analogues directly into the cell via a patch pipette, while the FRET response of the respective reporter is measured in parallel. By obtaining dose response curves for each type of FRET sensor, changes at the membrane and in the cytosol could be compared directly. From these readings we could then draw conclusions regarding effects of the same drug, on a specific target molecule, in different subcellular localisations.

4.2 Cell culture conditions optimisation for the human pulmonary microvascular endothelial cell line

This project was designed to study the role of cAMP compartmentalisation in pulmonary endothelial barrier function. As part of the project, we were interested to uncover GPCRs in the human pulmonary microvasculature that affected barrier function. Identified orphan GPCRs in pulmonary microvasculature could be interesting drug targets. Barrier dysfunction has been implicated in the pathophysiology of diseases including pulmonary oedema and chronic obstructive pulmonary disease. Therefore the human pulmonary microvascular endothelial cell line was the model of choice.

After having generated the reporters that allowed for CN monitoring in live cells, optimisation of cell conditions that allowed for FRET experiments in hPMEC was necessary. hPMECs have never before been used within a FRET setup. Therefore we set out to optimize cell culture conditions in order to obtain reproducible and reliable results.

hPMEC were not transfectable, therefore we infected cells with adenoviral particles that contained the FRET reporter of choice.

We found that addition of 28 mM HEPES to the cells decreased cell shrinkage and medium alkalization during the course of FRET experiments.

We did not find serum to affect FRET ratio changes when we stimulated hPMEC with forskolin, however, as we do not know the exact components of serum it may introduce variability in experiments. Therefore, we omitted serum in the bath solution to decrease variability in FRET measurements. Additionally, we omitted the auto fluorescing pH indicator phenol red to avoid interference

with FRET emission.

The FRET-setup employed in this study did not allow for maintenance of cells at 37 °C and 5% CO_2. Future additions of equipment that allow for temperature and carbon dioxide regulation could improve the physiological representation of our experiments.

Working with additional cell models in parallel with hPMEC, may be worth considering, as there is a vast variety in functionality, phenotype and expression patterns in different endothelial vascular cells[325].

Arteries and veins form a continuous endothelial barrier through adherens and tight junctions. Capillary endothelium can be continuous, discontinuous or fenestrated, depending on tissue type. Fenestrated endothelium contains large diaphragm-covered gaps and is found in organs involved in filtration or secretion, including glomeruli, gastric and intestinal mucosa, and the choroid plexus. Another example illustrating the phenotypical difference between types of endothelium is the longitudinal alignment pattern of endothelial cells, parallel to the blood flow. Arterial wall endothelium forms this longitudinal alignment pattern, whereas the venous segments of the vasculature lack this endothelial pattern. This may be due to the difference in blood pressure and flow[326].

Besides phenotypical differences, expression patterns can also vary between endothelial cells from different parts of the body. Endothelial differences in function and phenotype could partially be explained by dissimilarities in gene expression. *In vivo* proteomic approaches have revealed various vascular bed-specific phenotypes with very few markers in common[327,328]. Gene expression differences range from TJ proteins to ECM markers. For example, occludin expression levels were found to be 18 times higher in arterial compared with

venous vasculature[16]. Chi et al found marked contrasts in ECM protein expression between isolated endothelial cells from large or small vessels[329]. Collagen 41 and 42 and laminin were associated with microvessel endothelium, whereas fibronectin, and collagen 51 and 52 expression was more pronounced in macrovessels[329,330].

Having another cell line in parallel with hPMEC would allow us to compare findings in different types of endothelial cells. This would increase our understanding of the general barrier function mechanisms in endothelial cells. An alternative cell line could be the human cerebral microvessel endothelial cell (hCMEC/D3) line[278,279,308]. HCMEC/D3 are derived from human temporal lobe microvessels. They were immortalized by lentiviral vector transduction with the catalytic subunit of human telomerase (hTERT) and SV40 large T antigen. hCMEC/D3 are well characterized endothelial cells, proven to be a useful model. In addition they show easy and stable growth.

One major challenge that remains is optimisation of AJ and TJ tightness of hCMEC/D3 cell monolayers. Cells have shown an increase from 30-50 $\Omega \cdot cm^2$ to 300 $\Omega \cdot cm^2$, when grown in the presence of corticosteroids[331]. Most promising were hCMEC/D3 monolayers subjected to pulsatile flow. After seeding they showed a TER of 1-1.2 $k\Omega \cdot cm^2$[2,308].

The pulmonary microvascular barrier in alveoli is established by both endothelial vascular cells and epithelial alveolar cells. This barrier is crucial for adequate blood-gas exchange. Thus, an additional alveolar cell model would enable us to make more physiological assessments of pulmonary microvascular barrier function. For example, it would be interesting to compare findings in hPMEC with data from alveolar cells. Alveolar cells are in close

proximity with hPMEC in pulmonary alveoli. Both cell types are at the intersection of blood-gas exchange and maintain the cellular barrier in alveoli. Therefore, contrasting their responses to different stimuli would increase our understanding of the co-operation between alveolar and endothelial cells to orchestrate barrier function. Pulmonary alveolar epithelium has been shown to form a much tighter barrier against liquid flux and protein permeation than the capillary endothelium[1,332]. A representative *in vitro* model of the air-blood barrier would therefore include endothelial and epithelial cells and may have characteristically high TER values.

The epithelial pulmonary papillary adenocarcinoma cell line NCI H441 would be another possible cell line of interest. NCI H441 have previously been co-cultured with hPMEC to create a representative *in vitro* model of the alveocapillary barrier[279]. Comparable to endothelial cell lines, the low TER values remain a challenge. This co-culture however showed a significant increase of TER, 500 $\Omega \cdot cm^2$ compared to 30 $\Omega \cdot cm^2$, when cultured in dexamethasone containing medium. Dexamethasone is a glucocorticoid that has proven useful in the treatment of cerebral oedema, skin disease, chronic obstructive pulmonary disease and asthma[333]. It is thought to strengthen barrier function by modulating expression of TJ proteins[331]. Although promising, addition of dexamethasone to cell culture needs to be further characterised as it may interfere with signalling in barrier function experiments. For example, dexamethasone is thought to inhibit phospholipase A2, which could affect thrombin signalling[334]. Therefore, barrier function experiments should be conducted with cells grown with and without dexamethasone, respectively.

4.3 Assessment of FRET sensor dynamic range in human pulmonary microvascular endothelial cells

After having optimised cell culture conditions for FRET experiments in hPMEC, we assessed the maximal FRET change of our sensors expressed in hPMEC. This was necessary because the maximal change of FRET, characteristic for the specific reporter and cell line, enables us to compare data from different experiments.

The maximally saturating stimulus for the cAMP and PKA cytosolic sensors was found to be 20 µM forskolin and 500 µM IBMX and 20 µM forskolin and 100 µM IBMX, respectively. From previous observations it may be concluded that cAMP exhibits a lower affinity for Epac than it does for PKA[335,336]. In addition, results from PKA and cAMP reporters suggest changes in FRET ratio of the PKA sensor are induced at lower intracellular cAMP concentrations (unpublished results of the Zaccolo lab). These indications may explain the lower stimulus necessary to saturate the cytosolic PKA sensor. Twenty µM forskolin and 500 µM IBMX were used as the standard saturating stimulus for all our cAMP and PKA based reporters, respectively, in hPMEC. In the future, we will set out to determine the maximal saturating cGMP reporter stimulus.

4.4 Approaches to manipulate intracellular cAMP

We explored two approaches to modulate subcellular cAMP levels. By optimising usage of the sACI/II and IIaC we hoped to increase cytosolic cAMP

pools, which we could monitor with targeted FRET reports in parallel with barrier function measurements. The effects of localised cAMP increases and accompanying effects on endothelial barrier function would give a first indication of compartmentalisation and its regulation in hPMEC.

4.4.1 Soluble adenyl cyclaseI/II

We investigated the generation of a cytosolic cAMP pool by activation of a recombinant sAC expressed in transfectable epithelial cells. We obtained the sACI/II chimera from Sayner et al[119]. In their studies, Sayner et al. only showed indirect evidence of compartmentalisation and its effect on barrier function[118,119,299]. Therefore, we aimed to directly test the presence of compartmentalisation by employing the sACI/II in combination with FRET sensors. This allowed for high spatiotemporal resolution, in contrast to the immunoassays employed by Sayner et al., to investigate compartmentalisation in living cells.

This method did not prove to be useful for our purpose as the sACI/II was not able to increase cytosolic cAMP levels in our hands. The sACI/II was not tagged; thus, we could not validate expression of the construct. Therefore we cannot exclude that the sACI/II was not expressed in transfected cells. Expression could be validated with antibodies directed at either catalytic loop of the sACI/II; however, these are not on the market and would need to be costume made. Molecular cloning would allow addition to the sACI/II of a fluorescent tag or a short peptide sequence for immunoprecipitation. However,

we cannot predict how this would affect the conformation and ultimately the function of sACI/II.

Another limitation of this approach is that the sACI/II, comparable to all endogenous transmembrane ACs, is activated by forskolin and $G_s\alpha$ proteins[261]. This entails that the transmembrane ACs are always activated in addition to the cytosolic sACI/II. Indeed, Sayner et al. reported a substantial cAMP increase upon forskolin (100 µM) stimulation, in cellular plasma membrane fractions of lysed cells expressing the sACI/II[119]. In parallel, they found a small but significant cAMP increase in cytosolic cellular fractions, to which they attributed the observed endothelial gap formation. Therefore, observed results may not be solely attributable to the sACI/II, but could also be due to transmembrane AC activation and plasma membrane cAMP activation. Thus, it would be paramount to establish a significant cAMP increase in the cytosol, compared to the membrane before drawing conclusion in regard to the effect of a cytosolic cAMP increase.

We tried to observe increased cytosolic cAMP levels in sACI/II expressing cells, compared to controls, at varying doses of forskolin. However, we did not find cAMP increases upon treating cells with forskolin. Previous reports used significantly higher doses of forskolin (100 µM) than we have used. As the cAMP reporter we employed is saturated at 20 µM forskolin and 100 µM IBMX, addition of 100 µM forskolin would most likely saturate the FRET reporter. Therefore, we would not be able to measure differences in cytosolic cAMP concentrations, making this approach unfit for our purpose.

Due to the lack of success of this approach, we moved on to a near-infrared light activated adenyl cyclase, which had recently been published[304].

4.4.2 Near-infrared light-activated adenyl cyclase

In the context of this project, we explored the possibility of using IlaC to generate cytosolic cAMP pools in cells. Unfortunately, we were not able to use a previously published highly efficient bacterial photoactivatable AC, named bPAC[306]. bPAC's activation required a wavelength that also excited the donor chromophores of our FRET reporters, which would have resulted in continuous production of cAMP during FRET measurements. This would have made FRET experiments virtually impossible.

Unfortunately, this method has not proven successful, as of yet. Light sources we employed, a light bulb with 500 nm longpass filter and a 660 nm LED, respectively, did not result in an increase of cytosolic cAMP as indicated by increase in FRET ratio shift. Possible reasons may be that the light source was too weak, or the cAMP producing activity of the IlaC was not strong enough. Another possibility is that the exposure of cells to the respective light source was not long enough. Further testing of different illumination protocols is necessary to validate the function of the IlaC.

Additional limiting factors may have been limited intracellular supply of biliverdin or cAMP degradation by PDEs. As explained in the results section, biliverdin enables the IlaC to sense near-infrared light and to induce the conformational changes necessary for cAMP synthesis. Increased intracellular levels of biliverdin should therefore enable increased cytosolic cAMP generation.

Alternatively, the limiting factor could have been the cAMP hydrolysing activity of PDEs. Perhaps the catalytic activity of the IlaC was not strong enough to

override hydrolytic PDE activity.

In addition to the vector depicted in Figure 18A, we are in possession of a *BPHO* gene containing vector. This vector was a kind gift from Dr. Lyuksyutova (University of Wyoming). Downstream of the *IlaC* sequence, there is an internal ribosome entry site, followed by the *BphO* gene. *BphO* encodes heme oxygenase, which cleaves heme to form biliverdin. The theory behind employing this vector would be that the lack of cAMP production we have observed so far is due to biliverdin being the limiting factor. Increased heme oxygenase expression, should result in higher intracellular biliverdin concentrations and thus increase cytosolic cAMP production. Assuming that PDEs limit cAMP accumulation through their hydrolysing activity; another approach would be to inhibit all PDEs by pre-treatment of cells with IBMX, before starting the illumination protocols.

If the IlaC is able to increase subcellular cAMP pools, it may be worthwhile looking into producing a light activated cGMP producing IlaGC. The logic, on which construction of the IlaC was based, was that enzyme activation is predicted to occur via alignment of the rigid GGDEF domains rather than via intradomain conformational changes (refer to Figure 17). Therefore, proper alignment of homodimer catalytic domains of the GC could theoretically enable cGMP generation.

4.5 Approaches to measure endothelial permeability

4.5.1 Immunocytochemistry and FITC-dextran assays

Having explored and validated different approaches to address cAMP compartmentalisation, we still needed to establish methods for endothelial barrier function measurements. To assess the effect of various GPCR stimuli or possibly IlaC on barrier function we set out to optimise two types of approaches: immunocytochemistry and a FITC-dextran permeability assay. We optimised immunocytochemistry protocols to visualise VE-cadherin and actin expression and localisation in hPMEC. Expression and localisation changes of these proteins have often been employed as markers for barrier function alterations. Immunocytochemistry imaging allows for qualitative barrier function assessment. Although it gives an indication of barrier function by changes in VE-cadherin and/or actin distribution upon permeability inducing stimuli, we needed an alternative quantitative read-out. Therefore we set out to optimise the FITC-dextran permeability assay, in which permeability of a cellular monolayer is measured by the quantity of molecules that pass across it. Initial difficulties of cellular growth were overcome by coating inserts with a gelatin/fibronectin solution before cell seeding. We are now able to grow hPMEC monolayers on transwell inserts. These can be used in the FITC-dextran setup as well as the FRET-TER chamber, integrating both approaches nicely.

In future experiments we will be able to relate GPCR ligand induced changes in the hPMEC VE-cadherin and actin phenotype to barrier function. In addition,

we may able to combine immunocytochemistry with FITC-dextran assays. Assessment of hPMEC monolayer permeability by FITC-dextran can be followed up by staining the cells grown on transwell insert membranes after the initial experiment. This would give us two different read-outs of barrier function within the same cells, thus increasing the efficiency and validity of our experiments.

4.5.2 Construction of a FRET-TER measurement chamber

In order to provide definite evidence for the causative regulatory effect of cAMP compartmentalisation on barrier function, we ideally needed to measure barrier function in parallel with intracellular cAMP compartmentalisation. All approaches known from literature assess either barrier function or cAMP compartmentalisation. Thus, we aimed to engineer a novel FRET-TER chamber that combines both approaches. Parallel live cell cAMP and electrical barrier resistance measurements were validated in the prototype described in this report.

Initially we grew hPMEC on transwell inserts, before visualizing the cells with the FRET-TER setup. We found that cells grown at 40000 cells per 24 transwell insert grew to confluence within the first week of seeding. These results indicated that cells were already confluent after one week, which would explain the lack of decrease in permeability over the subsequent weeks of growth shown by the FITC-dextran assay. We validated hPMEC growth by adenoviral infection with the cAMP reporter, which allowed us to visualize the cells under a fluorescence microscope. Barrier function measurements with the EVOM^2 were

highly variable and showed low TER in hPMEC. Therefore we adapted the original TER electrode prongs into two parallel rings in a stable construction. This way, the electrodes permanently maintained the same distance to the cellular monolayer.

The low resistance we observed for hPMEC is consistent with findings by Hermanns et al[279].

In general literature TER is either presented as TER ($\Omega \cdot cm^2$) or as normalised TER. As barrier function has never been measured as presented here, we show $\Omega \cdot cm^2$ as well as normalised figures. In the future this will allow for TER ($\Omega \cdot cm^2$) comparison between different employed cell lines. For normalisation we subtracted background values, and divided all data points by an average of the values measured during stable resistance measurements before or after addition of 2 µM forskolin. We used this approach instead of normalising to TER before addition of ligands. This was because we struggled to obtain stable baseline measurements. This could be attributable to afore mentioned low basal TER of hPMEC. The drift in baseline that we observed is not large in absolute terms, therefore if basal TER values lay around several 100 $\Omega \cdot cm^2$ the drift may be minimal compared to a response to thrombin. To validate this hypothesis, further experiments in the FRET-TER chamber with endothelial or epithelial cell lines that have higher basal TER values are necessary. The value range after normalisation of the responses we detect is comparable to ECIS studies that have shown normalised resistance values[280](Refer to Figure S1). Further experiments are once again necessary to confirm these findings.

The low resistance we observed for hPMEC only allows for a small range of measurement. Several approaches including corticosteroid treatment, co-

culture or fluid shear stress exposure have been explored to increase *in vitro* TER values. Induction of shear stress proved most successful. Indeed, hCMEC/D3 monolayers subjected to pulsatile flow after seeding, presented a TER of 1-1.2 kΩ·cm^{2,} which rapidly dropped after flow cessation[308]. If we were able to successfully couple the FRET-TER prototype to a perfusion system, we could induce laminar flow across cellular monolayers during experiments, which may increase basal TER[308]. A successful increase of basal TER in hPMEC would allow us to produce more physiologically relevant data. Additionally, it may increase the changes in TER that we can observe after addition of barrier modulating stimuli, thus improving the dynamic range of our measurement.

Defining the dynamic range of hPMEC barrier function will be one of the future challenges. To assess the relevance of our measurements and the effect of stimuli compared to physiological barrier function, we would need to set a 'standard'. To assess the maximal and minimal barrier resistance of the monolayer, we would need to add both a maximally barrier enhancing stimulus as well as a barrier decreasing stimulus to the same cells. The addition of these stimuli upon other stimuli may not prove to be a representative maximal or minimal barrier resistance. For instance, if we were to add forskolin and IBMX after addition of a permeability inducing agent, we would not know whether the measured barrier resistance was maximal or sub-maximal. Certainty would only be provided by washing off the test stimulus before maximally increasing or decreasing the endothelial resistance. This necessitates a perfusion system that allows washing of the cells after stimulus addition.

Complete disruption of barrier function can be achieved by treatment of hPMEC

with Latrunculin B. Latrunculin B induces actin depolymerisation and would allow assessment of the minimal resistance. In contrast, sphingosine-1-phosphate has been shown to increase barrier function by up to 1.5 times (normalised), in endothelial cells in ECIS experiments and could therefore act as our 'positive' control[337].

Direct comparison of results obtained from the FRET-TER chamber and an ECIS system could give us an indication of how reliable and representative the TER chamber measurements are. Therefore, it would also be worthwhile comparing our FRET-TER data to results obtained from similar experiments, but assessed by immunocytochemistry and FITC-dextran assays.

4.6 Preliminary investigations into cAMP compartmentalisation in hPMEC

Having established the tools to investigate the association of CN compartmentalisation and barrier function in hPMEC we conducted pilot experiments with various GPCR agonists. These GPCR agonists were adenosine, histamine and thrombin, which have all been shown to play a role in endothelial barrier function.

4.6.1 Adenosine

Within the context of endothelial lung barrier function, cellular increases of adenosine have repeatedly been shown to enhance barrier function[310–312]. As previously mentioned, evidence suggests that cAMP increase in the cytosol

decreases barrier function, whereas increase of cAMP at the plasma membrane enhances it[118,119,299]. The barrier protective effect of adenosine may therefore result from a compartmentalised cAMP increase.

We set out to investigate the effect of adenosine on cytosolic cAMP levels and PKA activation in hPMEC. By means of FRET we found a small cytosolic cAMP increase in hPMEC upon adenosine addition and no increase in PKA activation. This was surprising as it may be concluded, from previous observations, that cAMP exhibits a lower affinity for Epac than it does for PKA[335,336]. In addition, results from PKA and cAMP reporters suggest that FRET ratio changes of the PKA sensor are induced at lower intracellular cAMP concentrations (unpublished results of the Zaccolo lab). Thus, in the presence of a cAMP-dependent signal an increased FRET ratio for the PKA reporter could be expected, even more so, as activated PKA would be able to phosphorylate more than only one FRET reporter. The observed lack of PKA FRET ratio change may suggest selective activation of Epac. This would be compatible with the notion of cAMP compartmentalisation in hPMEC.

Another theory would be that the cAMP reporter may be much more sensitive to low levels of cytosolic cAMP than the PKA sensor.

Alternatively, a small increase in cAMP in the cytosol with no detectable PKA activity may indicate that there is a larger cAMP increase, and presumably PKA activity, at the plasma membrane. Some cAMP spills into the cytosol but does not seem to be effective in activating PKA or to activate enough PKA to counteract the effect of cytosolic phosphatases. This would be compatible with the previously established barrier increasing Epac-cAMP signalling pathway (Figure 3 introduction). According to this pathway cAMP can lead to MLC

dephosphorylation and thus actin cytoskeleton stabilisation via the Epac/Rac/ROCK/MLC phosphatase signalling cascade. This pathway has been shown to act independently of the PKA signalling cascade[208,225]. Future experiments with the membrane bound cAMP and PKA sensors in hPMEC are necessary to establish whether adenosine induces a larger cAMP increase, and presumably PKA activity, at the plasma membrane. In addition, we would need to establish dose-response curves for cAMP induced FRET changes for both the cAMP and PKA reporter. This could be accomplished by our in-house patch-clamp micro-perfusion technology. The obtained dose response curves would allow us to directly compare FRET ratios of cytosolic and plasma membrane reporters for PKA and cAMP, respectively. We could then conclude whether cAMP and/or PKA concentrations are indeed higher at the plasma membrane and indicative of compartmentalisation.

Finally, future experiments with cytosolic and plasma membrane reporters for cAMP, PKA, and also cGMP, respectively, should be conducted in the FRET-TER setup. This would enable us to correlate observed changes in cyclic nucleotides and PKA activation with subsequent effects on endothelial barrier function.

The physiological role of adenosine in the lung depends on which of its four receptors it binds[338]. Interestingly, expression of both adenosine receptors A_{2A} and A_3 has been found to decrease in a lipopolysaccharide induced acute lung injury model in mice[311]. Treatment with adenosine abrogated the change in expression and decreased several factors associated with inflammation, including pulmonary neutrophil infiltration, TNF-α and IL-6 expression and fluid extravasation[311]. A_{2A} couples to a G_s protein, whereas A_3 couples to a G_i

protein, yet combined they seemed to have anti-inflammatory and barrier protective effects in the lung[339]. Cellular compartmentalisation could explain how these seemingly contradictory pathways may exert their individual function in separate cellular compartments to aid the same outcome. Therefore, it would be interesting to investigate the effect of adenosine on hPMEC in the FRET-TER setup. In addition to FRET-TER experiments, analysis of protein expression of the adenosine receptors in hPMEC would be necessary. Furthermore, expressed receptors could be targeted by specific agonists to define their individual responses and effects on barrier function. Based on previous reports, it would be most interesting to selectively inhibit A_{2B} and $A_{2A.}$ Examples of antagonists for A_{2B} and A_{2A} are SCH 58261 and PSB-603, respectively[340,341]. Selective inhibition of either receptor would allow assessment of their respective contribution to CN-regulated pulmonary barrier function by employing our FRET-TER chamber.

4.6.2 Histamine

Histamine has been found in blood and vessel walls[342,343], where it is thought to mediate an endothelial vasodilatory response through histamine receptors, as shown by Van de Voorde et al. in pre-contracted rat thoracic aorta[344]. Additionaly, histamine has been shown to decrease barrier function and induce intercellular gaps in several vascular cell models and *in vivo*[32,225,313–315].

To date, four histamine receptors have been identified: H1R- H4R, of which H1R and H2R have been found to be expressed in endothelial cells[345–347].

Interestingly, H1R has been shown to couple to a G_q protein and stimulate PLC, calcium and PKC signalling[348–350]. H2R couples to G_s proteins, thus stimulating the cAMP signalling cascade.

Histamine is a well-known inducer of vascular permeability[351,352]. Therefore, we expected to see a decrease in endothelial resistance alongside a possible decrease in cAMP, when we treated hPMEC with histamine. To observe this hypothetical decrease in cAMP, we pre-treated hPMEC with a small dose of forskolin. Surprisingly, we found no change in cytosolic cAMP in parallel with an increase in barrier function. Endothelial cells have been shown to express H1R and H2R, although we did not confirm this in hPMEC. H1R and H2R couple to G_q and G_s proteins, respectively. However, our results are difficult to explain on the basis of signalling through G proteins. Coupling to the G_q protein would explain the lack of change in cAMP; however, the ensuing calcium and PKC signalling would be expected to decrease barrier function. Activation of the H2R would coincide with the observed increase in barrier function, yet contradicts the lack of cAMP increase. A possible explanation would be that histamine increases cAMP at the membrane through H2R binding. This possibility implies cAMP compartmentalisation in hPMEC, which will be addressed in future experiments with the membrane targeted FRET cAMP reporter.

Alternatively, the pre-treatment of hPMEC with forskolin may have increased intracellular cAMP, thus improving barrier function and counteracting the histamine induced permeability. This has been previously observed by treatment of human dermal microvascular endothelial cells with the cAMP analogue dibutyryl cAMP before stimulation with histamine[353]. This would suggest a delicate balance of cellular cAMP which can be offset by histamine

treatment. A possible underlying mechanism would be inhibition of the calcium inhibited AC6, via calcium mediated increase of H1R-G_q signalling by addition of histamine[318]. Pre-treatment with forskolin could abrogate the ensuing barrier dysfunction by increasing intracellular cAMP levels. However, this does not explain why we do not see an increase in cAMP unless it was plasma membrane specific, which would suggest cAMP compartmentalisation. Overall, these preliminary findings suggest cAMP compartmentalisation may contribute to hPMEC barrier function. The balance of cAMP levels within specific cellular pools may also play a crucial role. A possible scenario compatible with our results is that a histamine-mediated increase in permeability secondary to intracellular calcium increase is counteracted by pre-treatment of hPMEC with forskolin. Forskolin may increase cAMP at the membrane, thus stabilising the barrier. This would coincide with barrier dysfunction after a small increase in cytosolic cAMP observed by Sayner et al, which could be rescued by a cAMP increase at the membrane[119].

Future experiments will aim to assess histamine receptor expression in hPMEC. In addition membrane-targeted cAMP FRET reporter-TER studies will investigate the role of compartmentalisation and the possible contribution of forskolin pre-treatment in histamine stimulated hPMEC.

4.6.3 Thrombin

Thrombin is predominantly known for its role in blood coagulation and tissue damage. Next to a plethora of effects in the vasculature, thrombin induces increased permeability and cell shape changes in cultured endothelial cells[315].

Thrombin exerts its function through cleavage of protease-activated receptors (PARs), which are GPCRs. Four human PARs are known, PAR1-4. PAR1, 3 and 4 can be cleaved by thrombin and are widely expressed in the vasculature[354].

The effect of thrombin is transient and resistance of monolayers returns to baseline after several hours, depending on thrombin dosage[28,106,355]. The accompanying expected decrease in cAMP has not been firmly established. Several radio-immunobased assays have shown a cAMP decrease in endothelial cells after 5 minutes of thrombin treatment[317,318]. This is in stark contrast with more recent FRET based findings that indicate a thrombin induced transient cAMP decrease, followed by a cAMP increase in endothelial cells[319,320]. Due to these discrepancies in results, we set out to investigate the relationship between thrombin decreased barrier function and cellular cAMP in the FRET-TER chamber.

As expected, hPMEC expressing the cytosolic cAMP reporter showed a FRET ratio increase after forskolin treatment. The following thrombin challenge indicated a small initial decrease in FRET signal. This was followed by substantial FRET ratio increase. These results coincided with a decrease in barrier function, suggesting that a transient decrease and subsequent increase in cytosolic cAMP were responsible for the observed barrier dysfunction. These findings support Sayner's model that increased cytosolic cAMP levels induce endothelial permeability[118,119,299].

Additionally, our results support findings by Werthmann et al. for the first time in hPMEC. Werthmann et al. found evidence that thrombin may induce accumulation of cAMP in human umbilical vein endothelial cells[319]. They found

thrombin dependent intracellular calcium increases that induced prostacyclin production. Calcium stimulates phospholipase A2 to release arachidonic acid from the plasma membrane. Interestingly, the increase in calcium was completely blocked by addition of acetylsalicylic acid. This cyclooxygenase inhibitor, better known as aspirin, is known to inhibit the conversion of arachidonic acid to prostaglandin H2. Ultimately, prostaglandin is converted to prostacyclin. Prostacyclin binds to prostacyclin receptors, which couple to G_s proteins[33,320]. The increase in cAMP we observed could depend on this mechanism. Additionally, Werthmann et al. showed that the the observed initial transient decrease in cAMP may be dependent on calcium effects[319]. siRNA interference with the calcium-inhibited AC5 and 6 diminished the transient cAMP decrease following thrombin stimulation[319]. Overall, our preliminary data seem compatible with an initial thrombin-calcium mediated decrease of cAMP as observed by Werthmann et al. Regardless; we would need to establish AC5 and AC6 gene expression in hPMEC, before we can elaborate on this theory.

Whether the initial peak in TER, after addition of thrombin, is due to cytosolic cAMP decrease or an artefact caused by addition of the stimulus is unclear. It should be noted that the ligands employed in the FRET-TER experiments were dissolved in a volume of 100 µl and the starting volume in the chamber was 200–300 µl. This approach was taken so that the two volumes would mix; rather than adding a very small volume to a big volume, which wouldn't allow the ligand to dissolve homogenously. Therefore, the observed peak could be an artefact due to (a combination of) the following factors: a change in osmolarity, an increase in volume, and the act of manually pipetting the solution

into the chamber. Interestingly, Malik et al. observed similar, yet smaller, peaks in an ECIS setup they developed[33,280]. They did not offer any insights as to how these peaks could be explained. Additionally, their traces were less noisy, possibly because they employed a lock-in amplifier to extract voltage signals from a noisy background[332,356]. Such an amplifier may be of benefit in our setup.

Overall, a mechanism that incorporates both the observed whole cell decrease in cAMP and cytosolic increase in cAMP following thrombin stimulation is postulated by Sayner et al[119,300]. According to Sayner's model a cytosolic cAMP increase disrupts endothelial barrier function, whereas membrane localised cAMP is barrier protective. Our preliminary findings seem compatible with this model. Repetition of experiments with hPMEC expressing the membrane targeted cAMP reporter should give us more insight into the role of cAMP compartmentalisation in barrier function upon thrombin stimulation.

4.7 Conclusion and summary

This body of work aimed to lay foundations and establish tools to investigate the relation between CN compartmentalisation and endothelial barrier function (in hPMEC) for the first time in parallel within the same living cell. Several approaches were taken to fulfil this aim. Membrane targeted FRET reporters for cAMP, cGMP and PKA were constructed, in addition to the cytosolic reporters that were already available. Localisation and functioning of the constructed reporters was confirmed. Thus, these reporters will enable future investigations into the presence of CN compartmentalisation in endothelial cells. For the first

time, cell culture conditions for hPMEC were optimized in order to use this cell line a FRET microscopy setup. To investigate the effect of an increased pool of cytosolic cAMP on endothelial barrier function, two constructs, sACI/II and IlaC were employed. By expressing and stimulating these two cytosolic cAMP-generating proteins in endothelial cells we aimed to observe an increase specifically in cytosolic cAMP. However, this increase was not shown; therefore, the sACI/II and IlaC have thus far not been validated as tools to investigate the relation between increases in cytosolic cAMP and endothelial barrier function.

To have a read-out for endothelial barrier function, immunocytochemistry to visualize changes in the distribution of cellular actin and VE-cadherin, and a FITC-dextran conjugate assay were established.

Here, the first setup of its kind to measure FRET and TER in parallel, in living cells, was described. Initial FRET-TER chamber experiments were conducted, confirming that both FRET and TER could be measured by using the chamber. Preliminary data, employing different stimuli and FRET reporters, were in line with the notion that cAMP is compartmentalised in hPMEC. Overall, findings reported here support the establishment of novel tools to investigate the presence of CN compartmentalisation and its potential effects on barrier function in endothelial cells.

4.8 Outlook

Results presented here show the first steps towards combining FRET methodology and endothelial barrier function measurements in one setup. This novel parallel approach will prove valuable in gaining a more thorough understanding of the effect of CN compartmentalisation and regulation within the context of cellular barrier function. Additionally, the FRET-TER chamber may prove useful in teasing apart the contribution of different signalling mechanism responsible for barrier regulation. Fluorescently tagged AJ and/or TJ proteins could be monitored in parallel with TER measurements, upon permeability inducing challenges. This would allow us to assess possible translocation and give us an indication of the contribution of both transcellular and paracellular permeability to endothelial resistance.

Additionally, the chamber could be used in conjunction with Rac FRET reporters[357]. Rac is thought to play a crucial role in barrier function (Figure 3) and would therefore be an interesting protein to study. Furthermore, the chamber could be used to monitor barrier function changes over time when blocking vesicular transcytosis. This could contribute to our understanding of the contribution of vesicular transcytosis to barrier function.

In addition to the FRET-TER chamber other methods could be employed, including permeability assays and immunocytochemistry, to validate the regulatory effect of CN compartmentalisation on endothelial permeability in hPMEC. Apart from optimising the tools described, we have made initial steps toward the validation of compartmentalisation in hPMEC. Future efforts will focus on confirming these findings by employing cAMP, cGMP and PKA FRET

reporters targeted to the membrane and cytosol, respectively. These sensors, in combination with the FRET-TER setup, will allow us to explore the regulatory mechanisms behind CN compartmentalisation and the associated effect on endothelial barrier function.

Ultimately, understanding the players in CN regulation may allow identification of novel drug targets that could contribute to amelioration of pathologies exacerbated by endothelial barrier dysfunction.

5.Supplements

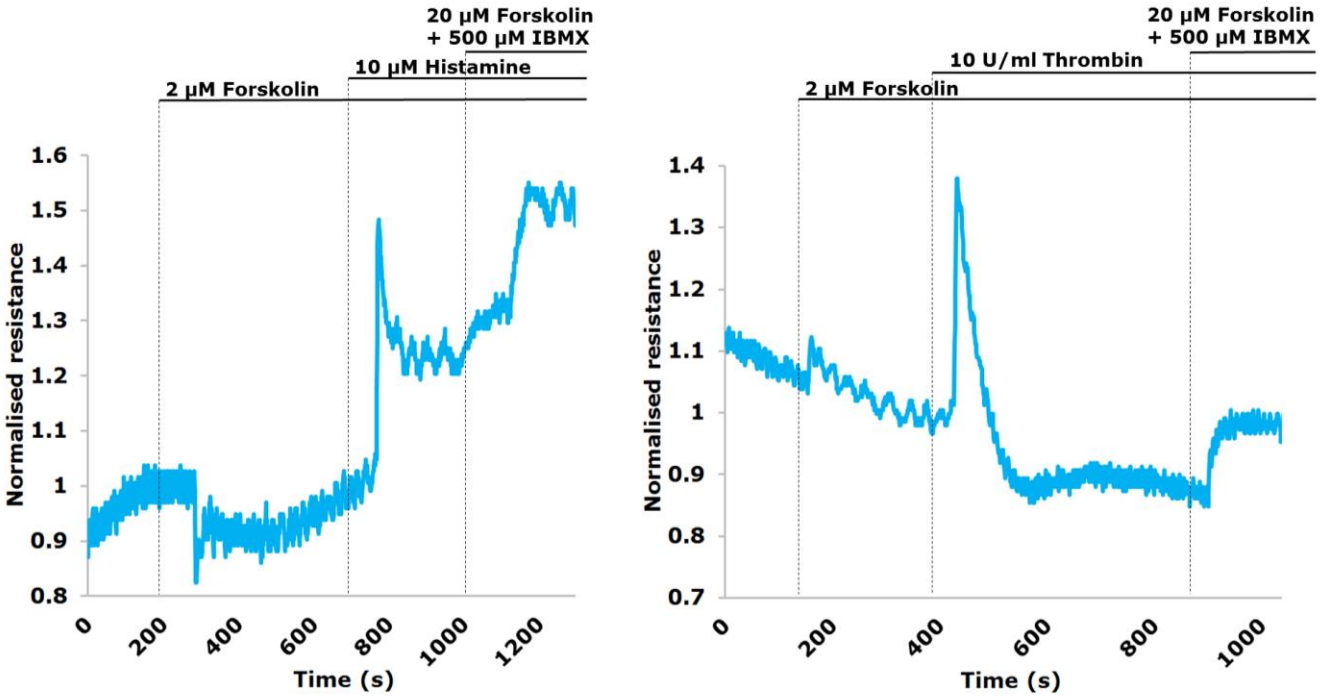

Figure S1: Assessment of barrier function by TER measurements in hPMEC treated with barrier modulatory GPCR ligands. A) Representative trace of n=2, showing a comparable result of normalised changes in TER over time after addition of 2 µM forskolin, 10 µM histamine and 20 µM forskolin with 500 µM IBMX, respectively. B) Representative trace of n=4, showing a comparable result of changes in normalised TER over time after addition of 2 µM forskolin, 10U/ml thrombin and 20 µM forskolin with 500 µM IBMX, respectively. Both measurements are from FRET-TER chamber measurements.

6.References

1. Vandenbroucke, E., Mehta, D., Minshall, R. & Malik, A. B. Regulation of endothelial junctional permeability. in *Annals of the New York Academy of Sciences* **1123,** 134–145 (2008).

2. Funk, S. D., Yurdagul, A. & Orr, A. W. Hyperglycemia and endothelial dysfunction in atherosclerosis: Lessons from type 1 diabetes. *International Journal of Vascular Medicine* **2012,** (2012).

3. Steyers, C. M. & Miller, F. J. Endothelial dysfunction in chronic inflammatory diseases. *International Journal of Molecular Sciences* **15,** 11324–11349 (2014).

4. Berliner, J. A. *et al.* Atherosclerosis: basic mechanisms. Oxidation, inflammation, and genetics. *Circulation* **91,** 2488–2496 (1995).

5. Daneman, R. The blood-brain barrier in health and disease. *Ann. Neurol.* **72,** 648–672 (2012).

6. Obermeier, B., Daneman, R. & Ransohoff, R. M. Development, maintenance and disruption of the blood-brain barrier. *Nat. Med.* **19,** 1584–96 (2013).

7. Michel, C. C. & Curry, F. E. Microvascular permeability. *Physiol. Rev.* **79,** 703–761 (1999).

8. Adamson, R. H. *et al.* Oncotic pressures opposing filtration across non-fenestrated rat microvessels. *J. Physiol.* **557,** 889–907 (2004).

9. Curry, F. E. & Michel, C. C. A fiber matrix model of capillary permeability. *Microvasc. Res.* **20,** 96–99 (1980).

10. Squire, J. M. *et al.* Quasi-periodic substructure in the microvessel endothelial glycocalyx: a possible explanation for molecular filtering? *J. Struct. Biol.* **136,** 239–255 (2001).

11. Dull, R. O. *et al.* Lung endothelial heparan sulfates mediate cationic peptide-induced barrier dysfunction: a new role for the glycocalyx. *Am. J. Physiol. Lung Cell. Mol. Physiol.* **285,** L986–L995 (2003).

12. Henry, C. B. & Duling, B. R. TNF-alpha increases entry of macromolecules into luminal endothelial cell glycocalyx. *Am. J. Physiol. Heart Circ. Physiol.* **279,** H2815–H2823 (2000).

13. Huxley, V. H. & Williams, D. A. Role of a glycocalyx on coronary arteriole permeability to proteins: evidence from enzyme treatments. *Am. J. Physiol. Heart Circ. Physiol.* **278,** H1177–H1185 (2000).

14. Desjardins, C. & Duling, B. R. Heparinase treatment suggests a role for the endothelial cell glycocalyx in regulation of capillary hematocrit. *Am. J. Physiol.* **258,** H647–H654 (1990).

15. Malik A and Siflinger-Birnboim A. Vascular endothelial barrier function and its regulation. (1993).

16. Mehta, D. & Malik, A. B. Signaling mechanisms regulating endothelial permeability. *Physiol. Rev.* **86,** 279–367 (2006).

17. Sunnergren, K. P., Fairman, R. P., deBlois, G. G. & Glauser, F. L. Effects of protamine, heparinase, and hyaluronidase on endothelial permeability and surface charge. *J. Appl. Physiol.* **63,** 1987–1992 (1987).

18. Sarrazin, S., Lamanna, W. C. & Esko, J. D. Heparan sulfate proteoglycans. *Cold Spring Harb. Perspect. Biol.* **3,** 1–33 (2011).

19. Florian, J. A. *et al.* Heparan sulfate proteoglycan is a mechanosensor on endothelial cells. *Circ. Res.* **93,** e136–e142 (2003).

20. Potter, D. R., Jiang, J. & Damiano, E. R. The recovery time course of the endothelial cell glycocalyx in vivo and its implications in vitro. *Circ. Res.* **104,** 1318–1325 (2009).

21. Dominguez, R. & Holmes, K. C. Actin structure and function. *Annu. Rev. Biophys.* **40,** 169–186 (2011).

22. Lum, H. & Malik, A. B. Mechanisms of increased endothelial permeability. *Can. J. Physiol. Pharmacol.* **74,** 787–800 (1996).

23. Garcia, J. G., Davis, H. W. & Patterson, C. E. Regulation of endothelial cell gap formation and barrier dysfunction: role of myosin light chain phosphorylation. *J. Cell. Physiol.* **163,** 510–522 (1995).

24. Van Nieuw Amerongen, G. P., Draijer, R., Vermeer, M. A. & van Hinsbergh, V. W. Transient and prolonged increase in endothelial permeability induced by histamine and thrombin: role of protein kinases, calcium, and RhoA. *Circ. Res.* **83,** 1115–1123 (1998).

25. Dudek, S. M. *et al.* Pulmonary endothelial cell barrier enhancement by sphingosine 1-phosphate. Roles for cortactin and myosin light chain kinase. *J. Biol. Chem.* **279,** 24692–24700 (2004).

26. Pekny, M. *et al.* Mice lacking glial fibrillary acidic protein display astrocytes devoid of intermediate filaments but develop and reproduce normally. *EMBO J.* **14,** 1590–1598 (1995).

27. Gu, L. H. & Coulombe, P. A. Keratin function in skin epithelia: a broadening palette with surprising shades. *Current Opinion in Cell Biology* **19,** 13–23 (2007).

28. Birukova, A. A. *et al.* Novel role of microtubules in thrombin-induced endothelial barrier dysfunction. *FASEB J.* **18,** 1879–1890 (2004).

29. Tian, X., Tian, Y., Moldobaeva, N., Sarich, N. & Birukova, A. A. Microtubule Dynamics Control HGF-Induced Lung Endothelial Barrier Enhancement. *PLoS ONE* **9,** (2014).

30. Hodivala-Dilke, K. M., Reynolds, A. R. & Reynolds, L. E. Integrins in angiogenesis: Multitalented molecules in a balancing act. *Cell and Tissue Research* **314,** 131–144 (2003).

31. Petit, V. & Thiery, J. P. Focal adhesions: structure and dynamics. *Biol. Cell* **92,** 477–494 (2000).

32. Moy, A. B. *et al.* Histamine alters endothelial barrier function at cell-cell and cell-matrix sites. *Am. J. Physiol. Lung Cell. Mol. Physiol.* **278,** L888–L898 (2000).

33. Wegener, J., Keese, C. R. & Giaever, I. Electric cell-substrate impedance sensing (ECIS) as a noninvasive means to monitor the kinetics of cell spreading to artificial surfaces. *Exp. Cell Res.* **259,** 158–166 (2000).

34. Cohler, L. F., Saba, T. M. & Lewis, E. P. Lung vascular injury with protease infusion. Relationship to plasma fibronectin. *Ann. Surg.* **202,** 240–247 (1985).

35. Daudi, I. *et al.* Fibronectin fragments in lung lymph after thrombin-induced lung vascular injury. *Lab. Invest.* **61,** 539–547 (1989).

36. Vincent, P. A., Rebres, R. A., Lewis, E. P., Hurst, V. & Saba, T. M. Release of ED1 fibronectin from matrix of perfused lungs after vascular injury is independent of protein synthesis. *Am. J. Physiol.* **265,** L485–L492 (1993).

37. Del Zoppo, G. J. & Milner, R. Integrin-matrix interactions in the cerebral microvasculature. *Arteriosclerosis, Thrombosis, and Vascular Biology* **26,** 1966–1975 (2006).

38. Wu, M. H. Endothelial focal adhesions and barrier function. *J. Physiol.* **569,** 359–366 (2005).

39. Lampugnani, M. G., Resnati, M., Dejana, E. & Marchisio, P. C. The role of integrins in the maintenance of endothelial monolayer integrity. *J. Cell Biol.* **112,** 479–490 (1991).

40. Guo, M. *et al.* Fibrinogen-γ C-Terminal fragments induce endothelial barrier dysfunction and microvascular leak via integrin-mediated and RhoA-dependent mechanism. *Arterioscler. Thromb. Vasc. Biol.* **29,** 394–400 (2009).

41. Vittet, D., Buchou, T., Schweitzer, A., Dejana, E. & Huber, P. Targeted null-mutation in the vascular endothelial-cadherin gene impairs the organization of vascular-like structures in embryoid bodies. *Proc. Natl. Acad. Sci. U. S. A.* **94,** 6273–6278 (1997).

42. Carmeliet, P. *et al.* Targeted deficiency or cytosolic truncation of the VE-cadherin gene in mice impairs VEGF-mediated endothelial survival and angiogenesis. *Cell* **98,** 147–157 (1999).

43. Garcia, J. G. & Schaphorst, K. L. Regulation of endothelial cell gap formation and paracellular permeability. *J. Investig. Med.* **43,** 117–126 (1995).

44. Nieset, J. E. *et al.* Characterization of the interactions of α -catenin with α -actinin and β-catenin/plakoglobin. *J. Cell Sci.* **110,** 1013–1022 (1997).

45. Jou, T. S., Stewart, D. B., Stappert, J., Nelson, W. J. & Marrs, J. A. Genetic and biochemical dissection of protein linkages in the cadherin-catenin complex. *Proc. Natl. Acad. Sci. U. S. A.* **92,** 5067–5071 (1995).

46. Imamura, Y., Itoh, M., Maeno, Y., Tsukita, S. & Nagafuchi, A. Functional domains of ??-catenin required for the strong state of cadherin-based cell adhesion. *J. Cell Biol.* **144,** 1311–1322 (1999).

47. Knudsen, K. A., Soler, A. P., Johnson, K. R. & Wheelock, M. J. Interaction of alpha-actinin with the cadherin/catenin cell-cell adhesion complex via alpha-catenin. *J. Cell Biol.* **130,** 67–77 (1995).

48. Vasioukhin, V., Bauer, C., Yin, M. & Fuchs, E. Directed actin polymerization is the driving force for epithelial cell-cell adhesion. *Cell* **100,** 209–219 (2000).

49. Kobielak, A., Pasolli, H. A. & Fuchs, E. Mammalian formin-1 participates in adherens junctions and polymerization of linear actin cables. *Nat. Cell Biol.* **6,** 21–30 (2004).

50. Beckman, D. L., Mehta, P., Hanks, V., Rowan, W. H. & Liu, L. Effects of peroxynitrite on pulmonary edema and the oxidate state. *Exp. Lung Res.* **26,** 349–359 (2000).

51. Piedra, J. *et al.* p120 Catenin-associated Fer and Fyn tyrosine kinases regulate beta-catenin Tyr-142 phosphorylation and beta-catenin-alpha-catenin Interaction. *Mol. Cell. Biol.* **23,** 2287–2297 (2003).

52. Reynolds, A. B. & Roczniak-Ferguson, A. Emerging roles for p120-catenin in cell adhesion and cancer. *Oncogene* **23,** 7947–7956 (2004).

53. Alcaide, P. *et al.* p120-catenin regulates leukocyte transmigration through an effect on VE-cadherin phosphorylation. *Blood* **112,** 2770–2779 (2008).

54. Sallee, J. L., Wittchen, E. S. & Burridge, K. Regulation of cell adhesion by protein-tyrosine phosphatases II. Cell-cell adhesion. *Journal of Biological Chemistry* **281,** 16189–16192 (2006).

55. Vincent, P. A., Xiao, K., Buckley, K. M. & Kowalczyk, A. P. VE-cadherin: adhesion at arm's length. *Am. J. Physiol. Cell Physiol.* **286,** C987–C997 (2004).

56. Wójciak-Stothard, B., Potempa, S., Eichholtz, T. & Ridley, A. J. Rho and Rac but not Cdc42 regulate endothelial cell permeability. *J. Cell Sci.* **114,** 1343–1355 (2001).

57. Abbott, N. J., Patabendige, A. A. K., Dolman, D. E. M., Yusof, S. R. & Begley, D. J. Structure and function of the blood-brain barrier. *Neurobiology of Disease* **37,** 13–25 (2010).

58. Hawkins, B. T. & Davis, T. P. The Blood-Brain Barrier / Neurovascular Unit in Health and Disease. *Pharmacol. Rev.* **57,** 173–185 (2005).

59. González-Mariscal, L. *et al.* MAGUK proteins: structure and role in the tight junction. *Semin. Cell Dev. Biol.* **11,** 315–24 (2000).

60. Graham, M. M. & Evans, M. L. A simple, dual tracer method for the measurement of transvascular flux of albumin into the lung. *Microvasc. Res.* **42,** 266–279 (1991).

61. Kevil, C. G. *et al.* Expression of zonula occludens and adherens junctional proteins in human venous and arterial endothelial cells: role of occludin in endothelial solute barriers. *Microcirculation* **5,** 197–210 (1998).

62. Huber, D., Balda, M. S. & Matter, K. Occludin modulates transepithelial migration of neutrophils. *J. Biol. Chem.* **275,** 5773–5778 (2000).

63. Bamforth, S. D., Kniesel, U., Wolburg, H., Engelhardt, B. & Risau, W. A dominant mutant of occludin disrupts tight junction structure and function. *J. Cell Sci.* **112 (Pt 1,** 1879–1888 (1999).

64. Hirase, T. *et al.* Occludin as a possible determinant of tight junction permeability in endothelial cells. *J. Cell Sci.* **110 (Pt 1,** 1603–1613 (1997).

65. Saitou, M. *et al.* Complex phenotype of mice lacking occludin, a component of tight junction strands. *Mol. Biol. Cell* **11,** 4131–4142 (2000).

66. Morita, K., Sasaki, H., Furuse, M. & Tsukita, S. Endothelial claudin: Claudin-5/TMVCF constitutes tight junction strands in endothelial cells. *J. Cell Biol.* **147,** 185–194 (1999).

67. Nitta, T. *et al.* Size-selective loosening of the blood-brain barrier in claudin-5-deficient mice. *J. Cell Biol.* **161,** 653–660 (2003).

68. Aurrand-Lions, M., Duncan, L., Ballestrem, C. & Imhof, B. A. JAM-2, a Novel Immunoglobulin Superfamily Molecule, Expressed by Endothelial and Lymphatic Cells. *J. Biol. Chem.* **276,** 2733–2741 (2001).

69. Aurrand-Lions, M., Johnson-Leger, C., Wong, C., Du Pasquier, L. & Imhof, B. A. Heterogeneity of endothelial junctions is reflected by differential expression and specific subcellular localization of the three JAM family members. *Blood* **98,** 3699–3707 (2001).

70. Aurrand-Lions, M. A., Duncan, L., Du Pasquier, L. & Imhof, B. A. Cloning of JAM-2 and JAM-3: an emerging junctional adhesion molecular family? *Curr. Top. Microbiol. Immunol.* **251,** 91–98 (2000).

71. Underwood, J. L. *et al.* Glucocorticoids regulate transendothelial fluid flow resistance and formation of intercellular junctions. *Am. J. Physiol.* **277,** C330–C342 (1999).

72. Youakim, A. & Ahdieh, M. Interferon-gamma decreases barrier function in T84 cells by reducing ZO-1 levels and disrupting apical actin. *Am. J. Physiol.* **276,** G1279–G1288 (1999).

73. Itoh, M., Yonemura, S., Nagafuchi, A., Tsukita, S. & Tsukita, S. A 220-kD undercoat-constitutive protein: Its specific localization at cadherin-based cell-cell adhesion sites. *J. Cell Biol.* **115,** 1449–1462 (1991).

74. Howarth, A. G., Hughes, M. R. & Stevenson, B. R. Detection of the tight junction-associated protein ZO-1 in astrocytes and other nonepithelial cell types. *Am. J. Physiol.* **262,** C461–C469 (1992).

75. González-Mariscal, L. *et al.* Molecular characterization of the tight junction protein ZO-1 in MDCK cells. *Exp. Cell Res.* **248,** 97–109 (1999).

76. Goodenough, D. A. & Paul, D. L. Beyond the gap: functions of unpaired connexon channels. *Nat. Rev. Mol. Cell Biol.* **4,** 285–294 (2003).

77. Van Rijen, H. *et al.* Gap junctions in human umbilical cord endothelial cells contain multiple connexins. *Am J Physiol* **272,** C117–30 (1997).

78. Van Rijen, H. V, van Kempen, M. J., Postma, S. & Jongsma, H. J. Tumour necrosis factor alpha alters the expression of connexin43, connexin40, and connexin37 in human umbilical vein endothelial cells. *Cytokine* **10,** 258–264 (1998).

79. Simon, A. M. & McWhorter, A. R. Vascular abnormalities in mice lacking the endothelial gap junction proteins connexin37 and connexin40. *Dev. Biol.* **251,** 206–220 (2002).

80. Minshall, R. D., Tiruppathi, C., Vogel, S. M. & Malik, A. B. Vesicle formation and trafficking in endothelial cells and regulation of endothelial barrier function. in *Histochemistry and Cell Biology* **117,** 105–112 (2002).

81. Nanbo, A. *et al.* Ebolavirus is internalized into host cells via macropinocytosis in a viral glycoprotein-dependent manner. *PLoS Pathog.* **6,** (2010).

82. Mercer, J. & Helenius, A. Virus entry by macropinocytosis. *Nat Cell Biol* **11,** 510–520 (2009).

83. Bruewer, M. *et al.* Interferon-gamma induces internalization of epithelial tight junction proteins via a macropinocytosis-like process. *FASEB J.* **19,** 923–933 (2005).

84. Morris, S. A., Ahle, S. & Ungewickell, E. Clathrin-coated vesicles. *Curr. Opin. Cell Biol.* **1,** 684–690 (1989).

85. McMahon, H. T. & Boucrot, E. Molecular mechanism and physiological functions of clathrin-mediated endocytosis. *Nat Rev Mol Cell Biol* **12,** 517–533 (2011).

86. Parton, R. G. & Simons, K. The multiple faces of caveolae. *Nat. Rev. Mol. Cell Biol.* **8,** 185–194 (2007).

87. Parton, R. G. & del Pozo, M. a. Caveolae as plasma membrane sensors, protectors and organizers. *Nat. Rev. Mol. Cell Biol.* **14,** 98–112 (2013).

88. Dvorak, A. M. *et al.* The vesiculo-vacuolar organelle (VVO): a distinct endothelial cell structure that provides a transcellular pathway for macromolecular extravasation. *J. Leukoc. Biol.* **59,** 100–115 (1996).

89. Bendayan, M. Morphological and cytochemical aspects of capillary permeability. *Microsc. Res. Tech.* **57,** 327–349 (2002).

90. Simionescu, M., Gafencu, A. & Antohe, F. Transcytosis of plasma macromolecules in endothelial cells: a cell biological survey. *Microsc. Res. Tech.* **57,** 269–288 (2002).

91. Bauer, P. M. *et al.* Endothelial-specific expression of caveolin-1 impairs microvascular permeability and angiogenesis. *Proc. Natl. Acad. Sci. U. S. A.* **102,** 204–209 (2005).

92. Gratton, J. P., Bernatchez, P. & Sessa, W. C. Caveolae and caveolins in the cardiovascular system. *Circulation Research* **94,** 1408–1417 (2004).

93. Lin, M. I., Yu, J., Murata, T. & Sessa, W. C. Caveolin-1 - Deficient mice have increased tumor microvascular permeability, angiogenesis, and growth. *Cancer Res.* **67,** 2849–2856 (2007).

94. Predescu, S. A., Predescu, D. N. & Malik, A. B. Molecular determinants of endothelial transcytosis and their role in endothelial permeability. *Am. J. Physiol. Lung Cell. Mol. Physiol.* **293,** L823–L842 (2007).

95. Zhang, Y., Zhang, L., Li, Y., Sun, S. & Tan, H. Different Contributions of Clathrin- and Caveolae-Mediated Endocytosis of Vascular Endothelial Cadherin to Lipopolysaccharide-Induced Vascular Hyperpermeability. *PLoS One* **9,** e106328 (2014).

96. Zimmerman, M. A. *et al.* Equilibrative nucleoside transporter (ENT)-1-dependent elevation of extracellular adenosine protects the liver during ischemia and reperfusion. *Hepatology* **58,** 1766–1778 (2013).

97. McGaraughty, S., Cowart, M., Jarvis, M. F. & Berman, R. F. Anticonvulsant and antinociceptive actions of novel adenosine kinase inhibitors. *Curr. Top. Med. Chem.* **5,** 43–58 (2005).

98. Dos Santos-Rodrigues, A., Pereira, M. R., Brito, R., de Oliveira, N. A. & Paes-de-Carvalho, R. Adenosine transporters and receptors: key elements for retinal function and neuroprotection. *Vitam. Horm.* **98,** 487–523 (2015).

99. Eckle, T., Grenz, A., Laucher, S. & Eltzschig, H. K. A2B adenosine receptor signaling attenuates acute lung injury by enhancing alveolar fluid clearance in mice. *The Journal of Clinical Investigation* **118,** 3301–3315 (2008).

100. Firestein, G. S. *et al.* Protective effect of an adenosine kinase inhibitor in septic shock. *J.Immunol.* **152,** 5853–5859 (1994).

101. Allison, R. C., Hernandez, E. M., Prasad, V. R., Grisham, M. B. & Taylor, A. E. Protective effects of O2 radical scavengers and adenosine in PMA-induced lung injury. *J. Appl. Physiol.* **64,** 2175–2182 (1988).

102. Jacobson, K. A. & Gao, Z.-G. Adenosine receptors as therapeutic targets. *Nat. Rev. Drug Discov.* **5,** 247–264 (2006).

103. Leach, L., Eaton, B. M., Westcott, E. D. & Firth, J. A. Effect of histamine on endothelial permeability and structure and adhesion molecules of the

paracellular junctions of perfused human placental microvessels. *Microvasc. Res.* **50,** 323–337 (1995).

104. Wu, N. Z. & Baldwin, A. L. Transient venular permeability increase and endothelial gap formation induced by histamine. *Am. J. Physiol.* **262,** H1238–H1247 (1992).

105. Carson, M. R., Shasby, S. S. & Shasby, D. M. Histamine and inositol phosphate accumulation in endothelium: cAMP and a G protein. *Am. J. Physiol.* **257,** L259–L264 (1989).

106. Laposata, M., Dovnarsky, D. K. & Shin, H. S. Thrombin-induced gap formation in confluent endothelial cell monolayers in vitro. *Blood* **62,** 549–556 (1983).

107. Majno, G., Shea, S. M. & Leventhal, M. Endothelial contraction induced by histamine-type mediators: an electron microscopic study. *J. Cell Biol.* **42,** 647–672 (1969).

108. Moy, A. B., Shasby, S. S., Scott, B. D. & Shasby, D. M. The effect of histamine and cyclic adenosine monophosphate on myosin light chain phosphorylation in human umbilical vein endothelial cells. *J. Clin. Invest.* **92,** 1198–1206 (1993).

109. Cirino, G. *et al.* Thrombin functions as an inflammatory mediator through activation of its receptor. *J. Exp. Med.* **183,** 821–827 (1996).

110. Peng, X. *et al.* Protective Effects of Sphingosine 1-Phosphate in Murine Endotoxin-induced Inflammatory Lung Injury. *Am. J. Respir. Crit. Care Med.* **169,** 1245–1251 (2004).

111. Finigan, J. H. *et al.* Activated protein C mediates novel lung endothelial barrier enhancement: Role of sphingosine 1-phosphate receptor transactivation. *J. Biol. Chem.* **280,** 17286–17293 (2005).

112. McVerry, B. J. *et al.* Sphingosine 1-Phosphate Reduces Vascular Leak in Murine and Canine Models of Acute Lung Injury. *Am. J. Respir. Crit. Care Med.* **170,** 987–993 (2004).

113. Saba, J. D. & Hla, T. Point-Counterpoint of Sphingosine 1-Phosphate Metabolism. *Circulation Research* **94,** 724–734 (2004).

114. Hait, N. C., Oskeritzian, C. A., Paugh, S. W., Milstien, S. & Spiegel, S. Sphingosine kinases, sphingosine 1-phosphate, apoptosis and diseases. *Biochimica et Biophysica Acta - Biomembranes* **1758,** 2016–2026 (2006).

115. Tauseef, M. *et al.* Activation of sphingosine kinase-1 reverses the increase in lung vascular permeability through sphingosine-1-phosphate receptor signaling in endothelial cells. *Circ. Res.* **103,** 1164–1172 (2008).

116. Srinivas, S. P., Satpathy, M., Gallagher, P., Lariviere, E. & Van Driessche, W. Adenosine induces dephosphorylation of myosin II regulatory light chain in cultured bovine corneal endothelial cells. *Exp. Eye Res.* **79,** 543–551 (2004).

117. Stelzner, T. J., Weil, J. V & O'Brien, R. F. Role of cyclic adenosine monophosphate in the induction of endothelial barrier properties. *J. Cell. Physiol.* **139,** 157–166 (1989).

118. Sayner, S. L. *et al.* Paradoxical cAMP-induced lung endothelial hyperpermeability revealed by pseudomonas aeruginosa ExoY. *Circ. Res.* **95,** 196–203 (2004).

119. Sayner, S. L., Alexeyev, M., Dessauer, C. W. & Stevens, T. Soluble adenylyl cyclase reveals the significance of cAMP compartmentation on pulmonary microvascular endothelial cell barrier. *Circ. Res.* **98,** 675–681 (2006).

120. Zaccolo, M. cAMP signal transduction in the heart: understanding spatial control for the development of novel therapeutic strategies. *Br. J. Pharmacol.* **158,** 50–60 (2009).

121. Zaccolo, M. Spatial control of cAMP signalling in health and disease. *Curr. Opin. Pharmacol.* **11,** 649–55 (2011).

122. Ignarro, L. J. Nitric oxide: A unique endogenous signaling molecule in vascular biology. in *Bioscience Reports* **19,** 51–71 (1999).

123. D'Souza, S. P., Davis, M. & Baxter, G. F. Autocrine and paracrine actions of natriuretic peptides in the heart. *Pharmacology and Therapeutics* **101,** 113–129 (2004).

124. Waldman, S. A. & Murad, F. Biochemical mechanisms underlying vascular smooth muscle relaxation: the guanylate cyclase-cyclic GMP system. *J. Cardiovasc. Pharmacol.* **12 Suppl 5,** S115–S118 (1988).

125. Litvin, T. N., Kamenetsky, M., Zarifyan, A., Buck, J. & Levin, L. R. Kinetic properties of 'soluble' adenylyl cyclase: Synergism between calcium and bicarbonate. *J. Biol. Chem.* **278,** 15922–15926 (2003).

126. Chen, Y. *et al.* Soluble adenylyl cyclase as an evolutionarily conserved bicarbonate sensor. *Science* **289,** 625–628 (2000).

127. Kaupp, U. B. & Seifert, R. Cyclic nucleotide-gated ion channels. *Physiol. Rev.* **82,** 769–824 (2002).

128. Surapisitchat, J., Jeon, K.-I., Yan, C. & Beavo, J. A. Differential regulation of endothelial cell permeability by cGMP via phosphodiesterases 2 and 3. *Circ. Res.* **101,** 811–818 (2007).

129. Zaccolo, M. & Movsesian, M. A. cAMP and cGMP signaling cross-talk: Role of phosphodiesterases and implications for cardiac pathophysiology. *Circulation Research* **100,** 1569–1578 (2007).

130. Stangherlin, A. & Zaccolo, M. cGMP-cAMP interplay in cardiac myocytes: a local affair with far-reaching consequences for heart function. *Biochem. Soc. Trans.* **40,** 11–4 (2012).

131. Stevens, R. C. *et al.* The GPCR Network: a large-scale collaboration to determine human GPCR structure and function. *Nat Rev Drug Discov* **12,** 25–34 (2013).

132. Overington, J. P., Al-Lazikani, B. & Hopkins, A. L. How many drug targets are there? *Nat. Rev. Drug Discov.* **5,** 993–996 (2006).

133. Tyndall, J. D. A. & Sandilya, R. GPCR agonists and antagonists in the clinic. *Med. Chem.* **1,** 405–421 (2005).

134. Klabunde, T. & Hessler, G. Drug design strategies for targeting G-protein-coupled receptors. *Chembiochem* **3,** 928–944 (2002).

135. Kroeze, W. K., Sheffler, D. J. & Roth, B. L. G-protein-coupled receptors at a glance. *J. Cell Sci.* **116,** 4867–4869 (2003).

136. Fredriksson, R., Lagerström, M. C., Lundin, L.-G. & Schiöth, H. B. The G-protein-coupled receptors in the human genome form five main families. Phylogenetic analysis, paralogon groups, and fingerprints. *Mol. Pharmacol.* **63,** 1256–1272 (2003).

137. Hollenstein, K. *et al.* Structure of class B GPCR corticotropin-releasing factor receptor 1. *Nature* **499,** 438–43 (2013).

138. Siu, F. Y. *et al.* Structure of the human glucagon class B G-protein-coupled receptor. *Nature* **499,** 444–449 (2013).

139. Fredriksson, R. & Schiöth, H. B. The repertoire of G-protein-coupled receptors in fully sequenced genomes. *Mol. Pharmacol.* **67,** 1414–1425 (2005).

140. Pal, K., Melcher, K. & Xu, H. E. Structure and mechanism for recognition of peptide hormones by Class B G-protein-coupled receptors. *Acta Pharmacologica Sinica* **33,** 300–311 (2012).

141. Pin, J.-P., Galvez, T. & Prezeau, L. Evolution, structure, and activation mechanism of family 3/C G-protein-coupled receptors. *Pharmacol. Ther.* **98,** 325–354 (2003).

142. Bjarnadóttir, T. K., Fredriksson, R. & Schiöth, H. B. The Adhesion GPCRs: A unique family of G protein-coupled receptors with important

roles in both central and peripheral tissues. *Cellular and Molecular Life Sciences* **64,** 2104–2119 (2007).

143. Adler, P. N. Planar signaling and morphogenesis in Drosophila. *Developmental Cell* **2,** 525–535 (2002).

144. Chandrashekar, J. *et al.* T2Rs function as bitter taste receptors. *Cell* **100,** 703–711 (2000).

145. Warne, T. *et al.* Structure of a beta1-adrenergic G-protein-coupled receptor. *Nature* **454,** 486–491 (2008).

146. Cherezov, V. *et al.* High-resolution crystal structure of an engineered human beta2-adrenergic G protein-coupled receptor. *Science* **318,** 1258–1265 (2007).

147. Shimamura, T. *et al.* Structure of the human histamine H1 receptor complex with doxepin. *Nature* **475,** 65–70 (2011).

148. Haga, K. *et al.* Structure of the human M2 muscarinic acetylcholine receptor bound to an antagonist. *Nature* **482,** 547–551 (2012).

149. Kruse, A. C. *et al.* Structure and dynamics of the M3 muscarinic acetylcholine receptor. *Nature* **482,** 552–556 (2012).

150. Hanson, M. A. *et al.* Crystal Structure of a Lipid G Protein-Coupled Receptor. *Science* **335,** 851–855 (2012).

151. Ramachandran, R. Developing PAR1 antagonists: minding the endothelial gap. *Discov Med* **13,** 425–431 (2012).

152. Chackalamannil, S. *et al.* Discovery of a novel, orally active himbacine-based thrombin receptor antagonist (SCH 530348) with potent antiplatelet activity. *J. Med. Chem.* **51,** 3061–3064 (2008).

153. Morrow, D. A. *et al.* Vorapaxar in the Secondary Prevention of Atherothrombotic Events. *New England Journal of Medicine* **366,** 1404–1413 (2012).

154. Tricoci, P. *et al.* Thrombin-Receptor Antagonist Vorapaxar in Acute Coronary Syndromes. *New England Journal of Medicine* **366,** 20–33 (2012).

155. Levoye, A., Dam, J., Ayoub, M. A., Guillaume, J.-L. & Jockers, R. Do orphan G-protein-coupled receptors have ligand-independent functions? New insights from receptor heterodimers. *EMBO Rep.* **7,** 1094–1098 (2006).

156. Schwartz, T. W., Frimurer, T. M., Holst, B., Rosenkilde, M. M. & Elling, C. E. Molecular mechanism of 7TM receptor activation--a global toggle switch model. *Annu. Rev. Pharmacol. Toxicol.* **46,** 481–519 (2006).

157. Nygaard, R., Frimurer, T. M., Holst, B., Rosenkilde, M. M. & Schwartz, T. W. Ligand binding and micro-switches in 7TM receptor structures. *Trends in Pharmacological Sciences* **30,** 249–259 (2009).

158. Katritch, V., Cherezov, V. & Stevens, R. C. Structure-function of the G protein-coupled receptor superfamily. *Annu. Rev. Pharmacol. Toxicol.* **53,** 531–56 (2013).

159. Deupi, X. & Standfuss, J. Structural insights into agonist-induced activation of G-protein-coupled receptors. *Current Opinion in Structural Biology* **21,** 541–551 (2011).

160. Premont, R. T. & Gainetdinov, R. R. Physiological roles of G protein-coupled receptor kinases and arrestins. *Annu. Rev. Physiol.* **69,** 511–534 (2007).

161. Luttrell, L. M. & Lefkowitz, R. J. The role of beta-arrestins in the termination and transduction of G-protein-coupled receptor signals. *J. Cell Sci.* **115,** 455–65 (2002).

162. May, L. T., Leach, K., Sexton, P. M. & Christopoulos, A. Allosteric modulation of G protein-coupled receptors. *Annu. Rev. Pharmacol. Toxicol.* **47,** 1–51 (2007).

163. Leach, K., Sexton, P. M. & Christopoulos, A. Allosteric GPCR modulators: taking advantage of permissive receptor pharmacology. *Trends Pharmacol. Sci.* **28,** 382–389 (2007).

164. Christopoulos, A. Allosteric binding sites on cell-surface receptors: novel targets for drug discovery. *Nat. Rev. Drug Discov.* **1,** 198–210 (2002).

165. Jensen, A. A. & Bräuner-Osborne, H. Allosteric modulation of the calcium-sensing receptor. *Curr. Neuropharmacol.* **5,** 180–186 (2007).

166. Wu, B. *et al.* Structures of the CXCR4 chemokine GPCR with small-molecule and cyclic peptide antagonists. *Science* **330,** 1066–1071 (2010).

167. Gomes, I. *et al.* Heterodimerization of mu and delta opioid receptors: A role in opiate synergy. *J. Neurosci.* **20,** RC110 (2000).

168. Jordan, B. A. & Devi, L. A. G-protein-coupled receptor heterodimerization modulates receptor function. *Nature* **399,** 697–700 (1999).

169. Bissantz, C. Conformational changes of G protein-coupled receptors during their activation by agonist binding. *J. Recept. Signal Transduct. Res.* **23,** 123–153 (2003).

170. Milligan, G., Canals, M., Pediani, J. D., Ellis, J. & Lopez-Gimenez, J. F. The role of GPCR dimerisation/oligomerisation in receptor signalling. *Ernst Schering Found. Symp. Proc.* 145–161 (2006). doi:10.1007/2789

171. Morris, A. J. & Malbon, C. C. Physiological regulation of G protein-linked signaling. *Physiol. Rev.* **79,** 1373–1430 (1999).

172. Malbon, C. C. G proteins in development. *Nat. Rev. Mol. Cell Biol.* **6,** 689–701 (2005).

173. Hermans, E. Biochemical and pharmacological control of the multiplicity of coupling at G-protein-coupled receptors. *Pharmacol. Ther.* **99,** 25–44 (2003).

174. Downes, G. B. & Gautam, N. The G protein subunit gene families. *Genomics* **62,** 544–552 (1999).

175. Oldham, W. M. & Hamm, H. E. Heterotrimeric G protein activation by G-protein-coupled receptors. *Nat. Rev. Mol. Cell Biol.* **9,** 60–71 (2008).

176. Simon, M. I., Strathmann, M. P. & Gautam, N. Diversity of G proteins in signal transduction. *Science* **252,** 802–808 (1991).

177. Rodriguez-Viciana, P. *et al.* Role of phosphoinositide 3-OH kinase in cell transformation and control of the actin cytoskeleton by Ras. *Cell* **89,** 457–467 (1997).

178. Hall, A. Rho GTPases and the Actin Cytoskeleton. *Science* **279,** 509–514 (1998).

179. Holinstat, M., Mehta, D., Kozasa, T., Minshall, R. D. & Malik, A. B. Protein kinase C??-induced p115RhoGEF phosphorylation signals endothelial cytoskeletal rearrangement. *J. Biol. Chem.* **278,** 28793–28798 (2003).

180. Neves, S. R., Ram, P. T. & Iyengar, R. G protein pathways. *Science* **296,** 1636–1639 (2002).

181. Wu, H. M., Yuan, Y., Zawieja, D. C., Tinsley, J. & Granger, H. J. Role of phospholipase C, protein kinase C, and calcium in VEGF-induced venular hyperpermeability. *Am J Physiol* **276,** H535–42 (1999).

182. Scott-Burden, T., Elizondo, E., Ge, T., Boulanger, C. M. & Vanhoutte, P. M. Simultaneous activation of adenylyl cyclase and protein kinase C induces production of nitric oxide by vascular smooth muscle cells. *Mol. Pharmacol.* **46,** 274–282 (1994).

183. Curry, F. E. Modulation of venular microvessel permeability by calcium influx into endothelial cells. *FASEB J.* **6,** 2456–2466 (1992).

184. Hurley, J. H. Structure, mechanism, and regulation of mammalian adenylyl cyclase. *J. Biol. Chem.* **274,** 7599–602 (1999).

185. Sunahara, R. K., Dessauer, C. W. & Gilman, A. G. Complexity and diversity of mammalian adenylyl cyclases. *Annu. Rev. Pharmacol. Toxicol.* **36,** 461–480 (1996).

186. Iyengar, R. Molecular and functional diversity of mammalian Gs-stimulated adenylyl cyclases. *FASEB J.* **7,** 768–775 (1993).

187. Xia, Z. & Storm, D. R. Calmodulin-regulated adenylyl cyclases and neuromodulation. *Current Opinion in Neurobiology* **7,** 391–396 (1997).

188. Hurley, J. H. Structure, Mechanism, and Regulation of Mammalian Adenylyl Cyclase. *J. Biol. Chem.* **274,** 7599–7602 (1999).

189. Defer, N., Best-Belpomme, M. & Hanoune, J. Tissue specificity and physiological relevance of various isoforms of adenylyl cyclase. *Am. J. Physiol. Renal Physiol.* **279,** F400–F416 (2000).

190. Steegborn, C. Structure, mechanism, and regulation of soluble adenylyl cyclases - similarities and differences to transmembrane adenylyl cyclases. *Biochim. Biophys. Acta* **1842,** 2535–2547 (2014).

191. Sadana, R. & Dessauer, C. W. Physiological roles for G protein-regulated adenylyl cyclase isoforms: Insights from knockout and overexpression studies. *NeuroSignals* **17,** 5–22 (2009).

192. Hanoune, J. & Defer, N. Regulation and role of adenylyl cyclase isoforms. *Annu. Rev. Pharmacol. Toxicol.* **41,** 145–174 (2001).

193. Manolopoulos, V. G., Liu, J., Unsworth, B. R. & Lelkes, P. I. Adenylyl cyclase isoforms are differentially expressed in primary cultures of endothelial cells and whole tissue homogenates from various rat tissues. *Biochem. Biophys. Res. Commun.* **208,** 323–331 (1995).

194. Garty, N. B. & Salomon, Y. Stimulation of partially purified adenylate cyclase from bull sperm by bicarbonate. *FEBS Lett.* **218,** 148–152 (1987).

195. Zippin, J. H. *et al.* Compartmentalization of bicarbonate-sensitive adenylyl cyclase in distinct signaling microdomains. *FASEB J.* **17,** 82–84 (2003).

196. Paunescu, T. G. *et al.* Association of soluble adenylyl cyclase with the V-ATPase in renal epithelial cells. *Am. J. Physiol. Renal Physiol.* **294,** F130–F138 (2008).

197. Braun, T. & Dods, R. F. Development of a Mn-2+-sensitive, 'soluble' adenylate cyclase in rat testis. *Proc. Natl. Acad. Sci. U. S. A.* **72,** 1097–1101 (1975).

198. Nomura, M., Beltrán, C., Darszon, A. & Vacquier, V. D. A soluble adenylyl cyclase from sea urchin spermatozoa. *Gene* **353,** 231–238 (2005).

199. Lucas, K. A. *et al.* Guanylyl cyclases and signaling by cyclic GMP. *Pharmacol. Rev.* **52,** 375–414 (2000).

200. Bellamy, T. C., Wood, J. & Garthwaite, J. On the activation of soluble guanylyl cyclase by nitric oxide. *Proc. Natl. Acad. Sci. U. S. A.* **99,** 507–510 (2002).

201. Collier, J. & Vallance, P. Second messenger role for NO widens to nervous and immune systems. *Trends Pharmacol. Sci.* **10,** 427–431 (1989).

202. Vallance, P., Collier, J. & Moncada, S. *Effects of endothelium-derived nitric oxide on peripheral arteriolar tone in man. Lancet* **2,** (1989).

203. Taskén, K. & Aandahl, E. M. Localized effects of cAMP mediated by distinct routes of protein kinase A. *Physiol. Rev.* **84,** 137–167 (2004).

204. Taylor, S. S., Buechler, J. A. & Yonemoto, W. cAMP-dependent protein kinase: framework for a diverse family of regulatory enzymes. *Annu. Rev. Biochem.* **59,** 971–1005 (1990).

205. Lee, D. C., Carmichael, D. F., Krebs, E. G. & McKnight, G. S. Isolation of a cDNA clone for the type I regulatory subunit of bovine cAMP-dependent protein kinase. *Proc. Natl. Acad. Sci. U. S. A.* **80,** 3608–3612 (1983).

206. Clegg, C. H., Cadd, G. G. & McKnight, G. S. Genetic characterization of a brain-specific form of the type I regulatory subunit of cAMP-dependent protein kinase. *Proc. Natl. Acad. Sci. U. S. A.* **85,** 3703–3707 (1988).

207. Scott, J. D. *et al.* The molecular cloning of a type II regulatory subunit of the cAMP-dependent protein kinase from rat skeletal muscle and mouse brain. *Proc. Natl. Acad. Sci. U. S. A.* **84,** 5192–5196 (1987).

208. Cheng, X., Ji, Z., Tsalkova, T. & Mei, F. Epac and PKA: A tale of two intracellular cAMP receptors. *Acta Biochimica et Biophysica Sinica* **40,** 651–662 (2008).

209. Beebe, S. J. *et al.* Molecular cloning of a tissue-specific protein kinase (C gamma) from human testis--representing a third isoform for the catalytic subunit of cAMP-dependent protein kinase. *Mol. Endocrinol.* **4,** 465–475 (1990).

210. Weber, I. T., Steitz, T. A., Bubis, J. & Taylor, S. S. Predicted structures of cAMP binding domains of type I and II regulatory subunits of cAMP-dependent protein kinase. *Biochemistry* **26,** 343–351 (1987).

211. Dudek, S. M. & Garcia, J. G. Cytoskeletal regulation of pulmonary vascular permeability. *J. Appl. Physiol.* **91,** 1487–1500 (2001).

212. Essler, M. *et al.* Thrombin inactivates myosin light chain phosphatase via Rho and its target Rho kinase in human endothelial cells. *J. Biol. Chem.* **273,** 21867–21874 (1998).

213. De Rooij, J. *et al.* Epac is a Rap1 guanine-nucleotide-exchange factor directly activated by cyclic AMP. *Nature* **396,** 474–477 (1998).

214. Kawasaki, H. *et al.* A family of cAMP-binding proteins that directly activate Rap1. *Science* **282,** 2275–2279 (1998).

215. Cohen, P. Protein kinases--the major drug targets of the twenty-first century? *Nat. Rev. Drug Discov.* **1,** 309–315 (2002).

216. Bos, J. L. Epac: a new cAMP target and new avenues in cAMP research. *Nat. Rev. Mol. Cell Biol.* **4,** 733–738 (2003).

217. Bos, J. L., de Rooij, J. & Reedquist, K. A. Rap1 signalling: adhering to new models. *Nat. Rev. Mol. Cell Biol.* **2,** 369–377 (2001).

218. Niimura, M. *et al.* Critical role of the N-terminal cyclic AMP-binding domain of Epac2 in its subcellular localization and function. *J. Cell. Physiol.* **219,** 652–658 (2009).

219. Grandoch, M., Roscioni, S. S. & Schmidt, M. The role of Epac proteins, novel cAMP mediators, in the regulation of immune, lung and neuronal function. *British Journal of Pharmacology* **159,** 265–284 (2010).

220. Schmidt, M., Dekker, F. J. & Maarsingh, H. Exchange protein directly activated by cAMP (epac): a multidomain cAMP mediator in the regulation of diverse biological functions. *Pharmacol. Rev.* **65,** 670–709 (2013).

221. Fukuhara, S. *et al.* Cyclic AMP potentiates vascular endothelial cadherin-mediated cell-cell contact to enhance endothelial barrier function through an Epac-Rap1 signaling pathway. *Mol. Cell. Biol.* **25,** 136–146 (2005).

222. De Rooij, J. *et al.* Mechanism of regulation of the Epac family of cAMP-dependent RapGEFs. *J. Biol. Chem.* **275,** 20829–20836 (2000).

223. Raaijmakers, J. H. & Bos, J. L. Specificity in Ras and Rap signaling. *Journal of Biological Chemistry* **284,** 10995–10999 (2009).

224. Kooistra, M. R. H., Corada, M., Dejana, E. & Bos, J. L. Epac1 regulates integrity of endothelial cell junctions through VE-cadherin. *FEBS Lett.* **579,** 4966–4972 (2005).

225. Cullere, X. *et al.* Regulation of vascular endothelial barrier function by Epac, a cAMP-activated exchange factor for Rap GTPase. *Blood* **105,** 1950–1955 (2005).

226. Adamson, R. H. *et al.* Epac/Rap1 pathway regulates microvascular hyperpermeability induced by PAF in rat mesentery. *Am. J. Physiol. Heart Circ. Physiol.* **294,** H1188–H1196 (2008).

227. Chrzanowska-Wodnicka, M., Smyth, S. S., Schoenwaelder, S. M., Fischer, T. H. & White, G. C. Rap1b is required for normal platelet function and hemostasis in mice. *J. Clin. Invest.* **115,** 680–687 (2005).

228. Knox, A. L. & Brown, N. H. Rap1 GTPase regulation of adherens junction positioning and cell adhesion. *Science* **295,** 1285–1288 (2002).

229. Ohba, Y. *et al.* Requirement for C3G-dependent Rap1 activation for cell adhesion and embryogenesis. *EMBO J.* **20,** 3333–3341 (2001).

230. Duchniewicz, M. *et al.* Rap1A-deficient T and B cells show impaired integrin-mediated cell adhesion. *Mol. Cell. Biol.* **26,** 643–653 (2006).

231. Birukova, A. A., Zagranichnaya, T., Alekseeva, E., Bokoch, G. M. & Birukov, K. G. Epac/Rap and PKA are novel mechanisms of ANP-induced Rac-mediated pulmonary endothelial barrier protection. *J. Cell. Physiol.* **215,** 715–724 (2008).

232. Lincoln, T. M., Komalavilas, P., Boerth, N. J., MacMillan-Crow, L. A. & Cornwell, T. L. cGMP signaling through cAMP- and cGMP-dependent protein kinases. *Adv. Pharmacol.* **34,** 305–322 (1995).

233. Lohmann, S. M., Vaandrager, A. B., Smolenski, A., Walter, U. & De Jonge, H. R. Distinct and specific functions of cGMP-dependent protein kinases. *Trends in Biochemical Sciences* **22,** 307–312 (1997).

234. Pfeifer, A. *et al.* Structure and function of cGMP-dependent protein kinases. *Rev. Physiol. Biochem. Pharmacol.* **135,** 105–149 (1999).

235. Uhler, M. D. Cloning and expression of a novel cyclic GMP-dependent protein kinase from mouse brain. *J. Biol. Chem.* **268,** 13586–13591 (1993).

236. Jarchau, T. *et al.* Cloning, expression, and in situ localization of rat intestinal cGMP-dependent protein kinase II. *Proc. Natl. Acad. Sci. U. S. A.* **91,** 9426–9430 (1994).

237. Francis, S. H., Noblett, B. D., Todd, B. W., Wells, J. N. & Corbin, J. D. Relaxation of vascular and tracheal smooth muscle by cyclic nucleotide analogs that preferentially activate purified cGMP-dependent protein kinase. *Mol. Pharmacol.* **34,** 506–517 (1988).

238. Butt, E. *et al.* Analysis of the functional role of cGMP-dependent protein kinase in intact human platelets using a specific activator 8-para-chlorophenylthio-cGMP. *Biochem. Pharmacol.* **43,** 2591–2600 (1992).

239. Jiang, H., Colbran, J. L., Francis, S. H. & Corbin, J. D. Direct evidence for cross-activation of cGMP-dependent protein kinase by cAMP in pig coronary arteries. *J. Biol. Chem.* **267,** 1015–1019 (1992).

240. Francis, S. H. & Corbin, J. D. Cyclic nucleotide-dependent protein kinases: intracellular receptors for cAMP and cGMP action. *Crit. Rev. Clin. Lab. Sci.* **36,** 275–328 (1999).

241. Hofmann, F., Bernhard, D., Lukowski, R. & Weinmeister, P. CGMP regulated protein Kinases (cGK). *Handbook of Experimental Pharmacology* **191,** 137–162 (2009).

242. Lorenz, R. *et al.* Transforming PKA into PKG – a structure-function approach to understand cyclic nucleotide selectivity. *BMC Pharmacol. Toxicol.* **14,** P41–P41 (2013).

243. Dousa, T. P. Cyclic-3',5'-nucleotide phosphodiesterase isozymes in cell biology and pathophysiology of the kidney. *Kidney International* **55,** 29–62 (1999).

244. Mika, D., Leroy, J., Vandecasteele, G. & Fischmeister, R. PDEs create local domains of cAMP signaling. *Journal of Molecular and Cellular Cardiology* **52,** 323–329 (2012).

245. Omori, K. & Kotera, J. Overview of PDEs and their regulation. *Circulation Research* **100,** 309–327 (2007).

246. Bender, A. T. & Beavo, J. A. Cyclic nucleotide phosphodiesterases: molecular regulation to clinical use. *Pharmacol. Rev.* **58,** 488–520 (2006).

247. Möglich, A., Ayers, R. A. & Moffat, K. Structure and Signaling Mechanism of Per-ARNT-Sim Domains. *Structure* **17,** 1282–1294 (2009).

248. Surapisitchat, J. & Beavo, J. A. Regulation of endothelial barrier function by cyclic nucleotides: The role of phosphodiesterases. *Handb. Exp. Pharmacol.* **204,** 193–210 (2011).

249. Rosman, G. J. *et al.* Isolation and characterization of human cDNAs encoding a cGMP-stimulated 3',5'-cyclic nucleotide phosphodiesterase. *Gene* **191,** 89–95 (1997).

250. Liu, X. *et al.* Adenylyl cyclase type 6 overexpression selectively enhances beta-adrenergic and prostacyclin receptor-mediated inhibition of cardiac fibroblast function because of colocalization in lipid rafts. *Naunyn. Schmiedebergs. Arch. Pharmacol.* **377,** 359–369 (2008).

251. Ostrom, R. S. & Insel, P. A. The evolving role of lipid rafts and caveolae in G protein-coupled receptor signaling: implications for molecular pharmacology. *Br. J. Pharmacol.* **143,** 235–245 (2004).

252. Blackman, B. E. *et al.* PDE4D and PDE4B function in distinct subcellular compartments in mouse embryonic fibroblasts. *J. Biol. Chem.* **286,** 12590–12601 (2011).

253. Rampersad, S. N. *et al.* Cyclic AMP phosphodiesterase 4D (PDE4D) Tethers EPAC1 in a vascular endothelial cadherin (VE-Cad)-based signaling complex and controls cAMP-mediated vascular permeability. *J. Biol. Chem.* **285,** 33614–22 (2010).

254. Zaccolo, M. & Pozzan, T. Discrete microdomains with high concentration of cAMP in stimulated rat neonatal cardiac myocytes. *Science* **295,** 1711–5 (2002).

255. Dodge-Kafka, K. L. *et al.* The protein kinase A anchoring protein mAKAP coordinates two integrated cAMP effector pathways. *Nature* **437,** 574–578 (2005).

256. Vo, N. K., Gettemy, J. M. & Coghlan, V. M. Identification of cGMP-dependent protein kinase anchoring proteins (GKAPs). *Biochem. Biophys. Res. Commun.* **246,** 831–835 (1998).

257. Radeva, M. Y., Kugelmann, D., Spindler, V. & Waschke, J. PKA compartmentalization via AKAP220 and AKAP12 contributes to endothelial barrier regulation. *PLoS One* **9,** e106733 (2014).

258. Sehrawat, S. *et al.* AKAP9 regulation of microtubule dynamics promotes Epac1-induced endothelial barrier properties. *Blood* **117,** 708–718 (2011).

259. Yuasa, K., Omori, K. & Yanaka, N. Binding and phosphorylation of a novel male germ cell-specific cGMP- dependent protein kinase-anchoring protein by cGMP-dependent protein kinase I?? *J. Biol. Chem.* **275,** 4897–4905 (2000).

260. Dejana, E. Endothelial cell-cell junctions: happy together. *Nat. Rev. Mol. Cell Biol.* **5,** 261–270 (2004).

261. Tang, W.-J. & Gilman, A. G. Construction of a Soluble Adenylyl Cyclase Activated by G$_s\alpha$ and Forskolin. *Science (80-.).* **268,** 1769–1772 (1995).

262. Van Nieuw Amerongen, G. P. & van Hinsbergh, V. W. M. Targets for pharmacological intervention of endothelial hyperpermeability and barrier function. *Vascul. Pharmacol.* **39,** 257–72 (2002).

263. Zimmerman, R. S., Trippodo, N. C., MacPhee, A. A., Martinez, A. J. & Barbee, R. W. High-dose atrial natriuretic factor enhances albumin escape from the systemic but not the pulmonary circulation. *Circ. Res.* **67,** 461–8 (1990).

264. Draijer, R., Atsma, D. E., van der Laarse, A. & van Hinsbergh, V. W. cGMP and nitric oxide modulate thrombin-induced endothelial permeability. Regulation via different pathways in human aortic and umbilical vein endothelial cells. *Circ. Res.* **76,** 199–208 (1995).

265. Hölschermann, H., Noll, T., Hempel, A. & Piper, H. M. Dual role of cGMP in modulation of macromolecule permeability of aortic endothelial cells. *Am. J. Physiol.* **272,** H91–H98 (1997).

266. Gupta, M. P. *et al.* Nitric oxide attenuates H(2)O(2)-induced endothelial barrier dysfunction: mechanisms of protection. *Am. J. Physiol. Lung Cell. Mol. Physiol.* **280,** L116–26 (2001).

267. Kuhn, M. Endothelial actions of atrial and B-type natriuretic peptides. *British Journal of Pharmacology* **166,** 522–531 (2012).

268. Seybold, J. *et al.* Tumor necrosis factor-alpha-dependent expression of phosphodiesterase 2: role in endothelial hyperpermeability. *Blood* **105,** 3569–3576 (2005).

269. PAPPENHEIMER, J. R., RENKIN, E. M. & BORRERO, L. M. Filtration, diffusion and molecular sieving through peripheral capillary membranes; a contribution to the pore theory of capillary permeability. *Am. J. Physiol.* **167,** 13–46 (1951).

270. Drake, R., Gaar, K. A. & Taylor, A. E. Estimation of the filtration coefficient of pulmonary exchange vessels. *Am. J. Physiol.* **234,** H266–H274 (1978).

271. Yuan, Y., Mier, R. A., Chilian, W. M., Zawieja, D. C. & Granger, H. J. Interaction of neutrophils and endothelium in isolated coronary venules and arterioles. *Am. J. Physiol.* **268,** H490–H498 (1995).

272. MILES, A. A. & MILES, E. M. Vascular reactions to histamine, histamine-liberator and leukotaxine in the skin of guinea-pigs. *J. Physiol.* **118,** 228–257 (1952).

273. Nakamura, Y. & Wayland, H. Macromolecular transport in the cat mesentery. *Microvasc. Res.* **9,** 1–21 (1975).

274. Witte, S., Goldenberg, D. M. & Schricker, K. T. [The propagation of fluorescent dyes in the hamster cheek pouch]. *Z. Gesamte Exp. Med.* **148,** 72–80 (1968).

275. Yuan, S. Y. & Rigor, R. R. *Regulation of Endothelial Barrier Function*. (2010).

276. Siflinger-Birnboim, A. *et al.* Molecular sieving characteristics of the cultured endothelial monolayer. *J. Cell. Physiol.* **132,** 111–117 (1987).

277. Crone, C. & Olesen, S. P. Electrical resistance of brain microvascular endothelium. *Brain Res.* **241,** 49–55 (1982).

278. Weksler, B., Romero, I. a & Couraud, P.-O. The hCMEC/D3 cell line as a model of the human blood brain barrier. *Fluids Barriers CNS* **10,** 16 (2013).

279. Hermanns, M. I., Unger, R. E., Kehe, K., Peters, K. & Kirkpatrick, C. J. Lung epithelial cell lines in coculture with human pulmonary microvascular endothelial cells: development of an alveolo-capillary barrier in vitro. *Lab. Invest.* **84,** 736–752 (2004).

280. Tiruppathi, C., Malik, A. B., Del Vecchio, P. J., Keese, C. R. & Giaever, I. Electrical method for detection of endothelial cell shape change in real time: assessment of endothelial barrier function. *Proc Natl Acad Sci U S A* **89,** 7919–7923 (1992).

281. Williams, C. cAMP detection methods in HTS: selecting the best from the rest. *Nat. Rev. Drug Discov.* **3,** 125–135 (2004).

282. Hailey, D. W., Dams, Trisha, N. & Muller, E. G. D. Fluorescence resonance energy transfer using color variants of green fluorescent protein. *Methods Enzymol.* **351,** 34–49 (2002).

283. Kurokawa, K., Takaya, A., Terai, K., Fujioka, A. & Matsuda, M. Visualizing the Signal Transduction Pathways in Living Cells with GFP-Based FRET Probes. *ACTA HISTOCHEMICA ET CYTOCHEMICA* **37,** 347–355 (2004).

284. Miyawaki, A. Visualization of the spatial and temporal dynamics of intracellular signaling. *Dev Cell* **4,** 295–305 (2003).

285. Klarenbeek, J. B., Goedhart, J., Hink, M. A., Gadella, T. W. J. & Jalink, K. A mTurquoise-based cAMP sensor for both FLIM and ratiometric read-out has improved dynamic range. *PLoS One* **6,** (2011).

286. Honda, A., Sawyer, C. L., Cawley, S. M. & Dostmann, W. R. G. Cygnets: in vivo characterization of novel cGMP indicators and in vivo imaging of intracellular cGMP. *Methods Mol. Biol.* **307,** 27–43 (2005).

287. Honda, A. *et al.* Spatiotemporal dynamics of guanosine 3',5'-cyclic monophosphate revealed by a genetically encoded, fluorescent indicator. *Proc. Natl. Acad. Sci. U. S. A.* **98,** 2437–2442 (2001).

288. Nikolaev, V. O., Gambaryan, S. & Lohse, M. J. Fluorescent sensors for rapid monitoring of intracellular cGMP. *Nat. Methods* **3,** 23–25 (2006).

289. Depry, C. & Zhang, J. Using FRET-based reporters to visualize subcellular dynamics of protein kinase A activity. *Methods Mol. Biol.* **756,** 285–294 (2011).

290. Nagai, T., Yamada, S., Tominaga, T., Ichikawa, M. & Miyawaki, A. Expanded dynamic range of fluorescent indicators for Ca(2+) by circularly permuted yellow fluorescent proteins. *Proc. Natl. Acad. Sci. U. S. A.* **101,** 10554–10559 (2004).

291. Klarenbeek, J., Goedhart, J., van Batenburg, A., Groenewald, D. & Jalink, K. Fourth-Generation Epac-Based FRET Sensors for cAMP Feature Exceptional Brightness, Photostability and Dynamic Range: Characterization of Dedicated Sensors for FLIM, for Ratiometry and with High Affinity. *PLoS One* **10,** e0122513 (2015).

292. Komatsu, N. *et al.* Development of an optimized backbone of FRET biosensors for kinases and GTPases. *Molecular Biology of the Cell* **22,** 4647–4656 (2011).

293. Chen, Y., Saulnier, J. L., Yellen, G. & Sabatini, B. L. A PKA activity sensor for quantitative analysis of endogenous GPCR signaling via 2-photon FRET-FLIM imaging. *Front. Pharmacol.* **5 APR,** (2014).

294. Schmidt, H. H. H. W., Hofmann, F. B. & Stasch, J.-P. *cGMP: Generators, Effectors and Therapeutic Implications*. (Springer, 2009).

295. Ni, Q., Titov, D. V. & Zhang, J. Analyzing protein kinase dynamics in living cells with FRET reporters. *Methods* **40,** 279–286 (2006).

296. Lambert, T. & Thorn, K. Fluorescent protein properties. at <http://nic.ucsf.edu/FPvisualization/>

297. Ponsioen, B. *et al.* Detecting cAMP-induced Epac activation by fluorescence resonance energy transfer: Epac as a novel cAMP indicator. *EMBO Rep.* **5,** 1176–1180 (2004).

298. Terrin, A. *et al.* PGE(1) stimulation of HEK293 cells generates multiple contiguous domains with different [cAMP]: role of compartmentalized phosphodiesterases. *The Journal of Cell Biology* **175,** 441–451 (2006).

299. Obiako, B. *et al.* Bicarbonate disruption of the pulmonary endothelial barrier via activation of endogenous soluble adenylyl cyclase, isoform 10. *Am. J. Physiol. Lung Cell. Mol. Physiol.* **305,** L185–92 (2013).

300. Sayner, S. L. Emerging themes of cAMP regulation of the pulmonary endothelial barrier. *Am. J. Physiol. Lung Cell. Mol. Physiol.* **300,** L667–78 (2011).

301. Maniatis, N. A. & Orfanos, S. E. The endothelium in acute lung injury/acute respiratory distress syndrome. *Curr. Opin. Crit. Care* **14,** 22–30 (2008).

302. Peinado, V. I. *et al.* Inflammatory reaction in pulmonary muscular arteries of patients with mild chronic obstructive pulmonary disease. *Am. J. Respir. Crit. Care Med.* **159,** 1605–1611 (1999).

303. Brunner, D. *et al.* Serum-free cell culture: the serum-free media interactive online database. *ALTEX* **27,** 53–62 (2010).

304. Ryu, M.-H. *et al.* Engineering adenylate cyclases regulated by near-infrared window light. *Proc. Natl. Acad. Sci. U. S. A.* **111,** 10167–10172 (2014).

305. Monterisi, S. *et al.* CFTR regulation in human airway epithelial cells requires integrity of the actin cytoskeleton and compartmentalized cAMP and PKA activity. *J. Cell Sci.* **125,** 1106–17 (2012).

306. Stierl, M. *et al.* Light modulation of cellular cAMP by a small bacterial photoactivated adenylyl cyclase, bPAC, of the soil bacterium Beggiatoa. *J. Biol. Chem.* **286,** 1181–1188 (2011).

307. Kim, J. H. *et al.* High cleavage efficiency of a 2A peptide derived from porcine teschovirus-1 in human cell lines, zebrafish and mice. *PLoS One* **6,** (2011).

308. Poller, B. *et al.* The human brain endothelial cell line hCMEC/D3 as a human blood-brain barrier model for drug transport studies. *J. Neurochem.* **107,** 1358–1368 (2008).

309. Weksler, B. B. *et al.* Blood-brain barrier-specific properties of a human adult brain endothelial cell line. *FASEB J.* **19,** 1872–1874 (2005).

310. Davies, J. *et al.* Adenosine promotes vascular barrier function in hyperoxic lung injury. *Physiol. Rep.* **2,** (2014).

311. Gonzales, J. N. *et al.* Protective effect of adenosine receptors against lipopolysaccharide-induced acute lung injury. *Am. J. Physiol. Lung Cell. Mol. Physiol.* (2014). doi:10.1152/ajplung.00086.2013

312. Van Linden, A. & Eltzschig, H. K. Role of pulmonary adenosine during hypoxia: extracellular generation, signaling and metabolism by surface adenosine deaminase/CD26. *Expert Opin. Biol. Ther.* **7,** 1437–1447 (2007).

313. Gschwandtner, M. *et al.* Histamine suppresses epidermal keratinocyte differentiation and impairs skin barrier function in a human skin model. *Allergy* **68,** 37–47 (2013).

314. Lin, T.-K. *et al.* Topical Antihistamines Display Potent Anti-Inflammatory Activity Linked in Part to Enhanced Permeability Barrier Function. *Journal of Investigative Dermatology* (2012). doi:10.1038/jid.2012.335

315. Lum, H. & Malik, A. B. Regulation of vascular barrier function endothelial. *Am. J. Physiol.* **262,** 223–241 (1994).

316. Alberelli, M. A. & De Candia, E. Functional role of protease activated receptors in vascular biology. *Vascular Pharmacology* **62,** 72–81 (2014).

317. Cioffi, D. L. *et al.* Dominant regulation of interendothelial cell gap formation by calcium-inhibited type 6 adenylyl cyclase. *J. Cell Biol.* **157,** 1267–1278 (2002).

318. Stevens, T. *et al.* Ca(2+)-inhibitable adenylyl cyclase modulates pulmonary artery endothelial cell cAMP content and barrier function. *Proc. Natl. Acad. Sci. U. S. A.* **92,** 2696–2700 (1995).

319. Werthmann, R. C., von Hayn, K., Nikolaev, V. O., Lohse, M. J. & Bünemann, M. Real-time monitoring of cAMP levels in living endothelial cells: thrombin transiently inhibits adenylyl cyclase 6. *J. Physiol.* **587,** 4091–4104 (2009).

320. Werthmann, R. C., Lohse, M. J. & Bünemann, M. Temporally resolved cAMP monitoring in endothelial cells uncovers a thrombin-induced [cAMP] elevation mediated via the Ca^{2}+-dependent production of prostacyclin. *J. Physiol.* **589,** 181–193 (2011).

321. Manolopoulos, V. G., Fenton, J. W. 2nd & Lelkes, P. I. The thrombin receptor in adrenal medullary microvascular endothelial cells is negatively coupled to adenylyl cyclase through a Gi protein. *Biochim. Biophys. Acta* **1356,** 321–332 (1997).

322. Francis, S. H., Busch, J. L., Corbin, J. D. & Sibley, D. cGMP-dependent protein kinases and cGMP phosphodiesterases in nitric oxide and cGMP action. *Pharmacol. Rev.* **62,** 525–563 (2010).

323. Huang, G. Y. *et al.* Structural basis for cyclic-nucleotide selectivity and cGMP-selective activation of PKG i. *Structure* **22,** 116–124 (2014).

324. Kim, J. J. *et al.* Co-crystal structures of PKG Iβ (92-227) with cGMP and cAMP reveal the molecular details of cyclic-nucleotide binding. *PLoS One* **6,** e18413 (2011).

325. Aird, W. C. Phenotypic heterogeneity of the endothelium: II. Representative vascular beds. *Circulation Research* **100,** 174–190 (2007).

326. Flaherty, J. T. *et al.* Endothelial nuclear patterns in the canine arterial tree with particular reference to hemodynamic events. *Circ. Res.* **30,** 23–33 (1972).

327. Aird, W. C. Endothelial cell heterogeneity. *Cold Spring Harb. Perspect. Med.* **2,** (2012).

328. Minami, T. & Aird, W. C. Endothelial cell gene regulation. *Trends in Cardiovascular Medicine* **15,** (2005).

329. Chi, J.-T. *et al.* Endothelial cell diversity revealed by global expression profiling. *Proc. Natl. Acad. Sci. U. S. A.* **100,** 10623–10628 (2003).

330. Swinscoe, J. C. & Carlson, E. C. Type II collagen is a major component of bovine retinal microvessel extracellular matrix. *Microcirculation* **2,** 253–265 (1995).

331. Salvador, E., Shityakov, S. & F??rster, C. Glucocorticoids and endothelial cell barrier function. *Cell and Tissue Research* 1–9 (2013). doi:10.1007/s00441-013-1762-z

332. Kim, K.-J. & Malik, A. B. Protein transport across the lung epithelial barrier. *Am. J. Physiol. Lung Cell. Mol. Physiol.* **284,** L247–L259 (2003).

333. Dexamethasone. at <http://www.drugs.com/monograph/dexamethasone.html>

334. Clark, M. A., Bomalaski, J. S., Conway, T. M., Wartell, J. & Crooke, S. T. Differential effects of aspirin and dexamethasone on phospholipase A2 and C activities and arachidonic acid release from endothelial cells in response to bradykinin and leukotriene D4. *Prostaglandins* **32,** 703–708 (1986).

335. Christensen, A. E. *et al.* cAMP analog mapping of Epac1 and cAMP kinase: Discriminating analogs demonstrate that Epac and cAMP kinase act synergistically to promote PC-12 cell neurite extension. *J. Biol. Chem.* **278,** 35394–35402 (2003).

336. Khanh, K. D. *et al.* Epac1 and cAMP-dependent protein kinase holoenzyme have similar cAMP affinity, but their cAMP domains have distinct structural features and cyclic nucleotide recognition. *J. Biol. Chem.* **281,** 21500–21511 (2006).

337. Garcia, J. G. N. *et al.* Sphingosine 1-phosphate promotes endothelial cell barrier integrity by Edg-dependent cytoskeletal rearrangement. *J. Clin. Invest.* **108,** 689–701 (2001).

338. Della Latta, V., Cabiati, M., Rocchiccioli, S., Del Ry, S. & Morales, M. A. The role of the adenosinergic system in lung fibrosis. *Pharmacol. Res.* **76,** 182–189 (2013).

339. Fredholm, B. B. *et al.* Structure and function of adenosine receptors and their genes. *Naunyn-Schmiedeberg's Archives of Pharmacology* **362,** 364–374 (2000).

340. Borrmann, T. *et al.* 1-Alkyl-8-(piperazine-1-sulfonyl)phenylxanthines: Development and characterization of adenosine A2B receptor antagonists and a new radioligand with subnanomolar affinity and subtype specificity. *J. Med. Chem.* **52,** 3994–4006 (2009).

341. Melani, A. *et al.* The selective A2A receptor antagonist SCH 58261 reduces striatal transmitter outflow, turning behavior and ischemic brain damage induced by permanent focal ischemia in the rat. *Brain Res.* **959,** 243–250 (2003).

342. Ryan, M. J. & Brody, M. J. Neurogenic and vascular stores of histamine in the dog. *J. Pharmacol. Exp. Ther.* **181,** 83–91 (1972).

343. Vugman, I. & Rocha e Silva, M. Biological determination of histamine in living tissues and body fluids. *Histamine and anti-histaminics. Handb. Exptl. Pharmakol.* **XVIII/I,** 81 (1966).

344. Van de Voorde, J. & Leusen, I. Role of the endothelium in the vasodilator response of rat thoracic aorta to histamine. *Eur. J. Pharmacol.* **87,** 113–120 (1983).

345. Togias, A. H1-Receptors: Localization and role in airway physiology and in immune functions. in *Journal of Allergy and Clinical Immunology* **112,** (2003).

346. Parsons, M. E. & Ganellin, C. R. Histamine and its receptors. *Br. J. Pharmacol.* **147 Suppl ,** S127–S135 (2006).

347. Repka-Ramirez, M. S. New concepts of histamine receptors and actions. *Curr. Allergy Asthma Rep.* **3,** 227–231 (2003).

348. Adjobo-Hermans, M. J. W. *et al.* Real-time visualization of heterotrimeric G protein Gq activation in living cells. *BMC Biol.* **9,** 32 (2011).

349. Mizuguchi, H. *et al.* Involvement of Protein Kinase C{delta}/Extracellular Signal-regulated Kinase/Poly(ADP-ribose) Polymerase-1 (PARP-1) Signaling Pathway in Histamine-induced Up-regulation of Histamine H1 Receptor Gene Expression in HeLa Cells. *J. Biol. Chem.* **286,** 30542–30551 (2011).

350. Notcovich, C. *et al.* Histamine acting on H1 receptor promotes inhibition of proliferation via PLC, RAC, and JNK-dependent pathways. *Exp. Cell Res.* **316,** 401–411 (2010).

351. Mikelis, C. M. *et al.* RhoA and ROCK mediate histamine-induced vascular leakage and anaphylactic shock. *Nat. Commun.* **6,** 6725 (2015).

352. Jie, Q. *et al.* Anti-allergic and anti-inflammatory properties of a potent histamine H1 receptor antagonist, desloratadine citrate disodium injection, and its anti-inflammatory mechanism on EA.hy926 endothelial cells. *Eur. J. Pharmacol.* **754,** 1–10 (2015).

353. Andriopoulou, P., Navarro, P., Zanetti, A., Lampugnani, M. G. & Dejana, E. Histamine induces tyrosine phosphorylation of endothelial cell-to-cell adherens junctions. *Arterioscler. Thromb. Vasc. Biol.* **19,** 2286–2297 (1999).

354. Coughlin, S. R. Thrombin signalling and protease-activated receptors. *Nature* **407,** 258–264 (2000).

355. Baumer, Y., Drenckhahn, D. & Waschke, J. cAMP induced Rac 1-mediated cytoskeletal reorganization in microvascular endothelium. *Histochem. Cell Biol.* **129,** 765–778 (2008).

356. Tiruppathi, C., Malik, A. B., Del Vecchio, P. J., Keese, C. R. & Giaever, I. Electrical method for detection of endothelial cell shape change in real time: assessment of endothelial barrier function. *Proc. Natl. Acad. Sci. U. S. A.* **89,** 7919–7923 (1992).

357. Hoppe, A. D. FRET-based imaging of rac and cdc42 activation during fc-receptor-mediated phagocytosis in macrophages. *Methods Mol. Biol.* **827,** 235–251 (2012).